Natural convection heating of liquids, with reference to sterilization of canned food

J. Hiddink

J. Hiddink

Natural convection heating of liquids, with reference to sterilization of canned food

Abstract

In a model system the physical transport phenomena that occur during the sterilization of a canned liquid food were investigated. Flow phenomena and heat transfer were studied experimentally as well as theoretically. Experiments on flow patterns and temperature profiles revealed a boundary layer flow at the vertical sidewall, a stratified core in the upper part of the container and a perfectly mixed, unstratified region in the lower part of the container. A dimensionless correlation for the overall heat transfer coefficient from steam to liquid was determined.

From the observed flow patterns and temperature profiles a simplified mathematical model was developed, with which temperature stratification in the liquid during heating could be simulated. The applicability of the simplified model for lethality calculations was briefly examined.

Some attention was also paid to the effect of solid particles on heating characteristics of the container contents.

Literature on the research of convection heating of liquids in closed containers was reviewed, as well as literature about the influence of temperature stratification on natural convection boundary layer flow.

Keywords: flow visualization, heating simulation model, lethality calculations, influence of solid particles on heat transfer.

Stellingen

1. Bij het bestuderen van warmteoverdracht door vrije convectie geeft het afleiden van stromingspatronen uit temperatuurprofielen gemakkelijk aanleiding tot onjuiste conclusies.

J. E. Reichert & H. J. Bielig. Confructa 18 (1973) 149–163.

2. De veronderstelling van Fujii et al. dat bij vrije convectie stromingsomkering in de grenslaag als gevolg van een temperatuurgradiënt in de bulk een artefact is, veroorzaakt door onnauwkeurigheden in de gevolgde rekentechnieken, is in elk geval voor hoge Prandtlgetallen onjuist.

T. Fujii, M. Takeuchi & I. Morioka. Fifth International Heat transfer Conference III (1974) 44–48.
Dit proefschrift, hoofdstuk 4.

3. De veronderstelling van Stumbo dat bij produkten van het convectietype tengevolge van stroming alle micro-organismen dezelfde hittebehandeling ondergaan, is voor visceuze produkten in bussen die stilstaand gesteriliseerd worden niet juist.

C. R. Stumbo. Thermobacteriology in Food Processing. Academic Press (1973).

4. Bij de sterilisatie van produkten van het convectietype is 'het koudste punt' een ambulant begrip.

Dit proefschrift, hoofdstuk 4.

5. Het gebruik van een verschillende terminologie waar het gaat om wetmatigheden betreffende eerste-ordereacties, belemmert de communicatie tussen de thermo-bacteriologie en de chemische reactietechniek.

6. Het gebruik van de term hyperfiltratie in plaats van omgekeerde osmose suggereert een te eenvoudig beeld van bij omgekeerde osmose optredende transportverschijnselen.

Symposium KNCV/KIVI, Sectie Chemische Technologie, 28 november 1974.

7. Gezien het uitbetalingsbeleid van melk op eiwitgehalte ligt het voor de hand consumptiemelk en consumptiemelkprodukten op eiwitgehalte te standaardiseren. Ultrafiltratie biedt hiertoe nu de mogelijkheid.

8. De stelling dat bij het concentreren van wei door middel van omgekeerde osmose bij een zo hoog mogelijke temperatuur gewerkt moet worden om een maximale flux te verkrijgen, is aanvechtbaar.

J. K. Donnelly, A. C. O'Sullivan & R. A. M. Delaney. J. Soc. Dairy Technol. 27 (1974) 128–140.

9. Biot moet blijven.

Concept norm NEN 999 (november 1974).

10. Dit proefschrift werpt nieuw licht op de betekenis van de ziel van de wijnfles.

Proefschrift van J. Hiddink
Natural convection heating of liquids, with reference to sterilization of canned food

Dankbetuiging

Curriculum vitae

De auteur werd geboren op 4 april 1943 te Zelhem. Hij behaalde in 1960 het MULO-B diploma aan de Ds. van Dijkschool te Doetinchem en vervolgens in 1962 het HBS-B diploma aan het Baudartiuslyceum te Zutphen. Na het vervullen van de militaire dienstplicht begon hij in 1964 zijn studie aan de Landbouwhogeschool te Wageningen. In januari 1969 werd het kandidaatsexamen afgelegd in de levensmiddelentechnologie met technologische specialisatie. De doctoraalstudie omvatte de vakken technologie, levensmiddelenchemie en natuurkunde. Na zijn afstuderen in september 1971 trad hij als promotie-assistent in dienst bij de Sectie Proceskunde van de Vakgroep Levensmiddelentechnologie van de Landbouwhogeschool, waar hij dit proefschrift bewerkte.

Sinds 15 oktober 1974 is hij werkzaam bij het Nederlands Instituut voor Zuivelonderzoek te Ede waar hij zich in het bijzonder bezighoudt met het onderzoek aan de membraanprocessen omgekeerde osmose en ultrafiltratie.

Contents

List of symbols most frequently used

A	= dimensionless parameter, Eqn (55)	—
A_c	= container surface in contact with product	(m²)
Bi	= $h_{out}l/\lambda$ = Biot number	—
c_B	= concentration of bacteria	(kg⁻¹)
c_p	= heat capacity of liquid (product)	(J/kg·K)
c_{pf}	= heat capacity liquid phase	(J/kg·K)
c_{ps}	= heat capacity solid phase	(J/kg·K)
D	= diameter of container	(m)
d_p	= diameter of solid sphere	(m)
d_w	= thickness of container wall	(m)
DRT	= decimal reduction time	(s)
f	= characteristic heating time, Eqn (3)	(s)
Fo	= $\alpha t/l^2$ = Fourier number	—
g	= acceleration of gravity	(m/s²)
Gr	= $l^3 g\beta \Delta T/\nu^2$ = Grashof number	—
H	= total liquid height in the container	(m)
h	= heat transfer coefficient	(W/m²·K)
h_{in}	= heat transfer coefficient inside container	(W/m²·K)
h_s	= heat transfer coefficient from liquid to solid particle	(W/m²·K)
h_{out}	= heat transfer coefficient outside container	(W/m²·K)
k_r	= reaction rate first order reaction, Eqn (73)	(s⁻¹)
L	= height of container	(m)
l	= characteristic length	(m)
m	= characteristic heating rate, Eqn (14)	(s⁻¹)
Nu	= $h_{in}l/\lambda$ = Nusselt number	—
$Pé$	= $Re.Pr$ = Péclet number	—
Pr	= ν/α = Prandtl number	—
q_b	= heat flux density at the bottom of a container	(W/m²)
q_s	= heat flux density at the sidewall of a container	(W/m²)
r	= radial coordinate (Fig. 9)	(m)
R	= dimensionless radial coordinate (Appendix A)	—
Ra	= $Gr Pr$ = Rayleigh number	—
Re	= lv/ν = Reynolds number	—
S	= specific area of packed bed	(m⁻¹)
t	= time	(s)
T	= instantaneous temperature of liquid (product)	(°C)
T_a	= temperature of the heating medium (steam)	(°C)

T_b	= temperature of the unstratified region	(°C)
T_{bl}	= temperature of boundary layer	(°C)
T_c	= temperature of liquid in stratified region	(°C)
T_{in}	= temperature of liquid entering boundary layer	(°C)
T_0	= initial temperature	(°C)
T_{ref}	= reference temperature	(°C)
T_w	= wall temperature	(°C)
T_l	= temperature of the liquid phase	(°C)
T_s	= temperature of the solid phase	(°C)
ΔT	= temperature difference $(T_a - T)$	(K)
ΔT_0	= temperature difference $(T_a - T_0)$	(K)
u	= velocity component in x direction (Fig. 9)	(m/s)
U	= dimensionless velocity in X-direction (Appendix A)	—
U	= overall heat transfer coefficient	(W/m$^2 \cdot$ K)
U_s	= overall heat transfer coefficient from liquid to solid particle	(W/m$^2 \cdot$ K)
U_{cond}	= overall heat transfer coefficient for conduction heating	(W/m$^2 \cdot$ K)
v	= velocity component in r direction (Fig. 9)	(m/s)
V	= dimensionless velocity in R direction (Appendix A)	—
v_c	= downward velocity in the core	(m/s)
v_{bl}	= liquid velocity in boundary layer flow	(m/s)
V_c	= liquid (product) volume	(m^3)
V_r	= reactor volume	(m^3)
W	= flow rate of boundary layer	(m^3/s)
x	= axial coordinate (Fig. 9)	(m)
X	= dimensionless axial coordinate (Appendix A)	—
X	= height of unstratified region	(m)
y	= distance from sidewall	(m)
z_t	= temperature coefficient of DRT	(K)
Z	= dimensionless height of unstratified region	—
α	= heat diffusivity	(m^2/s)
α_{eff}	= effective heat diffusivity	(m^2/s)
β	= thermal expansion coefficient	(K^{-1})
δ	= thickness of boundary layer	(m)
ε	= porosity	—
η	= dynamic viscosity	(N $\cdot$ s/m^2)
θ	= dimensionless temperature	—
κ	= reciprocal temperature gradient, Eqn (53)	(m/K)
λ	= heat conductivity of the liquid (product)	(W/m $\cdot$ K)
λ_{eff}	= effective heat conductivity	(W/m $\cdot$ K)
λ_s	= heat conductivity of the solid phase	(W/m $\cdot$ K)
λ_l	= heat conductivity of the liquid phase	(W/m $\cdot$ K)
λ_w	= heat conductivity of the container wall	(W/m $\cdot$ K)
ν	= kinematic viscosity	(m^2/s)
ρ	= liquid (product) density	(kg/m^3)
ρ_l	= density of the liquid phase	(kg/m^3)

ρ_s	= density of the solid phase	(kg/m^3)
τ	= dimensionless time	—
Φ	= heat flux	(W)
Ψ	= dimensionless stream function	—
ω	= dimensionless vorticity	—

1 Introduction

Heating of fluids in enclosed spaces is of interest, both scientifically and technologically. A common application is the heating of water for coffee or tea. More sophisticated technological applications are found in the thermal sterilization of liquid foods in cans or glass jars, the storage of liquid natural gas in large vessels, frictional heating of liquid fuels in missiles, heating of living rooms and internal cooling of gas turbine blades. This problem is also interesting from a scientific point of view: the question is whether the traditional boundary layer approach is adequate or not to describe the flow phenomena within the enclosed space. Are significant deviations to be expected from this simplified, but very useful picture?

The research described in this thesis was initiated from special interest in heat sterilization of canned liquid foods. In the food industry a considerable amount of literature is available about sterilization. There is much literature on conduction-heated products, solid foods, especially on the mathematical treatment of the heating process, see for example Hayakawa & Ball (1971). However there are few publications about convection-heated foods. Presumably the problem of convection heating was considered of minor importance because of its high heating rate and because it is too complicated for mathematical treatment. However, as will be outlined below, a study of convection heating of canned foods is still important.

To estimate the sterilizing effect, knowledge about the temperature history of the food is required. Conventional methods of thermal process evaluation determine the time-integrated lethal effect of heat at a fixed point in the container. This point is selected as the 'slowest heating point'; the rest of the container may be ignored since elsewhere in the product the time-integrated lethal effect of the heat treatment is undoubtedly higher. Examples of this method are described by Ball & Olson (1957). Another method for process evaluation is based on the volume-integrated probability of survival of micro-organisms over the whole container, see Stumbo (1953). For this method the temperature history at all points in the container must be known. For conduction-heated products the method of Stumbo is widely accepted, since the temperature distribution during heating can be calculated at any time from conduction heating theory. For convection-heated products no reliable methods are available for calculation of the temperature distribution during heating. Moreover it must be emphasized that the temperature history at a fixed point is not the temperature history experienced by a liquid element because convection currents cause product movement through the container. For these two reasons the method of Stumbo cannot be applied without modifications to convection-heated products. Therefore in sterilization of

liquid food the conventional calculation methods are used. To obtain the desired sterilization effects these methods are suitable. However, the required destruction of micro-organisms during the heating process is accompanied by an undesirable degradation of nutrients and flavour. Fortunately the dependency of reaction rate on temperature is different for thermal destruction of micro-organisms and for chemical reactions. Thus it will be clear that an optimum heating process can be defined for which the lethality is just sufficient and nutrient and flavour reduction is minimal. However, for a successful optimization the temperature history of all particles in the container should be known. For conduction-heated foods such optimizations have been done by Teixeira et al. (1969) and Jen et al. (1971). Although in the literature on food technology some attention has been paid to the development of mathematical models for predicting the heat transfer rate in convection heating, these models are too primitive to be used for process optimization. Only Stevens (1972) applied a more sophisticated theoretical treatment to convection heating and did lethality calculations including effects of product movement. However, as will be discussed later his results were not very satisfactory.

The aim of this study was to develop a better understanding of the mechanism of heat transfer within a liquid heated in a closed container. The study of the physical phenomena should provide a model for a mathematical treatment of the heating process, which can then be used to evaluate lethality and quality conservation. The study was restricted to cylindrical, non-agitated containers, positioned vertically in condensing steam, a situation often encountered in sterilization of canned foods. We must not forget, however, that in practice cans are often processed horizontally or even rotating. Nevertheless, it was considered that stable vertical orientation was most suitable for investigation and that the information obtained would surely be indicative in studying the other situations.

I studied flow phenomena and heat transfer experimentally as well as theoretically. The experimental set-up was especially designed to facilitate, besides temperature measurements, hydrodynamical observations by flow visualization techniques and by the laser-doppler method. Theoretically the problem was tackled by using dimensional analysis and mathematical models.

Organization of this thesis   A study was made of food technology literature and pertinent literature from other technological applications (Chapter 2).

In Chapter 3 the mathematical treatment of heating liquids in closed containers is reviewed. This review includes a study of the literature on natural convection boundary layers in environments of non-uniform temperature as well as a numerical solution of the differential equations with boundary conditions appropriate to the problem studied.

The experimental part of this thesis (Chapter 4) mainly consists of an assessment of flow patterns and temperature profiles for liquids of different viscosity. Important features were the development of flow patterns and temperature profiles in time, and the interaction between flow patterns and temperature profiles. A more detailed study of velocity profiles in the boundary layer at the sidewall was made with a laser-doppler velocimeter.

2

Many measurements were done to determine overall heat transfer coefficients (Chapter 5). This ultimately resulted in a dimensionless correlation for the overall heat transfer coefficient from the heating steam to the liquid in the container.

In Chapter 6 a simplified simulation model is developed based on the observed flow patterns and temperature profiles. With this model the temperature stratification in the liquid during heating can be predicted. The applicability of the simplified (reactor) model for lethality calculations was briefly examined.

In food canning very often solid particles are present in the liquid. Therefore, in Chapter 7 some attention was paid to the effect of solid particles on heating characteristics.

2 Literature

There is a considerable amount of literature about the heating of all kinds of food products in containers, under a wide variety of conditions. It has become common practice to distinguish between two main groups according to their heating characteristics: solid foods, where heat penetrates just by conduction and liquid foods, in which convection flows are generated throughout the heating process. This distinction between conduction-heated products and convection-heated products is not very sharp: there are many food products in which both mechanisms are of equal importance. Ball & Olson (1957) listed the various types of food products according to their heating characteristics. The most marked difference between conduction heating and convection heating is, of course, the much higher rate of heating for convection-heated products. Examples are given by Bigelow et al. (1920), Riedel (1947), Powers et al. (1952) and Board (1966).

I only studied convection heating in vertical, non-agitated containers. Thus only literature on this subject will be referred to in this survey. I often used Blaisdell's (1963) review of the literature on this subject as a guide line. This chapter successively deals with: (a) the effect of some internal and external factors on convection heating, (b) flow patterns and temperature profiles, (c) methods for calculating heat transfer by convection, (d) investigations on heating of liquids in closed containers for other technological applications.

2.1 Factors affecting the heating rate of convection-heated products

In food technology literature there are some reports about the effect of several internal and external factors on the heat penetration rate. Nearly all these investigations were qualitative and only indicate how the heat penetration rate can be influenced by varying only one single factor. These effects were listed by Blaisdell (1963). The significant part of his list is given in Table 1. Blaisdell distinguished between effects on an f factor and a j factor. These f and j factors are defined as: f = time required to reduce the difference between retort temperature and the temperature at a given point in the product to one-tenth of its initial value at some starting time; and j = the lag-factor, that is a measure of the lag in establishing a constant logarithmic heating rate. Fig. 1 shows a typical heat penetration curve from which the significance of the f and j factor can be seen. A more extensive description of these factors can be found in Ball & Olson (1957). The effects on j reported by Blaisdell are sometimes rather confusing and contradictory and it is often difficult to find an acceptable explanation. For a good understanding a proper definition of j is very important since it depends on the

4

dimensionless temperature $\left[\dfrac{T_a - T}{T_a - T_o}\right]$
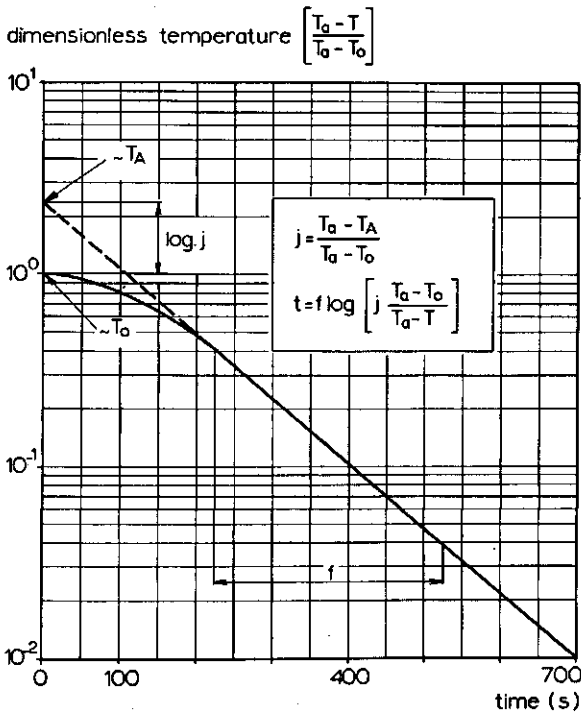
Fig. 1. Illustration of the definition of f and j. T_a = temperature heating medium, T_o = initial temperature of product, T_A = origin asymptote and T = instantaneous product temperature.

Table 1. Effect of change in some variables on convection heating as measured by the characteristic time f (Blaisdell, 1963).

Change in variable	Effect on f
Increase in diameter of container	increase
Increase in height of container	slight increase
Increase in viscosity of product	increase
Increase in T_a at constant $T_a - T_o$	decrease
Increase in temperature difference $T_a - T_o$ at	
constant T_o	decrease
constant T_a	decrease or increase
Glass instead of metal containers	increase
Increase in heat transfer coefficient h_{out}	decrease
Increase in size of solid particles added	
to the liquid contents of a can	decrease

position where j is measured in the container. As the j factor was judged of minor importance for a good understanding of the heat penetration, it is not further treated here.

We now return to the f factor, and its dependence on some parameters as listed in Table 1. These dependencies will be treated briefly and it will be seen that the

explanation of the effects is often rather trivial. To make the effect of the different parameters intelligible the approximation of Schultz & Olson (1938) is often followed. They postulated that the temperature can be considered to be uniform throughout the container at any instant. Then the heating can be described by the following ordinary differential equation:

$$V_c \rho c_p \frac{dT}{dt} = U A_c (T_a - T) \tag{1}$$

If ρ, c_p and the overall heat transfer coefficient U are assumed to be constant throughout the heating process, this results in:

$$\frac{T_a - T}{T_a - T_0} = \exp\left(-\frac{U A_c t}{V_c \rho c_p}\right) \tag{2}$$

Now we see at once that:

$$f = 2.303 \frac{V_c \rho c_p}{U A_c} \tag{3}$$

We will now discuss the influence of the parameters indicated in Table 1.

2.1.1 Container dimensions

Bigelow et al. (1920) and Magoon & Culpepper (1921) already reported that if the size of the container is increased, heating time also increases. Nicholas & Pflug (1961), Schmidt & Pflug (1966) and Blaisdell (1963) have tried to quantify this phenomenon. As the governing criterion they considered the ratio between heated surface and product volume $= A_c / V_c$. From Eqn (3) it is not surprising that they unanimously report an f value proportional to V_c / A_c. Schultz & Olson (1938) stated that if f has been determined for one container size, f can be calculated with Eqn (3) for any other container size, provided that U has the same value for the same product in containers of different size. If A_c is interpreted as the total container surface and the containers are cylindrical we obtain:

$$f_2 = f_1 \cdot \frac{D_2 L_2}{D_2 + 2L_2} \cdot \frac{D_1 + 2L_1}{D_1 L_1} \tag{4}$$

The ratio $DL/(D+2L)$ is the so-called 'can factor'. Schultz & Olson listed can factors for current container sizes. Ball & Olson (1957) called the product

$$\frac{D_2 L_2}{D_2 + 2L_2} \cdot \frac{D_1 + 2L_1}{D_1 L_1}$$

conversion factor for convection heating and listed some conversion factors for current container sizes. Blaisdell (1963) assumed, as is usually done, that the heat transfer through the top cover is negligible. Then

$$\frac{A_c}{V_c} = \frac{D + 4L}{DL} = \frac{1}{L} + \frac{4}{D} \tag{5}$$

If a certain product is heated in a container with a large instead of a small

6

diameter, with the same height L, then A_c/V_c is reduced and consequently f increases. Here Blaisdell assumed the overall heat transfer coefficient equal for both containers. If, on the other hand, the same product is heated in a container with a large instead of a small height, with the same diameter D, A_c/V_c is also reduced. Then Blaisdell stated that the inside heat transfer coefficient h_{in} from container wall to liquid is determined by the relation:

$$Nu = c(Gr\,Pr)^{\frac{1}{4}} \quad \text{or} \quad \frac{h_{in}L}{\lambda} = c\left(\frac{L^3 g\beta\,\Delta T}{\nu^2}\cdot\frac{\nu}{\alpha}\right)^{\frac{1}{4}} \tag{6}$$

in which L is used as characteristic length. Thus h_{in} is proportional to $L^{-\frac{1}{4}}$. According to Blaisdell this combination of factors should cause a slight increase of f.

I think the relation between f and the container size can be simplified as follows. From Eqn (5) it can easily be shown that:

$$\frac{A_c}{V_c} = \left(\frac{\pi}{4V_c}\right)^{\frac{1}{3}}\left\{\left(\frac{D}{L}\right)^{\frac{2}{3}} + 4\left(\frac{L}{D}\right)^{\frac{1}{3}}\right\} \tag{7}$$

Since for current food containers L and D are of the same magnitude, it can be concluded, that for convection heating of the same product in different sized containers f is approximately proportional to $(V_c)^{\frac{1}{3}}$:

$$f \propto (V_c)^{\frac{1}{3}} \tag{8}$$

It can be noted that $(V_c)^{\frac{1}{3}}$ is a linear measure associated with a container of volume V_c. In view of the approximate relation of Eqn (8) it is not surprising that Nicholas & Pflug (1961) and Schmidt & Pflug (1966) found a poor correlation when they assumed $f \propto V_c$.

Another approach for comparing heating rates in different sized containers is that of Charm (1963). His derivation is based on the assumption of similarity of natural convection in containers of different size. However, I think his method is of little practical value, as he introduced so many restrictive similarity assumptions.

2.1.2 Viscosity

With an increasing kinematic viscosity of the product the intensity of the convection decreases and the heating rate will be reduced. Examples are given by Bigelow et al. (1920), Ball & Olson (1957), Hersom & Hulland (1969) and Blaisdell (1963), e.g. for sucrose solutions and starch solutions. Pflug et al. (1965) found the same effect in heating cucumber pickles in sucrose solutions of 30 % and 50 %.

2.1.3 Temperature

Blaisdell (1963) applied three sets of temperature conditions, see Table 1. The first, a higher T_a with a constant $\Delta T_0 = (T_a - T_0)$, means that in the Grashof numbers for the different situations, ΔT_0 is equal. However, the kinematic

7

viscosity is temperature dependent and usually decreases with increasing temperature. During heating the kinematic viscosity decreases to some extent. If T_a is higher, as stated here, the effective viscosity based on this extent, will be smaller. The result will be a higher $Gr\,Pr$ product. In the natural convection equation (6) this means a higher h_{in}. According to Eqn (3) f should then decrease.

With the second set of conditions (a larger ΔT_0 at the same T_0, thus a higher T_a) the $Gr\,Pr$ product increases due to the larger ΔT_0 and the reduced effective kinematic viscosity. This means again a higher h_{in} and, consequently, a smaller f. The third situation, a larger ΔT_0 at the same T_a, is somewhat more complicated. In the $Gr\,Pr$ product ΔT_0 is increased, but the effective kinematic viscosity also increases. The ultimate influence on h_{in} and f depends on which of these factors dominates. Examples confirming the above are presented by Magoon & Culpepper (1921), Blaisdell (1963), Nicholas & Pflug (1961) and Schmidt & Pflug (1966).

2.1.4 *Heating medium and container wall*

In the old literature some investigations are reported in which heating rates were compared for heating cans and jars in water and in condensing steam. Bigelow et al. (1920) and Townsend et al. (1949) reported no difference in heating rates. Bigelow explained this result by arguing that, during heating in condensing steam, at the outside of the container a film of water (condensate) exists. The transfer of heat to the container would therefore be controlled by this film of water and thus the thermal resistance would be equal to that of massive water flow. This explanation is not correct.

For a better understanding we must distinguish between conduction heating and convection heating. For conduction heating the heat transfer to the product is governed by the relation:

$$\frac{\Delta T}{\Delta T_0} = \frac{T_a - T}{T_a - T_0} = f(Fo, Bi) \qquad (9)$$

in which the Biot number is defined as:

$$Bi = \frac{U \cdot \frac{1}{2}D}{\lambda} \qquad (10)$$

The overall heat transfer coefficient U is composed as:

$$\frac{1}{U} = \frac{1}{h_{out}} + \frac{d_w}{\lambda_w} \qquad (11)$$

From heat conduction theory (see e.g. Carslaw & Jaeger, 1959) we know that for large values of Bi the temperature is practically dependent on Fo only. Kopelman & Mizrahi (1972) state that if $Bi > 50$ the Biot number in Eqn (9) has no influence. A container radius $\frac{1}{2}D = 0.1\,m$ and $\lambda = 0.6\,W/m \cdot K$ results in $U > 300\,W/m^2 \cdot K$. For metal containers the wall resistance can be neglected. Thus, if the Biot number has no influence, $h_{out} > 300\,W/m^2 \cdot K$ must hold for metal containers. For glass jars with $(\lambda_w/d_w) \approx 600\,W/m^2 \cdot K$, $h_{out} > 600\,W/m^2 \cdot K$ for a non-limiting Biot number. Thorne & Jowitt (1972) calculated that for metal

8

containers with a radius $\frac{1}{2}D = 0.034$ m, if $h_{out} > 560$ W/m² · K the outside heat transfer coefficient had very little effect on the rate of heating. For their container dimensions this corresponds with $Bi > 15$. When heating in water or condensing steam these values for the outside heat transfer coefficient are easily reached. If heated in air at low velocities the outside thermal resistance could be limiting.

For convection heating the heat transfer is governed by the overall heat transfer coefficient U, here composed as:

$$\frac{1}{U} = \frac{1}{h_{out}} + \frac{d_w}{\lambda_w} + \frac{1}{h_{in}} \tag{12}$$

For metal containers $(\lambda_w/d_w) \approx 50000$ W/m² · K, while for glass and plastic containers (λ_w/d_w) is about 600 to 1000 W/m² · K. The value of h_{out} ranges from about 100 W/m² · K for air heating to about 12000 W/m² · K for condensing steam. The value for h_{in} can attain a value of about 1000 W/m² · K for low viscous products and decreases to about 30 W/m² · K for very viscous products.

For very viscous products the total thermal resistance $1/U$ will be determined by h_{in} only. For low viscous products the heat resistance of the wall of metal containers may be neglected. For glass and plastic containers the heat resistance of the wall cannot always be neglected; there U may be influenced by the wall. For condensing steam h_{out} is so large that its influence on U may be omitted, for other heating media like hot water and air this is commonly not allowed.

As could be expected from the foregoing, Merrill (1948) found different heating rates for metal containers, filled either with water or 1 % bentonite suspensions, being heated either in water or condensing steam. Pflug & Nicholas (1961a) found only small differences for glass jars containing water that were heated with condensing steam, in a water bath or with a water spray. Here the heat resistance of the glass wall predominates. They found steam-air mixtures to be considerably less effective. This is due to the small h_{out} caused by the high amount of air present and the weak convection in the steam-air mixture. Here h_{out} becomes limiting.

Hence we can conclude that for convection heating of low-viscous products, the heat transfer at the outside of the container and the heat resistance of the wall itself can become limiting. So for convection heating, metal containers are preferable and heating with condensing steam is more effective than heating with water or steam-air mixtures.

2.1.5 Presence of solid particles

For solid objects immersed in a liquid, heat is transferred by a combination of convection and conduction. According to Ball & Olson (1957) the ratio between conduction and convection in such products depends on: (a) the size and the shape of the solid objects, (b) arrangement of the solid elements and (c) viscosity of the liquid portion. This can be understood from the following. A large particle needs more time than a small one for a certain increase of temperature in its centre because heat is transferred in the solid by conduction alone. Size and shape of the objects have a direct influence on the thermal resistance but, as far as they

9

contact each other or the wall, they have also an indirect influence via the heat transmitting interface area. The size, shape and arrangement of the solid particles can also affect the flow resistance and therefore the heating rate, see Board (1966) and Pflug & Nicholas (1961b).

Blaisdell (1963) qualitatively analysed the influence of solid particles on the f value of the liquid portion in the container contents. The f value should be reduced by addition of solid particles because: (a) the ratio A_c/V_c, applied to the liquid part in the container increases, (b) the heat transfer rate between liquid and solid particles is smaller than between wall and liquid, since the liquid velocity in the core is smaller than in the boundary layer flow at the wall, and (c) the heat transfer by conduction in the solid usually proceeds much more slowly than by convection in the liquid. The facts (b) and (c) cause an accumulation of heat in the liquid. If small particles are added instead of large ones, while the total solid contents is kept the same, f of the liquid part will increase. The reason is that more heat can be transmitted to the solid particles, as the area of interface between liquid and solid is larger. Furthermore the increase of flow resistance would slightly decrease the heat transmission from wall to liquid and from liquid to solid particles.

More quantitative studies of the influence of solid particles on heat transfer rate are scarce. Schmidt & Pflug (1966) only did some work on heating water with glass marbles in glass jars. They used marbles of 9.5, 12.7 and 19.1 mm ($\frac{3}{8}$, $\frac{1}{2}$ and $\frac{3}{4}$ inch) diameter. They observed faster heating of the liquid part in comparison with jars filled with water only. This agrees with the above, as quoted from Blaisdell. They found no significant differences in f of the liquid part for the different marble sizes. This could be due to too small a variation in marble size.

As was reported by Nicholas et al. (1960a), Kitson (1962) and Mulvaney et al. (1960) a complication arises if fruits packed in syrup are processed. When we have fruit pieces in a syrup, common convection heating of the liquid part would be expected. However, water is extracted from the fruit pieces due to the high osmotic pressure of the syrup. The water leaving the product does not diffuse uniformly into the syrup throughout the container but instead rises to the top thereby producing a density gradient. This stratification begins as soon as the syrup is added to the product and is increased by heating. The product-induced stratification hampers the temperature-driven convection. This phenomenon was also investigated in a model system of water and sucrose solutions by Nicholas et al. (1960b). The water layer was on top of the sucrose solution. During heating it appeared that the convection currents did not cross the boundary between water and sucrose solution. Nicholas et al. (1960a) derived a formula to describe the theoretical conditions of syrup density and temperature gradients necessary to allow or prevent convection heating in a stratified syrup. For example, a difference of 7 % in sucrose concentration between two points in a container is sufficient to prohibit convection between these points even if the more dense syrup is 60° C higher in temperature.

2.2 Flow patterns and temperature profiles

A better insight in the mechanism of convection heating in liquid-filled containers is obtained by studying temperature profiles and flow patterns. These phenomena have been studied by several investigators. Jackson & Olson (1940) studied the temperature distribution in a 1 %-bentonite suspension heated in a can. They measured temperatures with thermocouples that were fixed along the vertical axis and in a horizontal plane through the geometric centre of the can. Along the vertical axis the temperature decreased from top to bottom. In the horizontal plane a steep temperature gradient was found at the wall, while in the core the temperature profile was nearly flat with a weak minimum at the centre, see also Ball & Olson (1957). From these temperature profiles, Jackson & Olson described the convection heating process as: a thin layer of hot liquid that ascends along the wall and, upon reaching the top, spreads out over the remaining liquid. The descending flow occurs by a slow downward movement in the rest of the container. Fagerson & Esselen (1950) studied flow patterns and temperature profiles in a 1 %-bentonite suspension in glass jars. With nine thermocouples they determined temperature profiles in three horizontal planes and along the vertical axis. Their temperature profiles, represented in Fig. 2, correspond rather well with those of Jackson & Olson. Flow patterns were visualized by adding methylene blue to water in glass jars. Additionally to the picture of Jackson & Olson they observed an upward flow starting from the centre of the bottom. At jar dimensions of 0.10 m diameter and 0.11 m height, these flows initially travelled to 0.025–0.040 m from the bottom. Later on this height gradually decreased with time until after 5 minutes it was ultimately reduced to about 0.020 m from the bottom. Blaisdell (1963) determined temperature profiles and flow patterns in water and 50 % sucrose solutions. The glass jars were heated in a stirred water
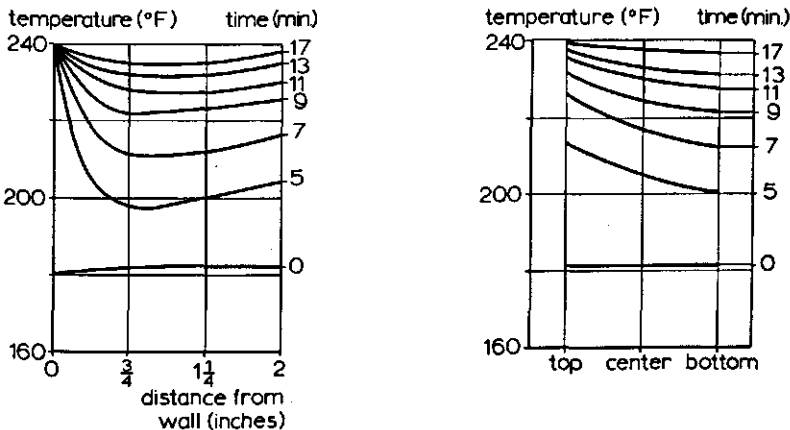

Fig. 2. Temperature profiles in 1%-bentonite suspension in cylindrical glass container at various times. Radial temperature profiles are presented for horizontal plane 73.5 mm from bottom of container (left). Vertical temperature profiles are presented for central axis (right). After Fagerson & Esselen (1950).
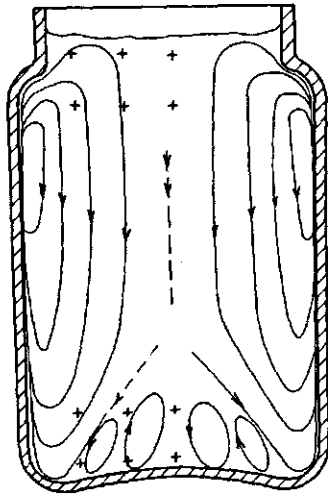
Fig. 3. Flow patterns in water in a glass jar; after Blaisdell (1963). Positions of thermocouples are indicated by +.

bath; with a number of thermocouples he determined temperature profiles along the vertical axis and in several horizontal planes (measuring points are indicated in Fig. 3). The horizontal temperature profiles were reported to be nearly flat, with some slight deviations just below the liquid surface where a 'cold ring' was found and just above the bottom where the existence of a 'hot ring' was reported. Blaisdell studied flow patterns by dye injection at different locations. From these dye injections and from the measured temperatures he constructed the flow patterns of Fig. 3. He reported eddies rising initially to 40 % of the liquid height, later on this height decreased to 20 %. An explanation of this latter phenomenon was not given. In the lower part of the jar fluctuations in the continuously measured temperatures occurred due to these eddies. These fluctuations decreased with time except at locations close to the bottom. Blaisdell postulated a cold point on the central axis where the eddies and the downward core flow meet (see Fig. 3). This cold point shifted downwards with time. A flow pattern similar to that of Blaisdell was earlier reported by Tani (1940). Tani studied flow patterns of water heated in rectangular glass containers, by adding aluminium powder. Recently Jowitt & Mynott (1974) reported a study of flow patterns in water contained in a cubical chamber heated by steam at the base and two vertical sides, while glass ends permitted observation of convection currents. The flow patterns were rendered visible by the addition of powdered carbon. Their diagrams also show flow patterns similar to those reported by Blaisdell (1963). Rao & Prabhu (1971) described temperature profiles during processing of canned prawns. They established a cold point on the central axis 10–13 mm above the bottom. Reichert & Bielig (1973) determined temperature profiles in canned potatoes (diameter 10–30 mm) in a 2 %-brine. Fig. 4 shows the temperature profiles found by these authors. From these profiles they concluded that a cold area exists, corresponding to a ring of 20 mm diameter, 11 mm above the bottom of the container. The explanation of Reichert & Bielig for this phenomenon is that the 'heat' ascends in the wall region of the container and along the central axis to the top and descends

12
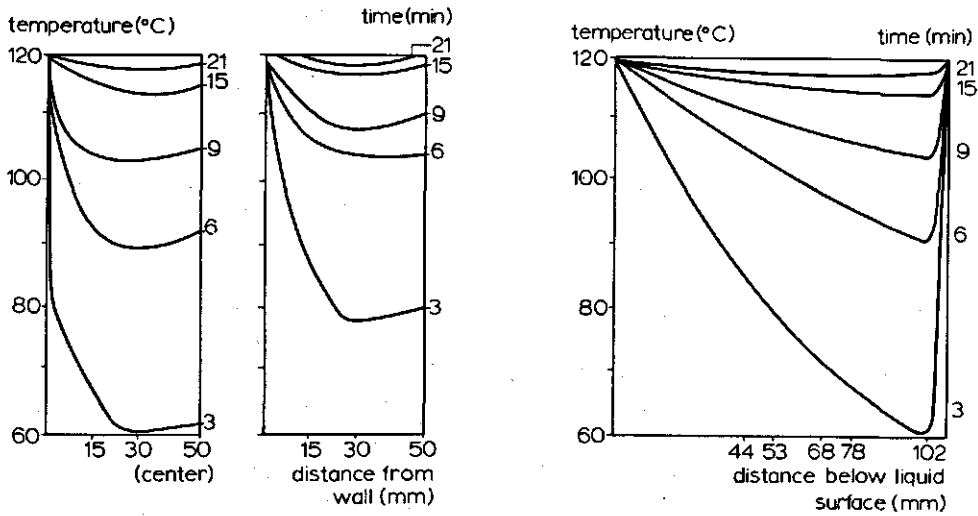
Fig. 4. Temperature profiles in canned potatoes; after Reichert & Bielig (1973). Radial temperature profiles are presented for the horizontal plane at 11 mm from bottom and the horizontal plane at the geometric centre (left). Axial temperature profiles are presented for the central axis (right).

in a cylinder with a radius of about 20 mm. This picture seems unrealistic in relation to the investigations discussed above.

From the studies of Fagerson & Esselen (1950), Blaisdell (1963) and Reichert & Bielig (1973), it could be concluded that the slowest heating point is not fixed on the vertical axis as usually presumed: see for example Townsend et al. (1949). According to the above mentioned authors, it should be located somewhere between axis and container wall (see Fig. 2 and 4). This phenomenon was also established by Fagerson et al. (1951) in convection-heated products like diced carrots, cut green beans and apple juice. The magnitude of the differences was less than in 1 %-bentonite suspension and was nearly absent in apple juice. The influence of the off-centre cold point on the sterilizing value was of minor importance.

Since the reported temperature differences in the horizontal plane are at most some degrees Kelvin and the horizontal temperature profiles of Fagerson & Esselen (1950) and Reichert & Bielig (1973) are only based on three measuring points in a horizontal plane, I think the accuracy of the measured temperature profiles is highly overestimated. Further it must be noted that in the interesting region bottom eddies do occur, which causes considerable temperature fluctuations. It is also somewhat surprising that Fagerson & Esselen (1950) reported an off-centre cold point for a 1 %-bentonite suspension while Jackson & Olson (1940) did not. I think the question of an off-centre cold point is of minor importance.

13

2.3 Methods for calculating convection heating of liquids in containers

So far the influence of some factors on convection heating was described qualitatively. In this section we will discuss possible methods to calculate heating rates for convection heating of liquids in containers. In literature some models have been proposed. However, most of the models are qualitative. Only Stevens (1972) developed a more detailed mathematical model, that will be dealt with in Section 2.3.4.

2.3.1 Effective-diffusivity model

In this model it is assumed that convection heating of a liquid in a container can be described by the heat diffusion equation in the same way as conduction heating. Then an effective thermal diffusivity is introduced which is the sum of thermal and eddy diffusivity. Thompson (1919) first used this effective-diffusivity approach. He stated that the convection currents only have a local nature and conduction heating theory could be applied to the container as a whole. Thompson determined an effective thermal diffusivity for some products (vegetables in brine). Riedel (1947), and more recently Thorne & Jowitt (1972) also applied this model. Thorne & Jowitt determined an effective thermal diffusivity for tomato soup and peas in brine. They used a plated brass tube with end pieces of perspex and a thermocouple mounted at its geometric centre. This tube was filled with the food-stuff and immersed in a water bath. The temperature of the bath was increased at a constant rate. From the ultimate constant temperature difference between water bath and geometric centre an effective thermal diffusivity was derived. These values were used to compute heating rates for baby-food cans filled with the considered food-stuff. Some discrepancy existed between measured and calculated heating rates, which is probably due to the inadequacy of the effective-diffusivity concept.

From what was said in Section 2.2 it will be obvious that the shape of convection heating profiles does not correspond at all with those for conduction heating. It is impossible to match the actual profiles with theory by adjusting the diffusivity. To match the calculated conduction heating profiles with the measured convection heating profiles, Tani (1940) had to assume an effective diffusivity dependent on the height in the container. I think there is no sound theoretical argument for doing so and in fact it is conceptually wrong to try and account for convective flow effects which are mainly in a vertical direction by changing thermal diffusivity in an axial direction. Because of the vertical direction of the flow one would have expected an effective thermal diffusivity in the vertical direction larger than in the horizontal direction, but not an effective thermal diffusivity dependent on height. Obviously the effective-diffusivity model is inadequate for calculation of the heating rate in convection heating. The difficulty is shifted to the determination of the effective thermal diffusivity, which has neither a well defined value nor a physical meaning because it depends on the intensity of the convection currents. Moreover the effective thermal diffusivity derived from an experiment can only be used to predict heating rates if similarity exists

14

between test apparatus and the can. The most practical method to achieve this is to heat a can with a thermocouple mounted in it under conditions that are as identical as possible with the operational conditions in the factory.

2.3.2 Uniform-temperature model

If one assumes that the entire heat resistance is located at the wall and the temperature is uniform throughout the container the heating can be described at any moment in time with Eqn (1). This model was used by Jones (1931), Schultz & Olson (1938) and Charm (1963). The application of this method requires a value of the heat transfer coefficient: the next section describes methods to obtain such values.

On the basis of the uniform temperature model Wideff et al. (1963) and Bimbenet & Michiels (1974) developed a method to calculate the temperature course of the product, if the temperature course of the heating medium is known. If the temperature of the heating medium, which is assumed to be time dependent, is called $T_{a,t}$ then the heating can be described by the following differential equation:

$$UA_c(T_{a,t} - T) = V_c \rho c_p \frac{dT}{dt} \tag{13}$$

An analytical solution of this differential equation exists for $T_{a,t}$ = constant (see Section 2.1) and if $T_{a,t}$ is linearly developing with time, see Wideff et al. (1963) and Bimbenet & Michiels (1974). Wideff defined a characteristic heating rate:

$$m = \frac{UA_c}{V_c \rho c_p} \tag{14}$$

and schematized the temperature course of the heating medium by distinguishing: (a) a starting period in which the retort temperature rises proportionally with time, (b) a period of constant retort temperature and (c) a cooling period in which the retort temperature falls proportionally with time. If for each period the value of m is known, the temperature course of the product can be calculated from the solution of Eqn (13) for each period. Bimbenet & Michiels (1974) defined a duration of a transfer unit (DTU), which is $1/m$. They extended the method proposed by Wideff to an arbitrary temperature course of the heating medium, by solving Eqn (13) numerically. If the value of DTU and the temperature course $T_{a,t}$ are known, Eqn (13) can be written in finite difference form and then heating can be simulated by choosing an appropriate time increment.

2.3.3 Dimensional analysis

For natural convection heating of liquids (with $Pr > 1$) in closed containers the heat transfer is governed by relations of the type:

$$Nu = f(Gr \cdot Pr) \tag{15}$$

In Fig. 5 such relations for transient convection heating of liquids in closed

15
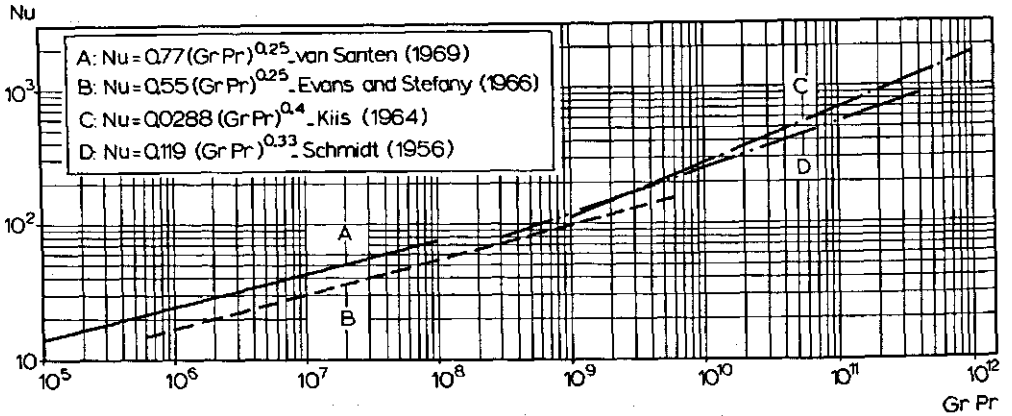
Fig. 5. Dimensionless relations for natural convection heating of liquids in closed containers as reported by different authors. Various liquids are studied, with $5 < Pr < 50000$.

containers, are shown. Evans & Stefany (1966) investigated heating of several liquids ($Pr = 7$–7000) in cans with diameters of 50.8 and 63.5 mm (2 and $2\frac{1}{2}$ inch) and aspect ratios $L/D = 0.75$–2.00. Their relation holds for both horizontally and vertically orientated cylinders. Van Santen (1969) studied several liquids ($Pr = 5$–50000) in two can sizes (0.89 and 0.36 litre), Kiis (1964) studied heating of milk in tins. The exponent of ($Gr\,Pr$) in the relation of Kiis deviates from what was usual up to that moment. However, in the review of Ede (1967) several authors are cited, who report an exponent between 0.33 and 0.5 for turbulent natural convection. Schmidt (1956) investigated heating of liquids ($Pr = 1$–100) in spherical containers with diameters of 100 and 500 mm.

Okada (1940), referred to in the review of Olson (1947), related the temperature at a certain time and location directly with factors obtained from a dimensional analysis. This results in:

$$\frac{T_a - T}{T_a - T_0} = f\left(\frac{x}{l}, \frac{y}{l}, \frac{z}{l}, \frac{\alpha t}{l^2}, Bi, Gr, Pr\right) \tag{16}$$

where x, y and z are coordinates of the point under consideration and l is a representative dimension of the container. As far as I know this proposal of Okada was not worked out by other authors. Of course it must be simplified to make it workable. For example the considerations must be restricted to a single point, say the geometric centre, then x/l, y/l and z/l can be dropped.

2.3.4 Mathematical model of Stevens

In the thesis of Stevens (1972) the thermal processing of liquid foods was modelled mathematically. The equations for momentum, energy and mass transport were written in non-dimensional form with the Grashof and Prandtl numbers as parameters. By evaluating the boundary conditions a third parameter, the geometric ratio H/D, was introduced. This system of equations was reduced to a

16

system containing the energy equation, the vorticity equation, the stream function equation, equations defining the velocities in terms of the stream function and the appropriate boundary and initial conditions. This closed set of partial differential equations was solved numerically, resulting in transient velocity and temperature fields. In his calculations Stevens used the temperatures he found experimentally, for thermal boundary conditions. Stevens verified his numerical results for ethylene glycol, by comparing numerically and experimentally obtained temperatures at three different heights in the liquid. The agreement between calculated and experimental temperatures was rather poor but at its best at very short times after initiation of heating. Stevens presumed that both experimental errors and computer limitations contributed to the poor agreement and that this can be overcome by larger computers.

I think Stevens' method has some shortcomings which were not recognized by Stevens. First he used experimentally determined wall temperatures for his boundary conditions. However, on evaluating his experiments, Stevens concluded that, due to incorrect thermocouple arrangement, his temperature measurements were erratic. Furthermore, I think, as he obviously did not study streamline patterns obtained either numerically or experimentally, he had too little insight in the heating process for a correct judgement of his numerical model. By only measuring temperatures at three selected heights in the liquid he did not recognize eddies rising from the bottom. As will be shown in Chapter 3 his numerical model does not account for convective heat transfer from the bottom of the container and thus is inadequate at boundary conditions which include bottom heating.

2.4 Similar problems in other fields of technology

There are of course many other fields of technology where natural convection heating of liquids in enclosed spaces is important. Some examples are:
1. In missiles stratification occurs in tanks with cryogenic propellants due to frictional heating. The stratification affects the rate of fluid vapourization and hence fuel supply rate to the propelling rocket engines, as well as the vessel design pressure (Bailey & Fearn, 1963). Such problems are also encountered in storage of liquid natural gas (LNG) and other cryogenic liquids. In LNG storage one encounters the so-called 'roll-over' problem. Then the contents of a storage tank develop an unstable stratification during filling or by convection heating, which leads to a sudden vigorous rolling over of the less dense layers to the top of the tank contents. This causes a sudden increase in pressure and a considerable boil-off, see Sarsten (1972).
2. Natural convection in cavities of which the opposite walls have different temperatures. In this situation heat is transferred from a hot to a cold wall. Sometimes the walls are flat (e.g. double-glazed windows), sometimes arranged as concentric cylinders (e.g. the annular fluid-filled cavity around a nuclear reactor core). Studies in this field were reviewed by Ostrach (1972).
3. Thermosiphons. The most common industrial thermosiphon applications include gas turbine blade cooling, nuclear reactor cooling and cooling systems for

internal combustion engines. A review on this subject was recently given by Japikse (1973).

In Examples 2 and 3 a steady state is reached. Heating of liquids in food containers, on the contrary, is a transient process by nature and therefore corresponds best with Example 1. In this section some studies on stratification in vessels with cryogenic liquids and model systems derived from it will be discussed.

If stratification occurs in a vessel with a cryogenic liquid it is important to know the liquid surface temperature. This temperature determines the vapour pressure in the head space of the vessel and consequently is important for the design of the vessel and for estimates of losses by excessive boil-off from the vessel. Several investigators have studied this and developed more or less empirical methods for calculating stratification. Often, however, the boundary conditions defining the problem, are quite different from those I applied. My study was concerned with a container partly filled with a liquid, heated on all sides, at a uniform temperature. Most of the studies however, consider only sidewall heating with a uniform heat flux, see for example Ruder (1964) and Bailey & Fearn (1963). Tatom et al. (1963) and Tatom & Carlson (1966) investigated stratification of liquid hydrogen and water in large vessels (1 to 3 m^3) under turbulent conditions. The H/D ratio ranged from 1 to 4.8 and the ratio of bottom to sidewall heat flux from 0 to 9.4. They found a stratified region in the upper part of the vessel with a region of uniform temperature below it. Schwind & Vliet (1964) extensively studied flow patterns and temperature profiles for heating of water in rectangular prismatic containers. The sidewall and the bottom could be heated separately with a constant heat flux. The experiments were in the range of $10^{11} < Gr\,Pr < 10^{14}$, thus turbulent conditions were to be expected. For flow visualization they used a
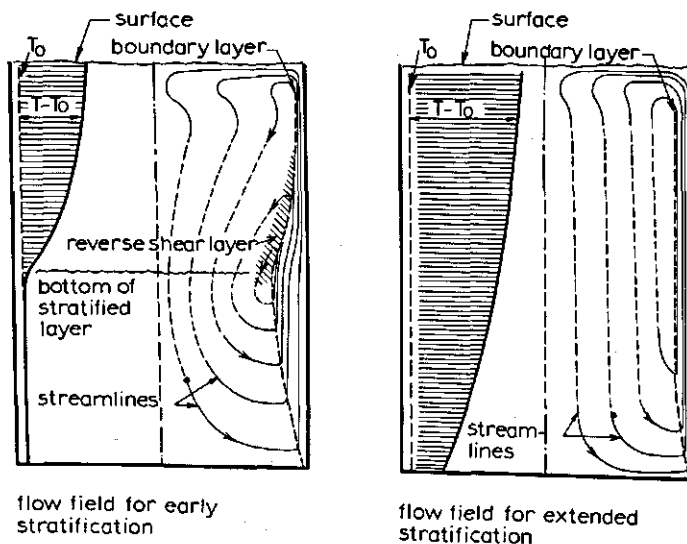

Fig. 6. Flow patterns and temperature profiles for heating water in a closed container with sidewall heating only; after Schwind & Vliet (1964). The axial temperature profile is projected on the left side of the flow field.

18

particle-streak method and the schlieren technique. Stream-line patterns at two times, for sidewall heating only are given in Fig. 6. The first indication of convection is observed about 5 to 15 s after start of heating at the liquid surface where the boundary layer liquid flows from the corners out across the surface. These shear layers meet at the centre of the tank and gradually spread to form a uniform stratified layer. Because of the continuous flow from the boundary layer into the top of the core, a downward flow of the stratified layer develops. Liquid flowing upwards in the boundary layer loses part of its buoyancy when it passes the lower end of the stratified layer and encounters liquid of increasing temperature at the outer edge of the boundary layer. Thus a part of the boundary layer liquid leaves the boundary layer and moves downwards and inwards. This liquid is indicated in Fig. 6 as a reverse shear layer. From the moment that the stratified layer reaches the bottom there is hardly any interaction between the stratified layer and the boundary layer. As a result no reverse shear layer will appear. The temperature profiles measured by Schwind & Vliet for simultaneous bottom and sidewall heating are similar to those measured by Pollard and Carlson (1969) as given in Fig. 7. Pollard & Carlson investigated the effect of horizontal baffles on stratification. These baffles appeared to reduce stratification considerably. In addition these authors determined temperature profiles for simultaneous bottom and sidewall heating without baffles (see Fig. 7).

Interesting analytical studies of exclusively sidewall heating are reported by Barakat & Clark (1966), Evans et al. (1968) and Matulevicius (1970). Barakat & Clark (1966) obtained a numerical solution of the momentum and energy equations for laminar flow. From this solution isotherms and streamlines in a cylindrical container could be constructed. In Fig. 8 their results are given at two different times. The experimental part of the investigation of Barakat & Clark was concerned with a water-filled cylinder of which the sidewall was electrically
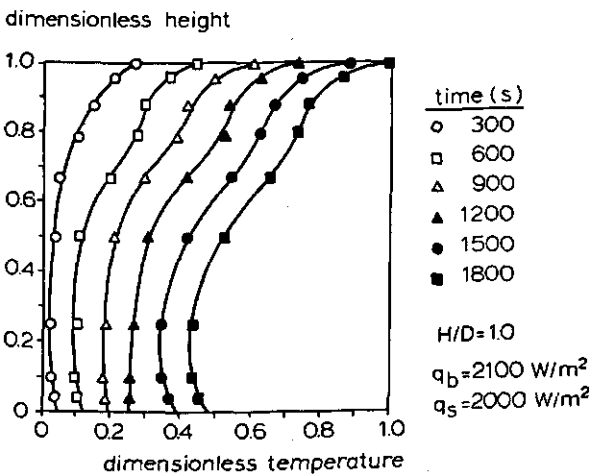
Fig. 7. Non-dimensional liquid temperature versus non-dimensional container height for simultaneous bottom and sidewall heating, q_b and q_s respectively. After Pollard & Carlson (1969).

19
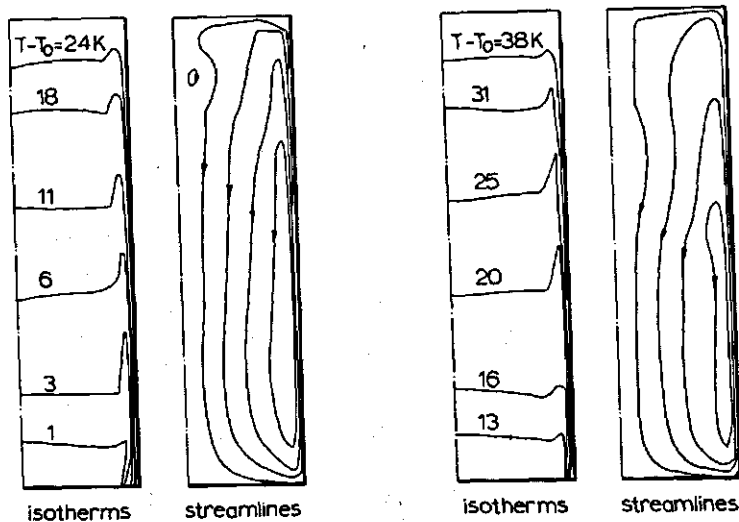
Fig. 8. Results of numerical solution of Barakat & Clark (1966) for heating water in a cylindrical container with sidewall heating only. Isotherms and streamline patterns are presented for two times.

heated. A good agreement between measured temperatures and calculated ones was reported. In fact the mathematical model of Stevens (1972), see Section 2.3.4, was similar to that of Barakat & Clark. The numerical solution of Barakat & Clark will be discussed in more detail in Section 3.2.

Evans et al. (1968) and Matulevicius (1970) developed a computation model for stratification, based on observations of flow patterns, which in fact were very similar to those reported by Schwind & Vliet (1964). By analysing the natural convection boundary layer flow at the wall, the velocity in the core and the core stratification could be calculated. Evans et al. (1968) and also Matulevicius (1970) performed experiments in a perspex cylinder (diameter 20 cm, height 60 cm) containing water and glycerol solutions. The sidewall was electrically heated, while the bottom was insulated. The authors reported a good agreement between the results of their model and the experiments. Finally Evans et al. (1971) investigated the effect of a non-uniform sidewall heat flux on the thermal stratification phenomena. They found that stratification might be reduced by non-uniform heating.

2.5 Conclusions

From the literature reviewed in this chapter it can be concluded that:
1. In food technology literature considerable attention has been paid to convection-heated products and especially to factors affecting the rate of heating. However, most of this work was only qualitative by nature and where it is quantitative, too simple and unrealistic physical models have been used.
2. The understanding of the mechanism of natural convection heating is incomplete, because; (a) the interaction between flow patterns and temperature profiles

20

has been *insufficiently analysed*, (b) *the flow pattern is mostly described as a steady state, while the heating process is transient*, (c) the study of flow patterns has been restricted to non-viscous products like water, and (d) mostly flow visualization studies were performed under not representative conditions, e.g. glass jars heated in a water bath with small temperature differences.

3. The storage of cryogenic fluids has been studied extensively. Although most of these studies have been concerned with boundary conditions different from those I applied, I feel the results of these basic studies are very valuable for food technology applications.

For a better understanding of the mechanism of heat transfer to convection-heated products and to be able to predict heating rates, I aimed at the following:

1. An experimental study of: (a) flow patterns and temperature profiles under actual sterilization conditions, that is in metal containers with condensing steam as the heating medium, for a wide range of viscosities, (b) interaction between flow patterns and temperature profiles, and (c) development of flow patterns and temperature profiles in time.

2. Adaption to the conditions of my study to one of the mathematical methods as used to compute stratification in cryogenic storage tanks.

3. The development of a more practicable, direct calculating model of the effectiveness of heat sterilization, based on the observed phenomena.

3 Theory

In this chapter the possible ways to describe mathematically the heating of a liquid in a closed container will be reviewed. The differential equations governing natural convection heating of a liquid in a container can easily be written out. But, an analytical solution of these equations is extremely difficult without drastic simplifications. To avoid simplifying the equations too much, numerical methods to solve the equations are of considerable help. Barakat & Clark (1966) used these and obtained a numerical solution of the complete momentum and energy equations for laminar flow.

The study of this problem can be simplified by applying the boundary layer theory. For this purpose the system is schematized by dividing it in a boundary layer flow upwards at the container wall and a liquid core which slowly flows downwards. Due to the heating process the core becomes stratified while this stratification in turn influences the boundary layer flow. A considerable amount of work, both analytical and experimental, has been done on natural convection boundary layers at walls in environments of uniform temperature. A review of this work was given by Ede (1967). However, the present case, natural convection in a thermally stratified environment is more complicated and has been less extensively studied. Fortunately the last few years some studies on this special situation were published by Cheesewright (1967), Eichhorn (1969), Yang et al. (1972), Piau (1974) and Fujii (1974). Evans et al. (1968) and Matulevicius (1970) developed a stratification model in which the boundary layer solutions for a thermally stratified environment were combined with the downward core flow. With this model temperature distributions in the liquid can be predicted.

For a mathematical treatment of the problem I chose a numerical method corresponding with that of Barakat & Clark (1966), but adapted it to my actual boundary conditions. At the end of this chapter results provided by this numerical method will be discussed.

3.1 The differential equations

In Fig. 9 the container configuration and coordinate system are presented. A cylindrical container with diameter D, is partially filled with a liquid to a height H. Initially the liquid has a uniform temperature T_0 and is at rest. At time $t = 0$ the sidewall and bottom temperature is suddenly raised to a value T_w. The following assumptions are made: (a) the thermal conductivity, viscosity and heat capacity are independent of temperature, (b) density variations are negligible except in the buoyancy effect, (c) the liquid is newtonian and the flow is laminar, (d) compressi-

22
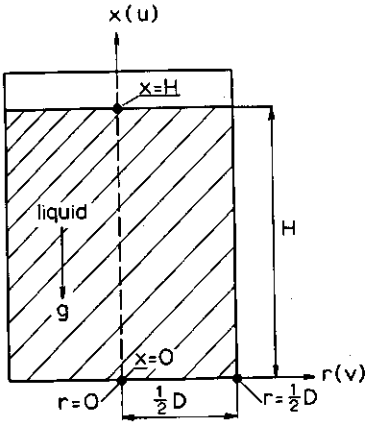
Fig. 9. Container configuration and coordinate system.

bility and viscous dissipation are negligible, and (e) cylinder symmetry holds. With these assumptions and with the assumption that the density can be approximated by

$$\frac{\rho_0}{\rho} = 1 + \beta(T - T_0) \tag{17}$$

the governing equations can be stated as follows (see Bird et al., 1960):
Energy equation:

$$\frac{\partial T}{\partial t} + u\frac{\partial T}{\partial x} + v\frac{\partial T}{\partial r} = \alpha\left(\frac{\partial^2 T}{\partial x^2} + \frac{1}{r}\frac{\partial T}{\partial r} + \frac{\partial^2 T}{\partial r^2}\right) \tag{18}$$

The x component of the equation of motion:

$$\frac{\partial u}{\partial t} + u\frac{\partial u}{\partial x} + v\frac{\partial u}{\partial r} = g\beta(T - T_0) + \nu\left(\frac{\partial^2 u}{\partial x^2} + \frac{1}{r}\frac{\partial u}{\partial r} + \frac{\partial^2 u}{\partial r^2}\right) \tag{19}$$

The r component of the equation of motion:

$$\frac{\partial v}{\partial t} + u\frac{\partial v}{\partial x} + v\frac{\partial v}{\partial r} = \nu\left(\frac{\partial^2 v}{\partial x^2} - \frac{v}{r^2} + \frac{1}{r}\frac{\partial v}{\partial r} + \frac{\partial^2 v}{\partial r^2}\right) \tag{20}$$

Continuity equation:

$$\frac{\partial u}{\partial x} + \frac{\partial v}{\partial r} + \frac{v}{r} = 0 \tag{21}$$

The initial conditions for the system under consideration are:

$$u(x, r, 0) = v(x, r, 0) = 0 \qquad T(x, r, 0) = T_0 \tag{22}$$

Under the assumption of cylinder symmetry, no slip at the wall and zero shear stress at the free surface, the boundary conditions are:

23

$$u(0, r, t) = v(0, r, t) = 0 \qquad T(0, r, t) = T_w \quad \text{(bottom)}$$

$$u(x, \tfrac{1}{2}D, t) = v(x, \tfrac{1}{2}D, t) = 0 \qquad T(x, \tfrac{1}{2}D, t) = T_w \quad \text{(sidewall)}$$

$$u(H, r, t) = \frac{\partial v}{\partial x}(H, r, t) = 0 \qquad \frac{\partial T}{\partial x}(H, r, t) = 0 \quad \text{(liquid surface)}$$

$$\frac{\partial u}{\partial r}(x, 0, t) = v(x, 0, t) = 0 \qquad \frac{\partial T}{\partial r}(x, 0, t) = 0 \quad \text{(centreline)}$$

$$(23)$$

Starting from these differential equations we obtain the dimensionless parameters, governing the heat transfer, by dimensional analysis (see Jakob, 1958 and Hellums & Churchill, 1961).

$$Nu = f\!\left(\frac{H}{D},\ Gr,\ Pr,\ \tau\right) \tag{24}$$

The Nusselt number, Grashof number and Prandtl number are very familiar in discussions on natural convection heating. The relevance of the aspect ratio H/D is obvious. Finally the process is time dependent by definition, which explains the role of dimensionless time τ.

3.2 Numerical solution of Barakat & Clark

Barakat & Clark (1966) developed numerical solutions of the equations of motion and energy for laminar natural convection in a closed container with sidewall heating only. The differential equations (18) to (21) are reduced to a set of three dimensionless partial differential equations. This is achieved by combining the equations of continuity and motion to obtain a time-dependent vorticity equation and an elliptic type equation relating the stream function and vorticity. The resulting equations are rendered non-dimensional by introducing dimensionless variables (see Appendix A).
Energy equation:

$$\frac{\partial \theta}{\partial \tau} + \frac{1}{R}\frac{\partial \Psi}{\partial R}\cdot\frac{\partial \theta}{\partial X} - \frac{1}{R}\frac{\partial \Psi}{\partial X}\cdot\frac{\partial \theta}{\partial R} = \frac{(\tfrac{1}{2}D)^2}{H^2}\frac{\partial^2 \theta}{\partial X^2} + \frac{1}{R}\frac{\partial \theta}{\partial R} + \frac{\partial^2 \theta}{\partial R^2} \tag{25}$$

Vorticity equation:

$$\frac{\partial \omega}{\partial \tau} + \frac{1}{R}\frac{\partial \Psi}{\partial R}\cdot\frac{\partial \omega}{\partial X} - \frac{1}{R}\frac{\partial \Psi}{\partial X}\cdot\frac{\partial \omega}{\partial R} = Pr\!\left[\frac{1}{R}\frac{\partial \theta}{\partial R} + \frac{(\tfrac{1}{2}D)^2}{H^2}\frac{\partial^2 \omega}{\partial X^2} + \frac{3}{R}\frac{\partial \omega}{\partial R} + \frac{\partial^2 \omega}{\partial R^2}\right] \tag{26}$$

Equation relating stream function and vorticity:

$$\frac{(\tfrac{1}{2}D)^2}{H^2}\frac{\partial^2 \Psi}{\partial X^2} - \frac{1}{R}\frac{\partial \Psi}{\partial R} + \frac{\partial^2 \Psi}{\partial R^2} = \omega R^2 \tag{27}$$

This set of equations is solved numerically by a finite-difference technique. Barakat & Clark assumed the sidewall temperature to be an arbitrary function of location and time, while heat transfer through the bottom was considered to be negligible. This is in contrast to the present situation where a constant and uniform bottom and sidewall temperature is assumed.

24

Besides the appropriate dimensionless temperature and velocity boundary conditions, Barakat & Clark defined additional boundary conditions for the stream function and vorticity.

Stream function boundary conditions:

$$\Psi(0, R, \tau) = 0 \qquad \frac{\partial \Psi}{\partial X}(0, R, \tau) = 0 \quad \text{(bottom)}$$

$$\Psi(X, 1, \tau) = 0 \qquad \frac{\partial \Psi}{\partial R}(X, 1, \tau) = 0 \quad \text{(sidewall)} \tag{28}$$

$$\Psi(1, R, \tau) = 0 \qquad \frac{\partial^2 \Psi}{\partial X^2}(1, R, \tau) = 0 \quad \text{(liquid surface)}$$

$$\Psi(X, 0, \tau) = 0 \qquad \frac{\partial}{\partial R}\left[\frac{1}{R}\frac{\partial \Psi}{\partial R}(X, 0, \tau)\right] = 0 \quad \text{(centreline)}$$

Vorticity boundary conditions:

$$\omega(1, R, \tau) = 0 \qquad \text{(liquid surface)} \tag{29}$$

$$\omega(X, 0, \tau) = 0 \qquad \text{(centreline)}$$

To solve the vorticity equation (26), additional boundary conditions at the sidewall and the bottom are required. Explicit expressions for the vorticity boundary conditions at these locations are difficult to obtain. In the method of Barakat & Clark this difficulty was solved.

The initial conditions are:

$$U(X, R, 0) = V(X, R, 0) = \Psi(X, R, 0) = \omega(X, R, 0) = \theta(X, R, 0) = 0 \tag{30}$$

The application of the method of finite differences results in values of θ, Ψ and ω for the grid points at each time step. Between these values of θ, Ψ and ω, isotherms and streamlines can be interpolated. An example of the results of Barakat & Clark for heating water in a container with sidewall heating is given in Fig. 8. In this figure streamlines and isotherms are given for two different times. In the bulk of the liquid the isotherms are nearly flat. This conclusion corresponds with observations of Evans et al. (1968) and Haug et al. (1968). The streamline pattern shows that the heated liquid rises in the vicinity of the wall and upon approaching the liquid surface gradually changes its direction to downward flow. Obviously part of the liquid returns downwards before reaching the liquid surface, indicating the presence of a reverse shear layer as reported by Schwind & Vliet (1964). Another surprising feature is the temperature reversal in the vicinity of the wall. Near the wall the temperature gradient points to the wall but at some distance from the wall it points into the bulk. In the bulk the radial temperature gradient vanishes. This phenomenon was experimentally confirmed by Haug et al. (1968) with a Mach-Zehnder interferometer. The flow and temperature reversal are characteristic for natural convection in non-isothermal surroundings. This will be explained in more detail in Section 3.3.

Barakat & Clark reported an agreement within 10 % between measured and calculated temperatures. They did not verify streamline patterns experimentally, but their calculated velocity field corresponds fairly well with that presented by

25

Schwind & Vliet (1964) and given in Fig. 6. According to Torrance (1968) the appearance of a vortex near the centre line (see Fig. 8) could be caused by an incorrect evaluation of the vorticity at the centre line.

3.3 Natural convection in a thermally stratified fluid

Natural convection at a vertical surface in an isothermal fluid has been studied at length by several investigators and extensively reviewed by Ede (1967). A profound analytical study was made by Ostrach (1953). Ostrach calculated velocity and temperature profiles for a wide range of Prandtl numbers (0.01 to 1000). For $Pr \gg 1$ the hydrodynamic boundary layer is thicker than the thermal boundary layer (see also Soehngen, 1969). The buoyancy force in the boundary layer ranges from a maximum value at the wall to zero at the outer edge of the thermal boundary layer. For $Pr \gg 1$ the fluid elements in the outer region of the hydrodynamic boundary layer, outside the thermal boundary layer, thus experience no buoyancy forces. Nevertheless, these fluid elements are moving upward because the warmer fluid in the thermal boundary layer exerts a drag force.

However, if the bulk fluid is stratified a different situation arises. This situation is shown qualitatively in Fig. 10, which illustrates temperature and velocity profiles at a location x_1, from the leading edge. The bulk of the fluid is assumed to be stratified from the plane $x = x_1$ upward to the top. Since the fluid in the thermal boundary layer is heated by the wall, the temperatures in the boundary layer at height $(x_1 + \Delta x)$ will exceed those at height x_1. As stated above for $Pr \gg 1$ the fluid in the outer region of the hydrodynamic boundary layer is not heated. Due to stratification the bulk temperature at height $(x_1 + \Delta x)$ is higher than the bulk temperature at height x_1. The fluid in the outer region of the hydrodynamic boundary layer at height $(x_1 + \Delta x)$ coming from below, therefore will be colder than the bulk fluid at that height. So this fluid will experience a negative buoyancy force and will decelerate.

Different situations will arise depending on the magnitude of the bulk temperature gradient. Schwind & Vliet (1964) distinguished three regimes.
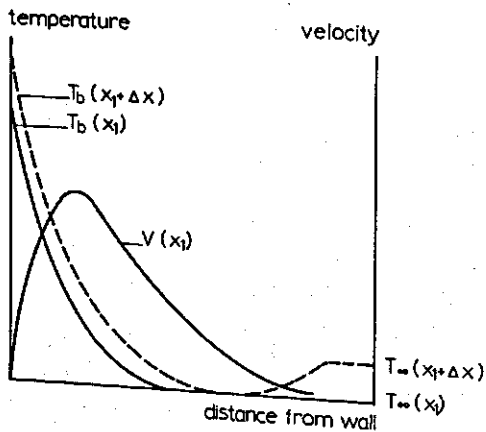

Fig. 10. Qualitative velocity and temperature profiles for $Pr > 1$, in the presence of a temperature stratified bulk. $T_b =$ temperature in the boundary layer, $T_\infty =$ bulk liquid temperature.

26

In *Regime A* the vertical bulk temperature gradient is favourable (temperature decreasing in upward direction), zero or slightly adverse. Then the boundary layer grows since the heat flux from the wall is sufficient to heat additional mass and set it in motion.

In *Regime B* the bulk temperature gradient is moderately adverse. Here all the wall heat flux is required to keep the average temperature level of the boundary layer liquid increasing at the same rate as that of the bulk liquid. Consequently there is no thermal energy available for additional growth of the boundary layer.

In *Regime C* the bulk temperature gradient is largely adverse. Here the heat flux from the wall is not sufficient to prevent deceleration of the boundary layer liquid. Part of the liquid in the outer region of the boundary layer leaves the boundary layer and joins the adjacent bulk fluid, or if a very large adverse bulk temperature gradient exists, the flow is reversed because of the negative buoyancy force.

Analytical studies of natural convection at a vertical wall in the presence of a vertical bulk temperature gradient were made by Cheesewright (1967), Eichhorn (1969), Yang et al. (1972) Goodman (1973), Piau (1974) and Fujii (1974). Cheesewright (1967) and Yang et al. (1972) obtained similarity solutions for natural convection in non-isothermal surroundings. The study of Cheesewright was restricted to natural convection in air ($Pr = 0.708$) from an isothermal vertical wall with a non-isothermal bulk. Yang studied a wider range than Cheesewright, since he also considered non-isothermal walls immersed in a stratified environment. Yang's work covered a Prandtl number range of 0.1 to 20. As I was mainly interested in a uniform wall temperature and a temperature gradient in the upward direction, only results related to this situation will be discussed here. Yang et al. (1972) started from the well-known boundary layer equations for laminar natural convection at a flat, vertical plate. They assumed the following boundary conditions:

$$y = 0 \quad u = v = 0 \quad T = T_w(x)$$
$$y \to \infty \quad u \to 0 \quad T \to T_\infty(x) \tag{31}$$

In Fig. 11 temperature profiles calculated by Yang et al. are presented for $Pr = 0.72$ and $Pr = 10$. Yang et al. stated that when the ambient temperature increases with height there is a minimum in the temperature profile, accompanied by flow reversal in the outer part of the boundary layer. However, they did not give velocity profiles. From their calculated results we can also conclude that the steeper the bulk temperature gradient and the higher the Prandtl number the more pronounced the phenomena of temperature defect and flow reversal will be.

Eichhorn (1969) considered the problem of a vertical flat plate of uniform temperature immersed in a fluid of which the temperature increases linearly with height. He presented velocity and temperature profiles, obtained by the technique of solutions in series, for $Pr = 0.7$ and $Pr = 6$. The more interesting value for my work, $Pr = 6$, is presented in Fig. 12. In this figure the dimensionless temperature and velocity are plotted against a dimensionless distance from the wall. From this figure again a minimum in the temperature profile below the local ambient temperature can be seen, while from the velocity profiles it can be concluded that
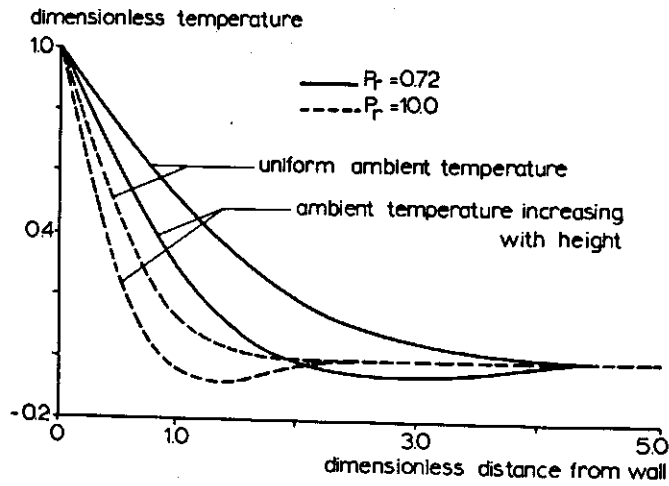
Fig. 11. Dimensionless temperature profiles after Yang et al. (1972) for constant wall temperature and ambient temperature increasing with height.
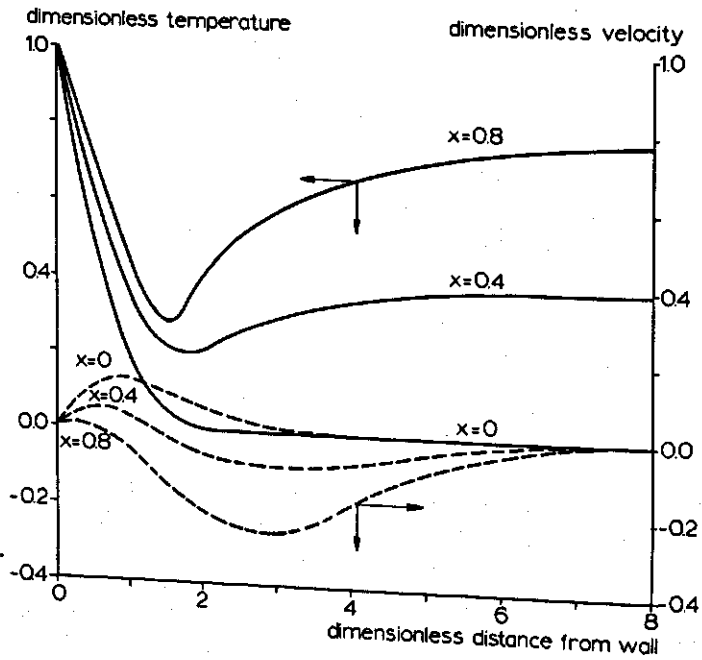

Fig. 12. Dimensionless temperature and velocity profiles at various distances (x) from the leading edge for constant wall temperature and ambient temperature increasing with height, $Pr = 6.0$. After Eichhorn (1969).

28

there is a region with reversed flow. Eichhorn stated that for low Prandtl numbers (air) no sizeable regions of reverse flow or temperatures below the local ambient one occur, whereas for large Prandtl numbers considerable regions of reversed flow and temperature defects are obtained.

Piau (1974) presented an experimental temperature profile for natural convection at a vertical wall in water with a temperature gradient. This profile shows a temperature defect. Also Haug et al. (1968) reported such a defect in their temperature profiles under similar experimental conditions. Piau (1974) compared his experimental temperature profile with a calculated one, obtained in a similar way to that of Yang et al. (1972). Piau reported a very good agreement between experimental and calculated temperature profiles.

Fujii et al. (1974) obtained calculated temperature and velocity profiles by using successively a similarity solution, a pertubation method and a finite difference approximation. For $Pr = 6.5$ all three methods showed that local temperature defects occurred, but there was no flow reversal. Experiments done in water in a vessel, were reported to confirm these findings. Fujii et al. assumed that flow reversal as predicted by Yang et al. (1972) and Eichhorn (1969) was caused by inaccuracy of numerical calculations. However there are strong indications for the real existence of a flow reversal at large Prandtl numbers, as will be shown in Chapter 4 of this thesis.

The concept of natural convection at a vertical wall in a non-isothermal surrounding was used in an analytical model for calculating stratification of a liquid in a closed container by Evans et al. (1968) and Matulevicius (1970). Evans et al. divided the system in three regions: a thin boundary layer flow rising along the heated wall, a mixing region at the top where the boundary layer flow dissolves and mixes with the upper core liquid and a main core where downward plug flow exists. They assumed that within the core horizontal temperature gradients can be neglected and that a vertical temperature gradient exists due to stratification. The separate equations describing the behaviour of the mixing region, central core and boundary layer were combined and solved simultaneously to predict the overall behaviour of the system. Evans et al. made a boundary layer analysis for a flat plate, by the Karman-Pohlhausen integral method which allows for temperature variation at the outer edge of the boundary layer. In their stratification model no liquid exchange between boundary layer and core was assumed. Effects such as a temperature and flow reversal in the boundary layer could not be predicted by this model.

The stratification model of Matulevicius (1970) is analogous to that of Evans et al. (1968). However, the hypothetical mixing region at the top of the core was dropped. Matulevicius also made a boundary layer analysis, by the Karman-Pohlhausen integral method, using more suitable velocity and temperature profiles than Evans et al. In the stratification model of Matulevicius temperature and flow reversal is allowed for. Thus in his model part of the boundary layer liquid leaves the boundary layer towards the core before reaching the top of the container.

3.4 Results of numerical model

As referred to in Section 3.2, Barakat & Clark (1966) obtained a numerical solution of the equations of motion and energy for laminar natural convection in a closed container with sidewall heating only. Their method applied to water in a closed cylindrical container provided results which look very reasonable. As the physical model of Barakat & Clark could easily be adapted to the conditions I applied an attempt was made to use this method here too.

Here the same set of dimensionless equations (25) to (27) is obtained and has to be solved. The following dimensionless thermal boundary conditions hold for this system:

$$\frac{\partial \theta}{\partial X}(1, R, \tau) = 0 \qquad \text{(liquid surface)}$$

$$\frac{\partial \theta}{\partial R}(X, 0, \tau) = 0 \qquad \text{(centre line)}$$

$$\theta(0, R, \tau) = \frac{(\frac{1}{2}D)^4 g\beta(T_w - T_0)}{H\nu\alpha} \qquad \text{(bottom)}$$

$$\theta(X, 1, \tau) = \frac{(\frac{1}{2}D)^4 g\beta(T_w - T_0)}{H\nu\alpha} \qquad \text{(sidewall)}$$

(32)

The boundary conditions for the stream function and vorticity are equal to Eqns (28) and (29) respectively, while the initial conditions correspond with those of Eqn (30). The method of solution was the same as that of Barakat & Clark (1966), only some slight modifications were applied to some finite difference approximations. The transformation of the partial differential equations in finite difference equations, the treatment of the boundary conditions and the procedure of the calculations are given in Appendix A.

Numerical results were obtained for the following parameter values:

$Pr = 300$

$Gr = \dfrac{(\frac{1}{2}D)^3 g\beta(T_w - T_0)}{\nu^2} = 10^5$ in which $T_w = 120°$ C and $T_0 = 30°$ C

$D = 0.178$ m

$H = 0.200$ m

These parameter values correspond to some extent with the conditions in my experiments, see Chapter 4.

In Fig. 13 for three dimensionless times, radial temperature profiles and streamline patterns are presented. These graphs look similar to those of Barakat & Clark for sidewall heating only (see Fig. 8). Except initially, the radial temperature profiles are almost flat outside the boundary layer. They show a minimum at a distance of about 15 mm from the wall. This temperature reversal will be caused by the temperature stratified core. From the streamline pictures it can be seen that part of the boundary layer liquid leaves the boundary layer before reaching the top of the container. This is an indication for reversed boundary layer flow.

30

Fig. 13. Streamline patterns and radial temperature profiles resulting from the numerical solution of the differential equations at three dimensionless times. $Pr = 300$, $Gr_w = 10^5$, $H/D = 1.12$.

The effects of temperature defect and flow reversal are in agreement with Section 3.3. In Fig. 14 the axial temperature profiles at the same three dimensionless times are given. The data presented in Fig. 14 were obtained 20 mm from the centre line. The real centre line values were not presented because of the irregularity in the horizontal temperature profiles at that location at early times. If we compare the axial temperature profiles from Fig. 14 with some reported in literature for simultaneous bottom and sidewall heating (Chapter 2) one notices an important difference. The experimental profiles show a region of uniform temperature in the lower part of the liquid and a temperature increasing with height in the upper part. The calculated profiles from Fig. 14 correspond closely

31

distance from bottom (mm)
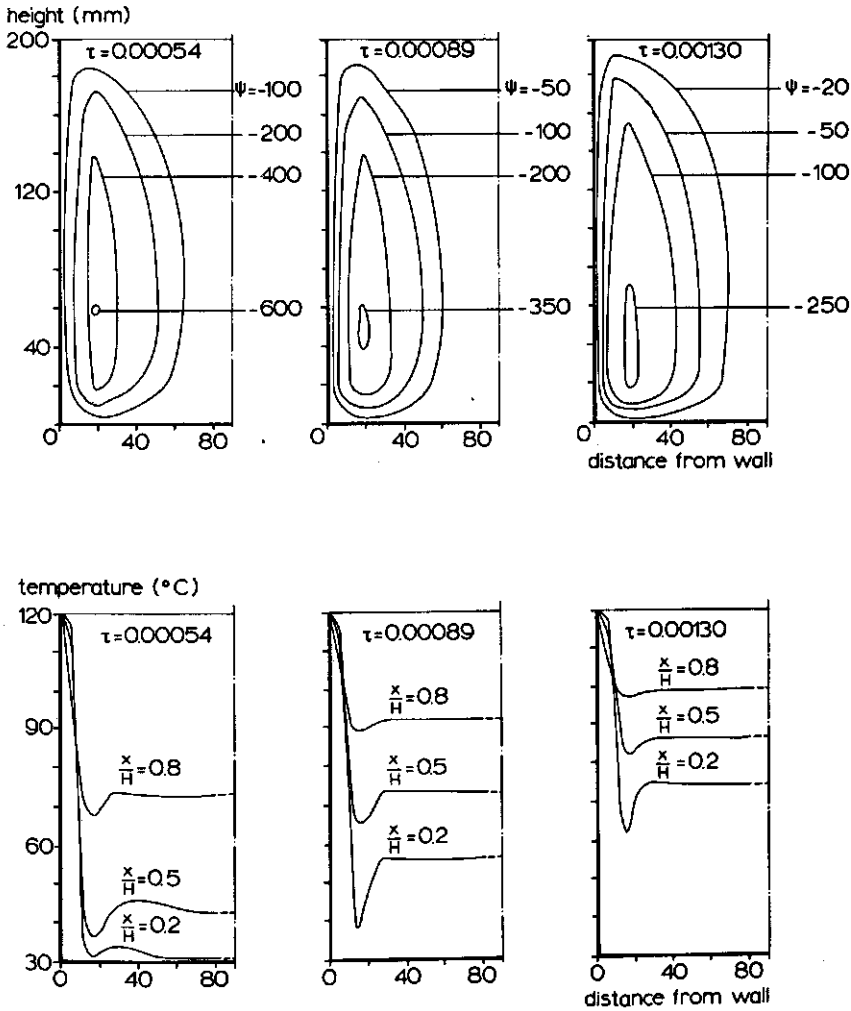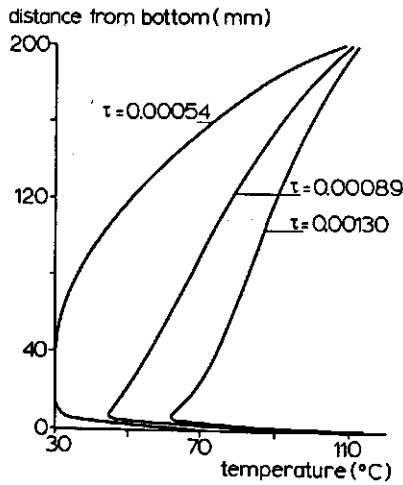

Fig. 14. Axial temperature profiles obtained from the numerical solution of the differential equations at three dimensionless times. $Pr = 300$, $Gr_w = 10^5$, $H/D = 1.12$.

to profiles experimentally obtained for only sidewall heating, see for example Schwind & Vliet (1964), while the streamline pattern also corresponds with those for only sidewall heating. Evidently the heat transfer from the bottom to the liquid is restricted to conduction in my situation, while under experimental conditions there is considerable convective heat transfer from the bottom. If we look at studies of natural convection in horizontal liquid layers heated from below, it becomes apparent that here there should even be turbulent natural convection from the bottom because $Gr\,Pr = 3 \times 10^7$ (Chu & Goldstein, 1973 and Somerscales & Dougherty, 1970).

By using a pertubation technique laminar natural convection in a fluid layer heated from below can be theoretically analysed, which results in streamline patterns (Bénard cells) and temperature profiles, see for example Charlson & Sani (1970). In such an analysis vertical convective heat transfer from a horizontal plate can be accounted for. It will be clear that this is not possible in my simulation model, which does not include a pertubation technique. As the conductive heat transfer is much less than the convective heat transfer from bottom it is not surprising that in this model the heat transfer from the bottom to the liquid is largely underestimated.

3.5 Discussion and conclusions

From a comparison of streamline patterns and temperature profiles from my numerical model, with experimental results from literature (and also with own experimental results, see Chapter 4) a poor correspondence between model and experiment was found. Especially the eddies, generated by bottom heating, are not incorporated in the numerical results. This shortcoming makes the numerical model inadequate for a prediction of the heating process.

As already mentioned in Section 2.3.4, Stevens (1972) tried to obtain a numerical solution for the same problem. He followed the approach of Torrance

32

(1968). Torrance used somewhat different finite difference approximations than Barakat & Clark (1966). Torrance stated that though the flow pattern and temperature profiles predicted by the method of Barakat & Clark are qualitatively correct, their method does not conserve energy and vorticity within the system. However, Torrance only proved this statement empirically for a situation with quite different boundary conditions than here. Essentially the approach of Stevens (Torrance) is the same as applied here. Though not recognized by Stevens, his model has the same shortcoming as this one: it does not account for convective heat transfer from the bottom.

Only if it were possible to introduce the effect of convective heat transfer from the bottom in such approaches, could reliable results be expected. Since it seems extremely difficult to do so, I think simplified models analogous to those of Evans et al. (1968) and Vliet (1966) are more promising.

4 Flow patterns and temperature profiles

The literature review given in Chapter 2 shows that a good understanding of the heating of liquids in closed containers requires a thorough knowledge of flow patterns and temperature profiles. In Section 2.5 we noted that there are gaps in our knowledge of flow patterns and temperature profiles, especially for simultaneous bottom and sidewall heating and for liquids much more viscous than water. This chapter describes experiments aimed at filling these gaps.

The organization of this chapter is as follows: first experimental methods, applicable for detection of flow patterns and temperature profiles will be viewed. Then the methods actually applied in our experiments will be treated in more detail. Flow patterns were observed by the 'particle-streak method', while temperature profiles were determined by means of inserted thermocouples. For a more detailed investigation of the boundary layer flow we used the laser-doppler method. Next a global preliminary discussion of flow patterns and temperature profiles is given to illustrate the interaction between both. Further flow patterns and temperature profiles are dealt with separately but thoroughly for water and two types of silicone oil, one with medium and the other with very high viscosity. Special attention was paid to the transient character of the flow pattern. Further points of investigation were the influence of the liquid height in the container and the level of the initial temperature of the liquid.

4.1 Methods and materials

4.1.1 Methods to determine flow patterns and temperature profiles

Various methods can be used to determine flow patterns. One group of methods uses a velocity measuring device such as a pitot tube, a hot-wire anemometer or a thermistor anemometer; with this device, which is inserted into the liquid a velocity profile can be determined. The disadvantage of this group of methods is that the measuring device itself disturbs the velocity distribution and therefore cannot be used at low liquid velocities and in thin boundary layers. Moreover the sensitivity becomes relatively weak at the low velocities occurring under the conditions I applied.

A second group of methods uses flow visualization techniques by adding tracers to the liquid. These methods enable the observation of the flow pattern and an estimation of the flow velocity. Examples are dye injection as well as techniques where hydrogen bubbles are generated or radioactive materials are used. The 'particle-streak method' also belongs to this group. In this method small glittering

34

particles are suspended in the liquid. The particles are illuminated by a flat narrow slit of light, exposed against a dark background and photographed. Detailed descriptions of the particle-streak method are given by Van Meel & Vermij (1958) and Powe et al. (1973). A modern version in this group is the laser-doppler velocimeter. This method is based on the fact that scattering of light against a moving particle causes a frequency shift. This frequency shift is called the Doppler effect. For a description of this method see Adrian & Goldstein (1971) and Appendix B.

The following methods can be used to measure temperature profiles:

1. Insertion of thermocouples or other small temperature sensors. By measuring temperatures at several points in the liquid a temperature profile can be determined.

2. Light deflection by 'schlieren'. This method is based on the fact that the refractive index of a fluid depends on temperature. The 'schlieren' method yields shadow pictures which show the space limits, in which the temperature of the fluid is influenced by the heated surface. From the shadow picture temperature gradients can be directly determined and used for an estimate of the heat transfer rate from the heating surface. See Jakob (1958) and Hauf & Grigull (1970) for a more detailed description.

3. Interferometric method. This method is based on the change of the density of a fluid with temperature. The pattern of fringes produced by the interferometer represents the temperature distribution in the fluid. From the interference fringes isotherms can be achieved. For more detailed descriptions see again Jacob (1958) and Hauf & Grigull (1970).

4. Infrared radiation. Temperature differences on the surface of an adiathermanous object are detected utilizing the natural infrared radiation which varies with the surface temperature. The wavelength distribution at any point is a measure for its surface temperature. By scanning the object a temperature map can be drawn up. For a description of this method see Sörenfirs (1974).

In this investigation the particle-streak method was used to determine the flow patterns. This method gives a clear picture of the overall flow pattern, during the whole heating process. For a detailed study of velocity profiles in the boundary layer the laser-doppler method was adopted. This method facilitates a more detailed observation in a small region than the particle streak method does. For temperature measurements we inserted thermocouples in the liquid, because this method is readily applicable in a closed container. For a special purpose incidentally a Thermovision Infrared camera was used.

4.1.2 Experimental set-up

Determination of temperature profiles For the measurement of temperature profiles I used a cylindrical copper container. On eight locations in the sidewall and four locations in the top cover thermocouples could be inserted through the walls (see Fig. 15). Iron-constantan thermocouples with a stainless-steel sheath of 1 mm outer diameter were used. The construction of the thermocouple fittings in the sidewall and top cover enabled a radial or axial displacement of the ther-

35
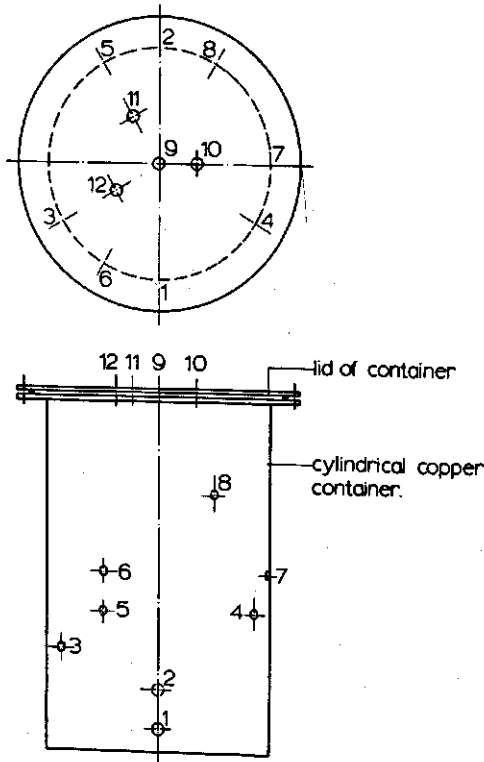
Fig. 15. Cylindrical copper container, used for determining temperature profiles. $D = 178$ mm and $L = 277$ mm. Location of thermocouple fittings is indicated by numbers 1 to 12.

mocouples. Since the thermocouples also could be bent easily it was possible to measure temperatures at any desired position in the liquid. For temperature measurements in the vicinity of the wall a considerable length of the thermocouple tube is preferably led through the liquid to prevent heat leakage along the thermocouples (see also Packer & Gamlen, 1974). The container was heated in a retort by condensing steam. The steam was supplied tangentially to get a high flow rate at the wall of the container ensuring a high heat transfer rate. About 30 s after opening the steam valve the desired values of pressure and temperature of the condensing steam in the retort were reached. In the wall of the retort 10 brass fittings were mounted for leading the thermocouples through the wall.

With this experimental set-up cylinder symmetry may be assumed. Deviation from the vertical position or unequal heating around the container wall could disturb the symmetry. However, no important deviations from cylinder symmetry in the temperature field were found in a special test with water.

Flow visualization   As already mentioned in Section 4.1.1 the particle-streak method was used. For this method a container with at least one transparent flat wall is needed so that the flow visualization studies were performed in a half-cylindrical brass container with a diameter of 0.18 m and a height of 0.20 m. The sidewall and bottom of the container could be heated with condensing steam. The flat front wall and top cover were made of double-windowed pyrex glass, see

1 = half cylindrical brass
    container
2 = pyrex glass windows
3 = vessel for test-liquid
4 = valves for in-and outlet liquid
5 = steam chamber
6 = steam inlet
7 = condensate trap
8 = air chamber (insulation)
9 = inlet hot air
10 = connections to pressure
    controller
11 = thermocouple arrangement
12 = liquid containing slit
    (insulation)

detail A

detail B
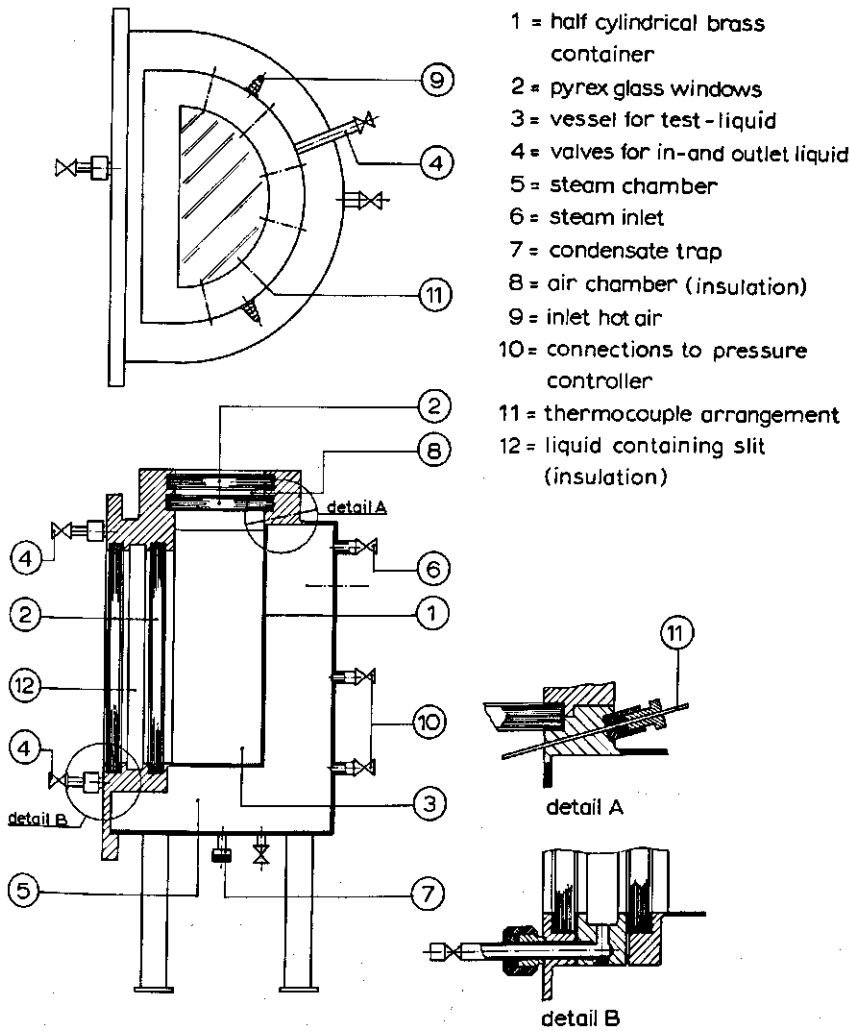
Fig. 16. Half-cylindrical container used for flow visualization.

Fig. 16. The mutual distance of the glass windows of the front wall was 30 mm. The compartment in between was also filled with liquid and also heated with condensing steam at sidewall and bottom. As a result the temperature distribution in this compartment matches well with that in the liquid inside the half cylinder. Thus the heat loss through the front wall from the liquid in the half container can be neglected in comparison with the heat supply via the brass wall and the bottom. The centre line of the half-cylindrical container was situated 10 mm behind the second glass window, see Fig. 16. The thermal and hydrodynamic boundary layers have a thickness of about 5 mm. Thus in the vertical plane through the centre line, disturbance of flow patterns due to the presence of the glass window is negligible. As a result of these precautions the situation in the half

1 = half cylindrical container
2 = glass windows
3 = steam chamber
4 = liquid
5 = slide projector
6 = slit of light
7 = camera
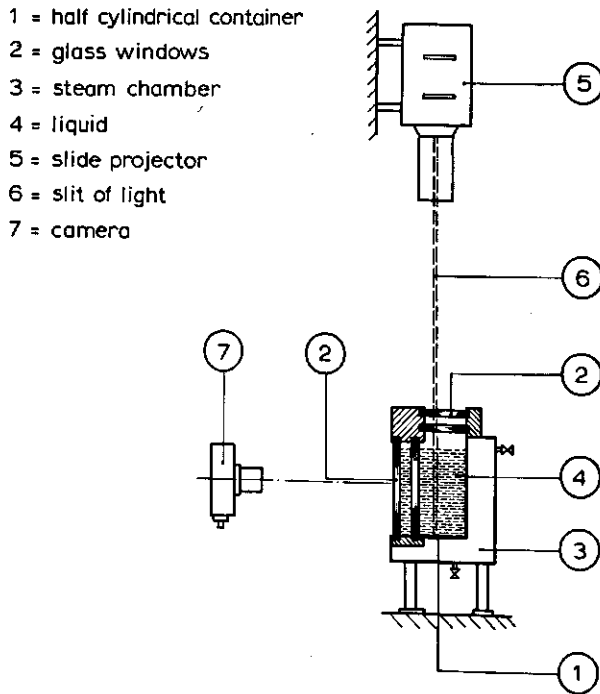
Fig. 17. Experimental set-up for flow visualization.

container is as alike that in the complete container as possible. If cylinder symmetry is assumed, the whole flow pattern can be presented in two-dimensional graphs. During the experiments the compartment between the glass windows on top was continuously purged with hot air to prevent condensation on the lower side of the lower glass window and to suppress heat losses through the top cover.

Temperatures in the liquid were measured with thermocouples in a similar way as described for the copper vessel. As tracer particles a suspension of 1 mg/kg 'Mearlin-A Pearlwhite' was used. This material consists of silica plates coated with TiO_2, with a particle size of 5 to 30 μm. In the plane through the centre line these particles were illuminated by a high-intensity lamp focussed through a narrow slit. The thickness of this slit was about 10 mm. As light source a slide projector was used. In front of the half container a camera was placed. The flow patterns were photographed by making time exposures of 1 to 40 s. The experimental set-up is shown in Fig. 17 and Plate 1.

Velocity measurements with a laser-doppler velocimeter The measurements with the laser-doppler velocimeter were done in the half-cylindrical container, since this method also requires a partly transparent vessel wall. The experimental set-up is presented in Fig. 18. The special measuring technique used in this investigation was developed by Technisch Physische Dienst TNO-TH Delft (Institute of Applied Physics, Netherlands Organization for Applied Scientific Research—Technological University, Delft), while the experiments were also

38
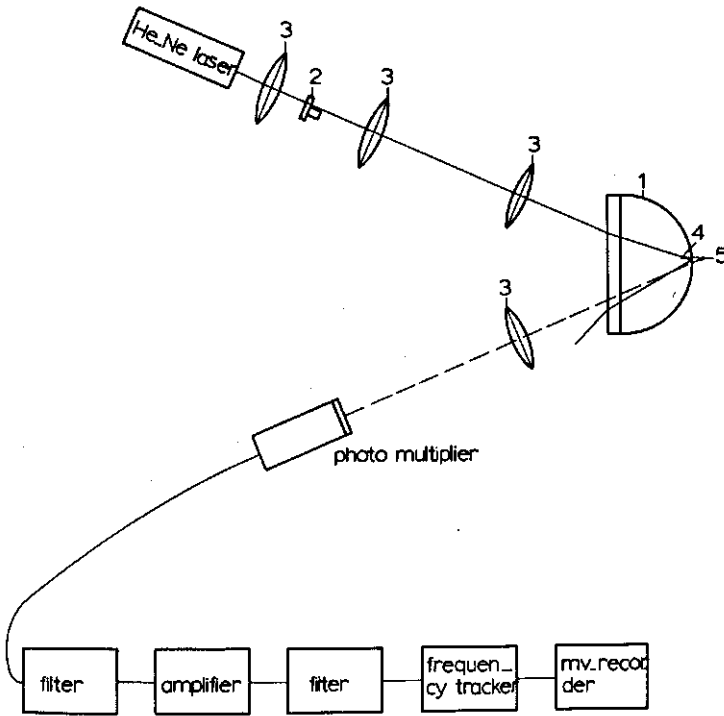
Fig. 18. Experimental set-up for measurements with laser-doppler velocimeter: (1) container with reflecting backwall, (2) rotating grating, (3) lens, (4) probe volume, (5) image probe volume.

performed by TPD-TNO/TH. In Appendix B a description of the laser-doppler method and the experimental set-up is given. The laser-doppler method requires the presence of small particles in the liquid. In water a milk suspension was used, while in silicone fluid a centrifuged suspension of 'Mearlin-A Pearlwhite', with a particle size of 5 to 10 μm, was used.

Test liquids For a qualitative study of the flow pattern a 75 % glycerol solution was used, which gave excellent pictures of the flow pattern. For the definite measuring programme I abandoned this liquid because of its doubtful physical uniformity. For the definite study of flow patterns and temperature profiles I used three liquids with strongly differing viscosities, namely water, silicone fluid F111/100 (medium viscosity) and silicone fluid F111/10000 (very high viscosity). Laser-doppler measurements were performed in water and silicone fluid F111/100. The most important physical properties of the test liquids are given in Appendix C.

4.2 Qualitative discussion of flow patterns and temperature profiles

A qualitative description of flow patterns and related temperature profiles will be based on those observed for heating a 75% glycerol solution. In Plate 2 and 3

39

photographs of flow patterns observed in the half-cylindrical container (Fig. 17) are shown. In Fig. 19 these flow patterns are schematized, while in the same figure corresponding axial temperature profiles are given. At the onset of heating the temperature of the container wall was suddenly increased from 30°C to about 115°C. The liquid near the wall is heated and buoyancy forces drive the liquid upwards. This results in an upward boundary layer flow at the wall. In the upper corner this boundary layer flow is interrupted because the liquid changes direction and spreads inwards over the free liquid surface. This liquid forms a more or less uniform horizontal layer which then slowly moves downward. The distribution in the core is stabilized as a result of hot liquid from the boundary layer piling up continuously on the slightly cooler core: a phenomenon known as 'thermal stratification'. In the lower part of the container the flow pattern is very complex. At the bottom we observe a kind of liquid eruption. These eruptions are generated by the heating of the bottom. The liquid near the bottom will attain a higher temperature (and thus a lower density) than the adjacent liquid at some
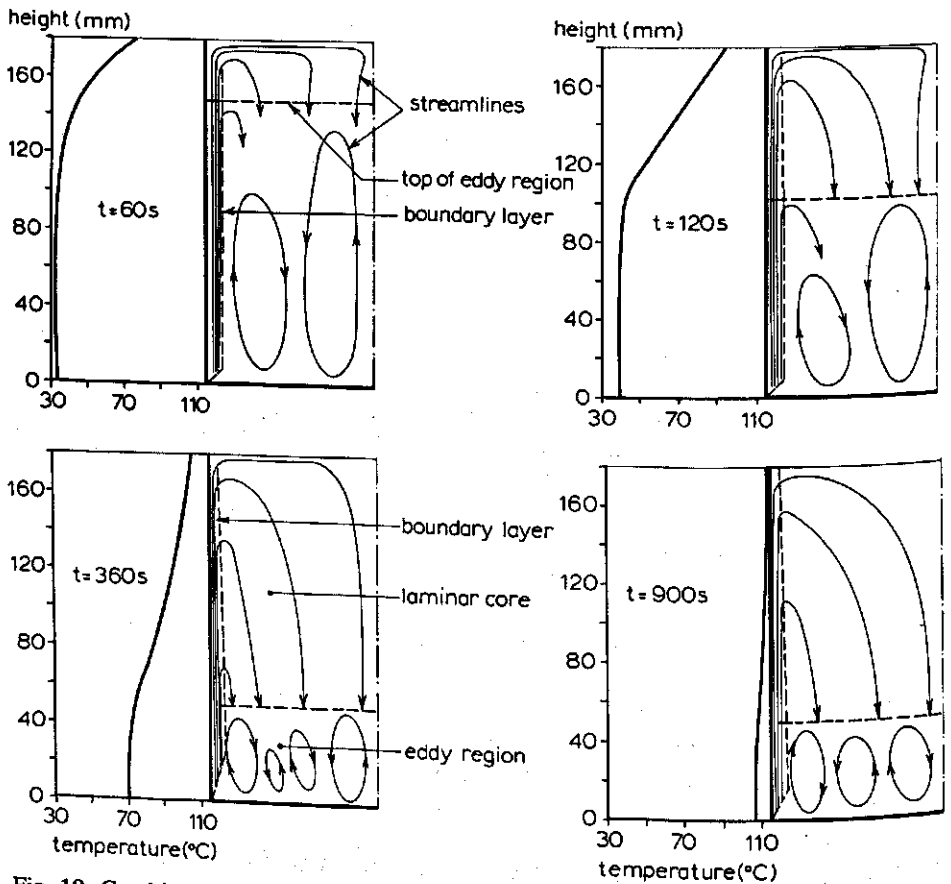

Fig. 19. Combined flow patterns and axial temperature profiles for heating 75 % glycerol, at four different times. Liquid height 180 mm, initial temperature 30°C and steam temperature 115°C.

40

distance from the bottom. This situation is unstable and heated liquid will rise from bottom in a rather unpredictable way. For ease we shall call these liquid eruptions 'eddies', though they are quite different from eddies that occur in turbulent flow. The 'eddies' penetrate over a certain height in the liquid. From the pictures of Plate 2 it can be seen that there are several of these eddies emerging over the bottom plate. The height of the eddy region decreases as heating proceeds. At the beginning the height of the eddy region is about 80 % of the total liquid height. After about six minutes an equilibrium height of about 30 % is reached. This height remains essentially unchanged during the remainder of the heating process.

In Fig. 19 both flow patterns and temperature profiles are presented at four different times. The times of Plate 2 and Fig. 19 do not correspond exactly. The flow patterns of Fig. 19 are not drawings from the photographs of Plate 2, but are interpreted from several series of photographs of the flow pattern.

Fig. 19 elucidates the relation between flow patterns and temperature profiles. First we see that at any time the temperature in the lower part of the container is nearly uniform, while above this uniform temperature region the temperature is increasing towards the free liquid surface. The temperature gradient in the upper part originates from the stratification process mentioned above. The thermally stratified core causes the flow reversal of boundary layer liquid as shown in Plate 3 and Fig. 19. This phenomenon was extensively treated in Section 3.3.

From Fig. 19 we can conclude that the top of the eddy region corresponds with the bend in the temperature profile. The heating process in the lower part of the container may be conceived as follows: Liquid which is vigorously heated at the bottom rises in eddies. The upward flow of these eddies continues until a liquid parcel heated at the bottom enters a region with a higher temperature (thus a lower density) than its own. Then the buoyancy force of the liquid parcel vanishes and flow returns. According to the equation of continuity any ascending flow must be compensated by some descending flow. The combination of these flows leads to the rather complicated picture in the lower part of the container as seen in Plate 2. As a result of these phenomena in the eddy region a rather intensive mixing of liquid in the axial direction occurs. This causes a nearly uniform temperature in the whole eddy region.

The liquid above the eddy region, in the upper part of the container, is heated as a result of the boundary layer flow along the container wall. By this phenomenon continuously hot liquid is added at the top of this stratified region. The upper part of the container is thus mainly heated from above. Initially the stratified region is heated faster from above than the eddy region is heated from below, while the volume of the former is small compared with the volume of the latter. The interface between eddy region and stratified region is thus pushed downward until the heating of the stratified region from above and the heating of the eddy region from below balance each other. In Plate 2 this asymptotic situation was reached after about six minutes.

4.3 Flow patterns and temperature profiles for silicone fluid of intermediate viscosity

4.3.1 Temperature profiles

Radial temperature profiles   Radial temperature profiles were measured at six different levels in the silicone fluid. The liquid height was 200 mm, while the diameter of the container was 178 mm. Two thermocouples were inserted axially through the top cover and six thermocouples radially through the sidewall. In the first run the radially inserted thermocouples were located on the central axis, in each of the following runs they were bent into positions nearer to the wall. In this way temperature courses were measured at six different positions between central axis and container wall. No measurements were done within a distance of 5 mm from the sidewall. Flow visualization indicated that the boundary layer was within this 5 mm. It is impossible to make a significant temperature measurement within a boundary layer of less than 5 mm by inserting a 1 mm thermocouple. The two thermocouples inserted through the top cover were fixed during all runs, to check reproducibility of the successive runs.

The above procedure ultimately results in radial temperature profiles at six different levels in the container. In Fig. 20 radial temperature profiles are presented for four different levels. The other two radial temperature profiles are similar to those presented. From Fig. 20 it appears that the horizontal temperature profiles are flat within the above mentioned limits. This fact, together with the upward direction of the temperature gradient, supports the concept of a core with downward plug flow, continuously fed on top by uniformly spread layers of ever increasing temperatures. Only for $t = 120$ s at $x = 136$ mm and $x = 195$ mm could a small radial temperature gradient be detected. Probably the plug flow in the core was not completely established at that moment.
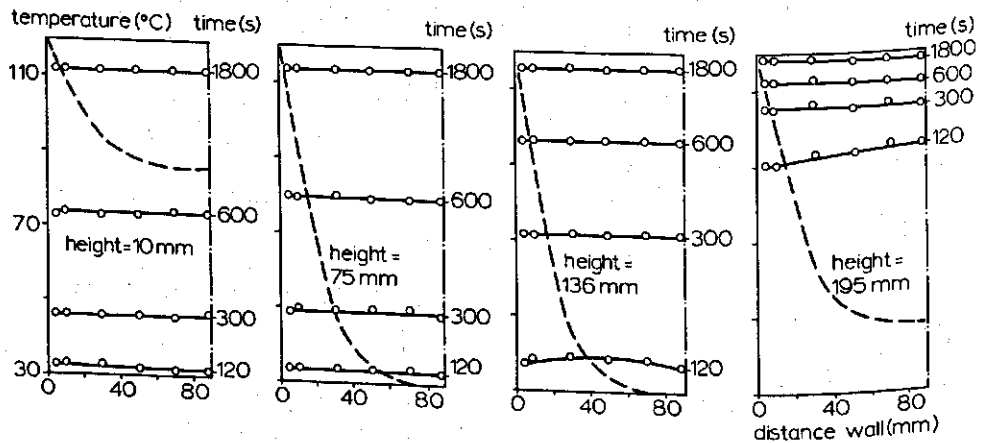
Fig. 20. Radial temperature profiles for heating silicone fluid F111/100, at four different levels. Calculated radial temperature profile for pure conduction heating at $t = 1800$ s is added for comparison (broken curve). $H = 200$ mm, $T_0 = 30°$ C and $T_* = 120°$ C.

42

Plate 1. Photograph of experimental set-up for flow visualization, showing half cylindrical container and slide projector. This photograph corresponds with Fig. 17.
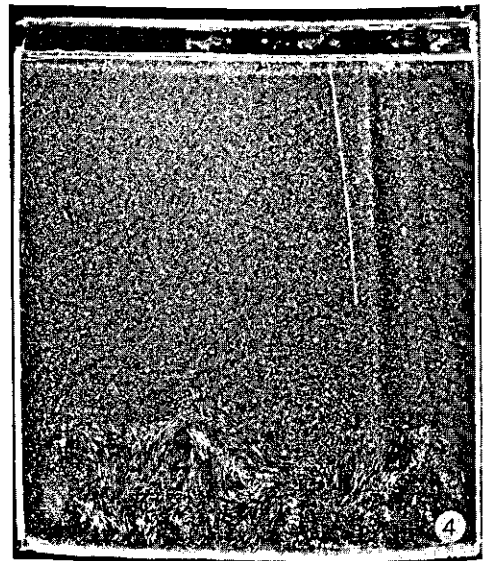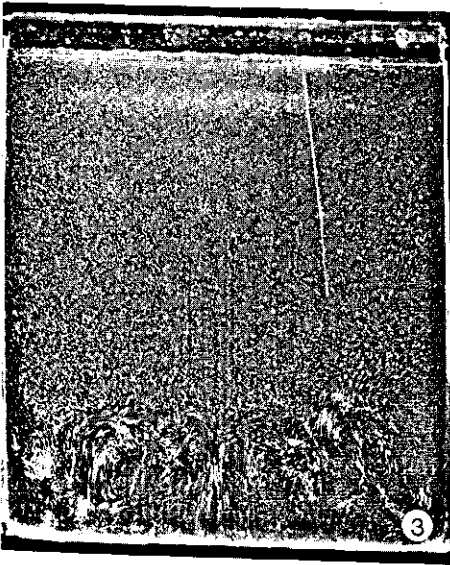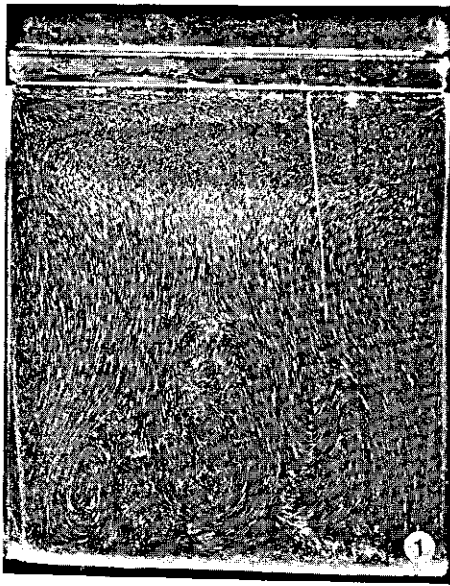
Plate 2. Photographs of flow patterns observed in 75% glycerol. Exposure time 1 s. (1) 20 s after start of heating; (2) 120 s after start of heating; (3) 360 s after start of heating; (4) 1080 s after start of heating.
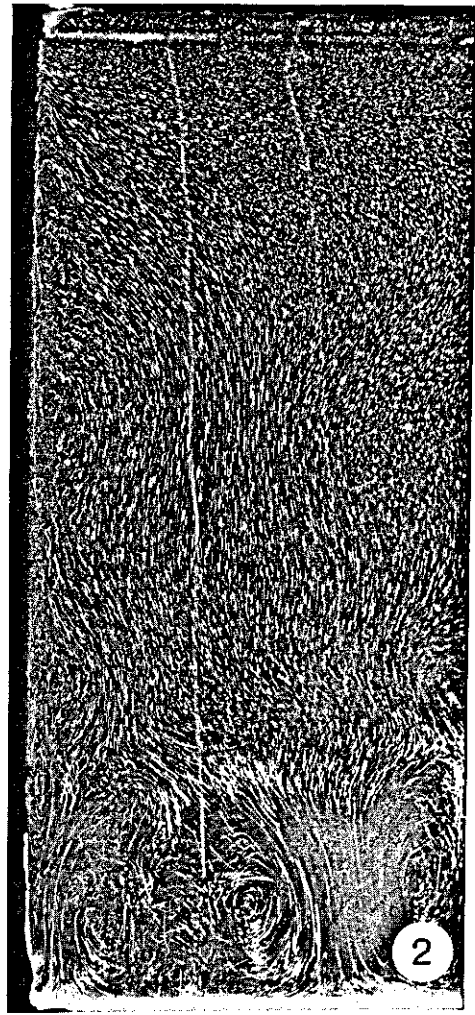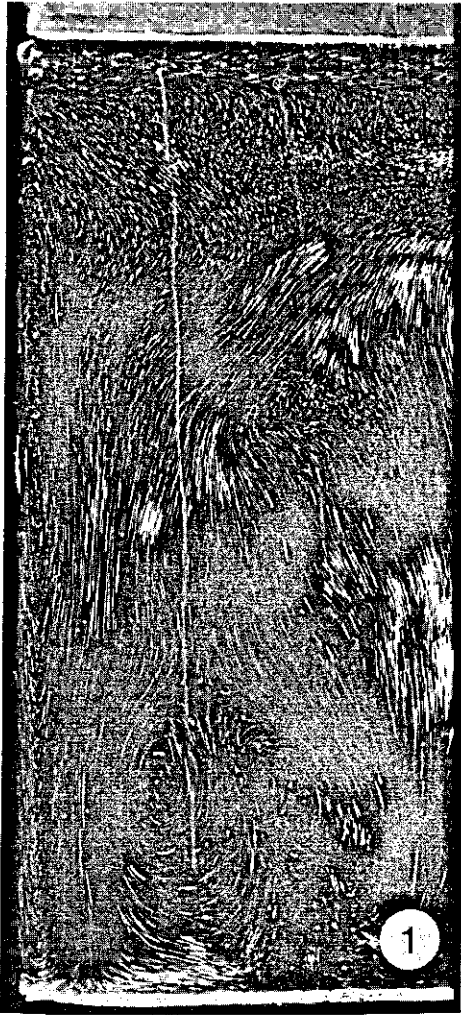
Plate 3. Photographs of flow patterns observed in 75% glycerol. Only the left half of the container is shown. (1) 40 s after start of heating, exposure time 1 s; (2) 900 s after start of heating, exposure time 5 s. On both pictures eddies developing at the bottom can be seen. Picture 2 also shows a flow reversal in the boudary layer at the sidewall.
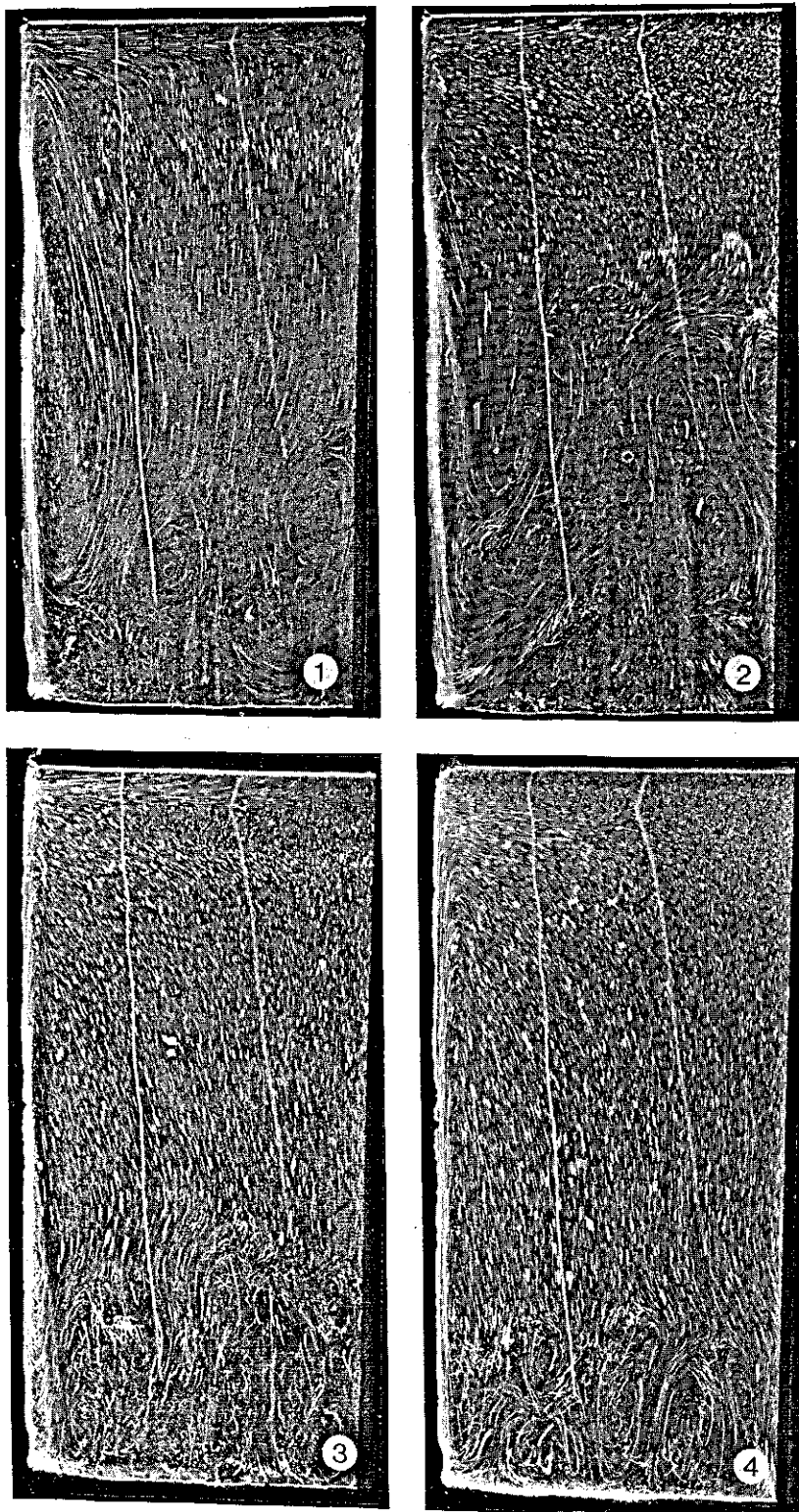
Plate 4. Photographs of flow patterns observed in silicone fluid F111/100. Only the left half of the container is shown. (1) 30 s after start of heating, exposure time 3 s; (2) 120 s after start of heating, exposure time 3 s; (3) 480 s after start of heating, exposure time 8 s; (4) 1800 s after start of heating, exposure time 15 s.
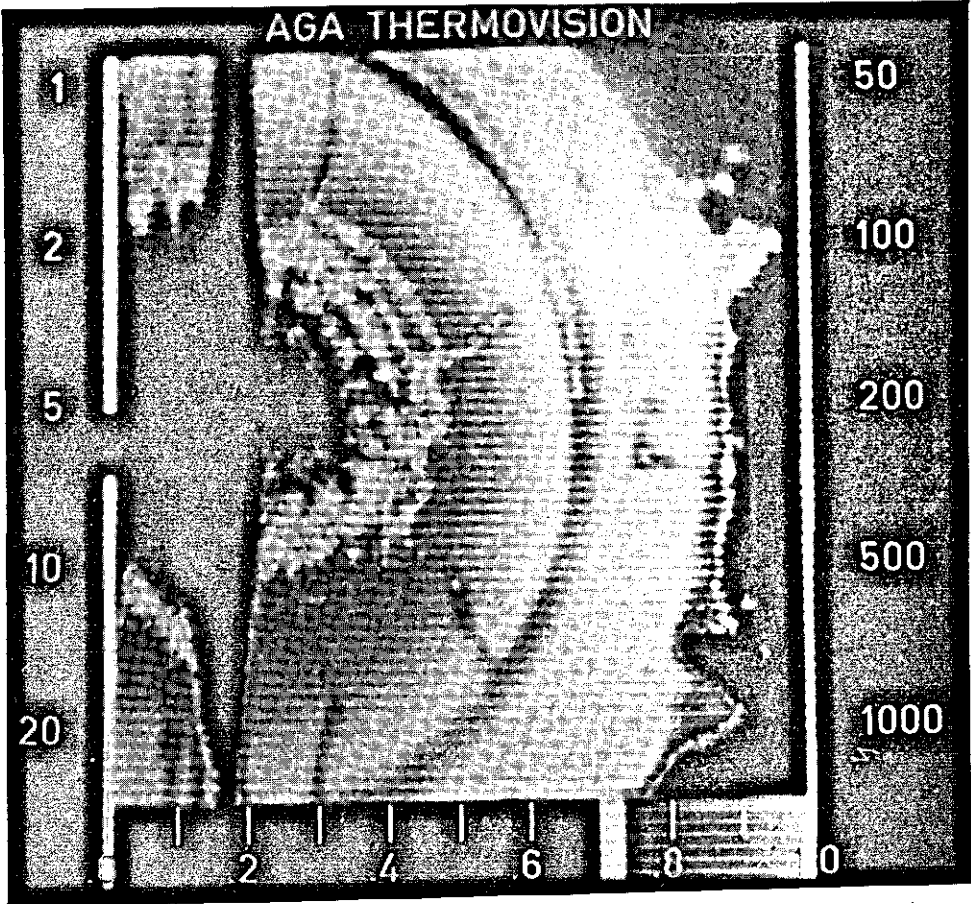
Plate 5. Infrared picture of free liquid surface of silicone fluid F111/100 420 s after start of heating. Temperature range 5 °C (difference between black and white). White bond is contourline, width 0.2 °C (see lower scale between 0.7 and 0.8).
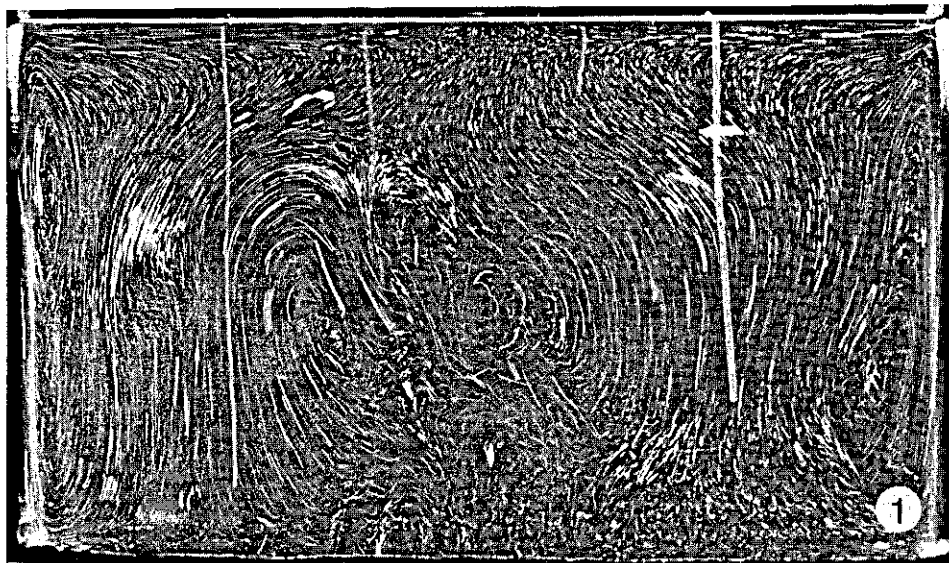
Plate 6. Photographs of flow patterns observed in silicone fluid F111/100 at a total liquid height of 100 mm. (1) 45 s after start of heating, exposure time 3 s; (2) 180 s after start of heating, exposure time 5 s; (3) 480 s after start of heating, exposure time 8 s; (4) 1440 s after start of heating, exposure time 15 s.

3

4
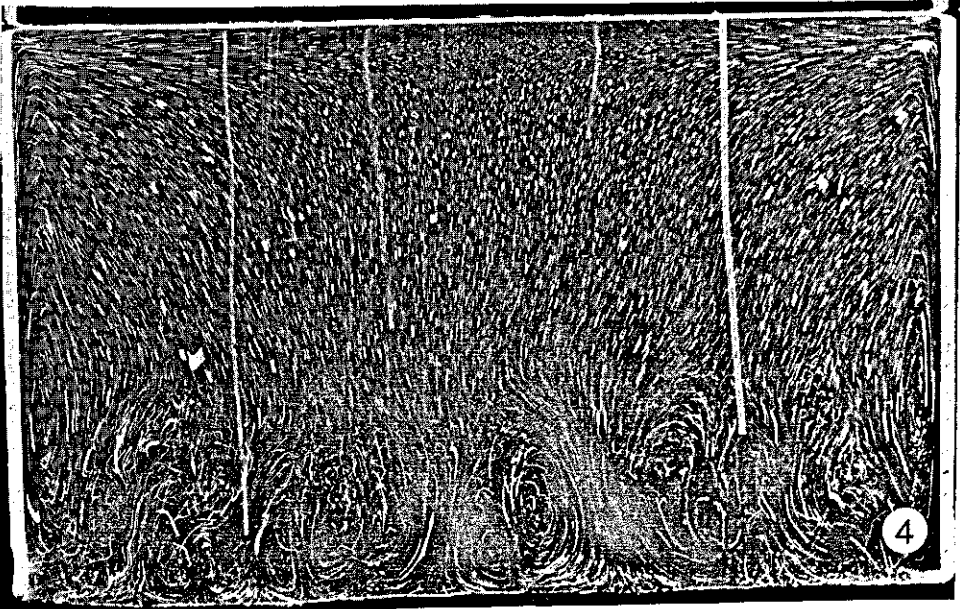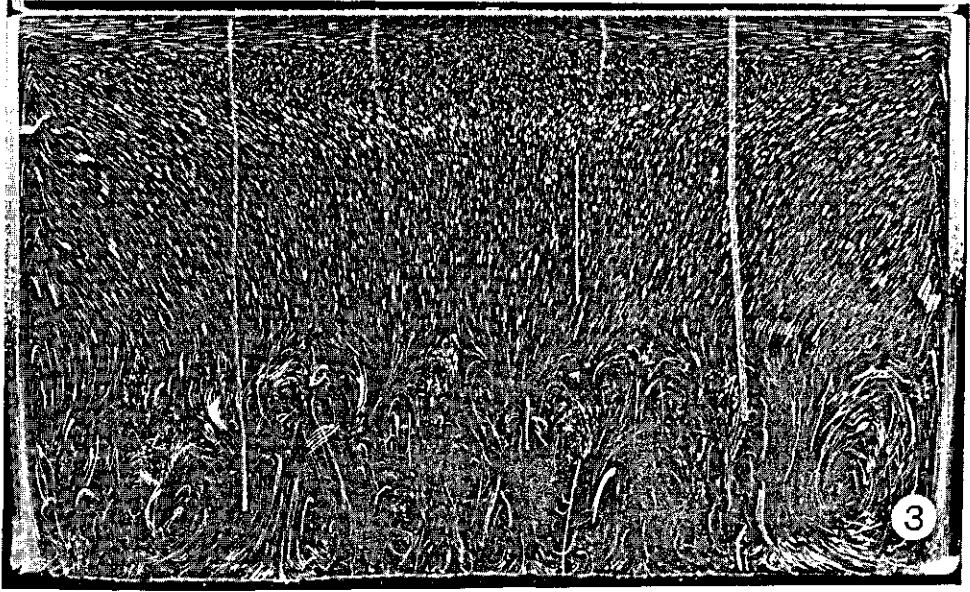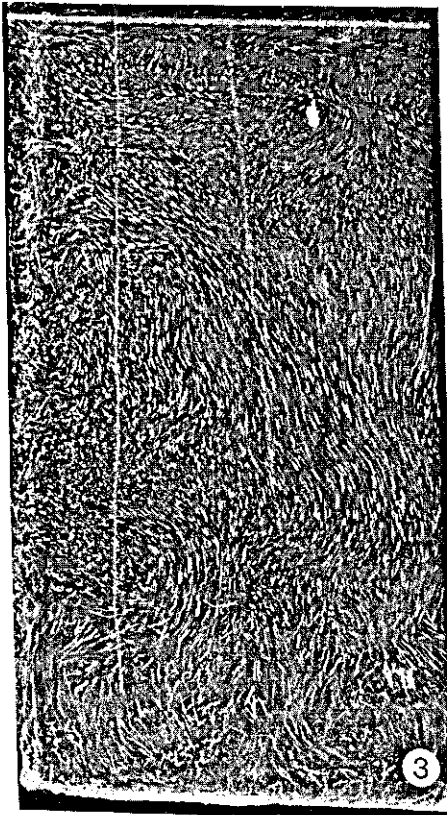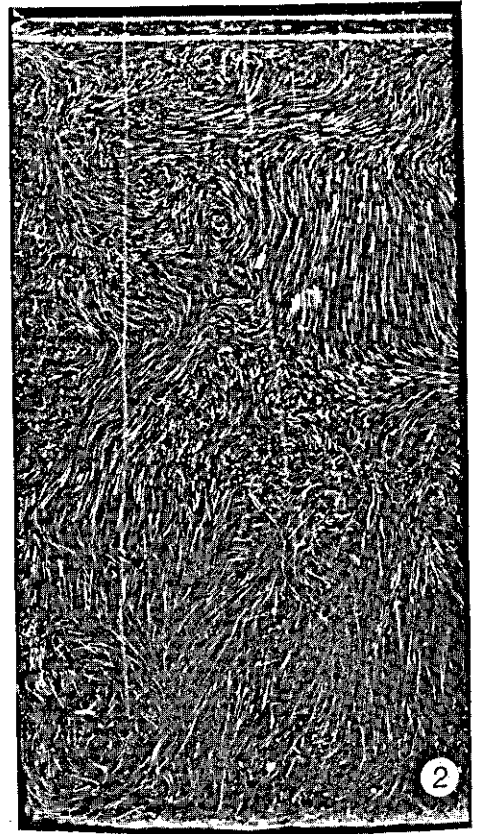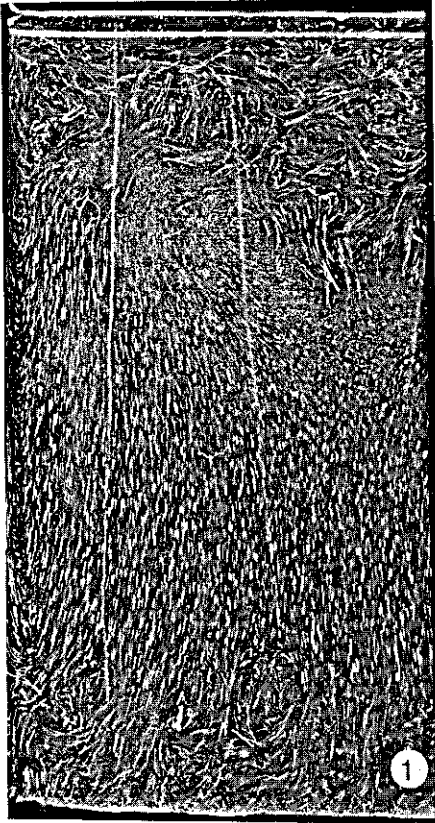
Plate 7. Photographs of flow patterns observed in water. Only the left half of the container is shown. Exposure time 1 s. (1) 15 s after start of heating; (2) 45 s after start of heating; (3) 120 s after start of heating.

In the same Fig. 20 calculated temperature profiles at $t = 1800$ s are given assuming only conduction heating (see for calculation method Appendix D). In this calculation a slight heat transfer through the head space is supposed, mainly by radiation. The calculated conduction profiles are obviously quite different from the actual profiles. Heating by conduction would proceed much more slowly and the slowest heating would be somewhere in the centre.

The measured radial temperature profiles are qualitatively in good agreement with those reported for similar cases in literature, see Chapter 2.

Axial temperature profiles To determine axial temperature profiles, thermocouples were inserted at eight different heights in the liquid. The exact radial position of a thermocouple was not very important because of the flatness of the radial temperature profiles. In Fig. 21 axial isochronic temperature profiles are drawn for four different times. As with 75 % glycerol solution it appears that at a certain time the temperature is nearly uniform in the lower part of the container, while in the upper part the temperature increases towards the liquid surface. The temperature gradients in the upper part are rather steep, particularly in the initial stage of heating. At $t = 120$ s the temperature at the liquid surface is already
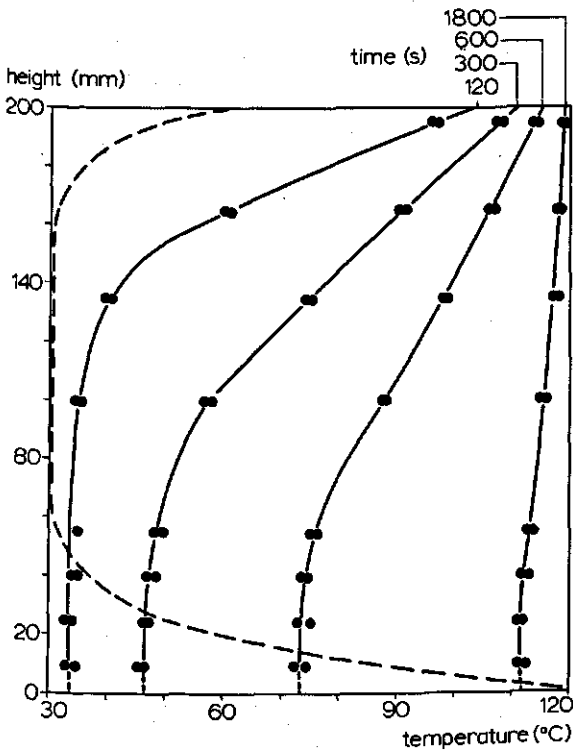
Fig. 21. Axial temperature profiles for heating silicone fluid F111/100 at four different times. Calculated axial temperature profile for pure conduction heating at $t = 1800$ s is added for comparison (broken curve). The two dots at any time and height are successive runs. $H = 200$ mm, $T_0 = 30°$ C and $T_a = 120°$ C.

above 100° C while in the lower part the temperature is between 30 and 35° C. Here too the height of the uniform temperature region as well as the temperature gradient in the upper part diminish in time. However, the shape of the axial temperature profiles remains unaltered.

The calculated axial temperature profile at $t = 1800$ s for pure conduction heat transfer is also drawn in Fig. 21. It appears from that curve that after half an hour a marked temperature increase is found only just above the bottom and just below the liquid surface. We may conclude, that in this relatively large container convection heating proceeds much faster than conduction heating, even for this rather viscous silicone fluid.

Similar axial temperature profiles for convection heat transfer for simultaneous bottom and sidewall heating were reported by Schwind & Vliet (1964), Vliet (1966) and Pollard & Carlson (1969), see also Chapter 2.

4.3.2   Flow patterns

In Plate 4 a series of photographs is given of the flow pattern of silicone fluid F111/100. Here the liquid height amounted to 180 mm. The flow pattern is similar to the one already described for a 75 % glycerol solution. It seems appropriate to give some more details of the flow pattern at this stage of the report. During heating two periods can be distinguished: an initial or starting period, during which the flow starts and establishes itself, and subsequently a quasi-steady state.

Initial period   Heating is initiated by bringing the walls of the container quickly to nearly the steam condensation temperature. A few seconds later the liquid at the wall is set in motion and a boundary layer flow develops. From Plate 4 ($t = 30$ s) this boundary layer is estimated to be about 8 mm thick. Demanding continuity the average upward velocity in the boundary layer can be roughly estimated from the downward core flow, by:

$$\pi D\, \delta \bar{v}_{bl} = \tfrac{1}{4}\pi D^2 \bar{v}_c$$

(33)

From the length of the streaks the downward velocity in the core is estimated to be about 2 mm/s, which implies that the average velocity in the boundary layer should be about 11 mm/s. During the initial period the thickness of the hydrodynamic boundary layer decreases with time, while the velocity of the boundary layer flow decreases too. The decrease of the hydrodynamic boundary layer thickness can be understood from the decreasing viscosity of the liquid. At the onset of convection the liquid near the wall is only moderately heated. When the heating progresses, more heat penetrates into the boundary layer and the overall temperature of the liquid increases, so the viscosity decreases. Since the thickness of the hydrodynamic boundary layer is proportional to $Pr^{\frac{1}{4}}$ (Ostrach, 1953), the thickness will be reduced during the initial period. For silicone fluid F111/100 the kinematic viscosity is reduced approximately by factor 4 (see Appendix C), so the thickness of the hydrodynamic boundary layer will be reduced by a factor 2. Qualitatively this agrees rather well with my observations.

44

The onset of natural convection near a suddenly heated vertical flat plate was studied theoretically by Siegel (1958). Siegel found that initially heat is transferred by conduction only. Hence heat transfer is equivalent to heat conduction into a semi-infinite slab and it may be described as penetration of isotherms parallel to the surface into the liquid. From the analysis of Siegel, an estimate can be made of the time at which pure one-dimensional heat conduction terminates. For the conditions I applied, at $100\,mm$ from the bottom, this estimation results in a termination of pure conduction $15\,s$ after initiation of heating ($F_0 = 4.2 \times 10^{-5}$). From flow visualization it appeared that it took about $10\,s$ after initiation of heating to set the liquid in motion. These times are in rather good agreement. According to Siegel the early velocity distribution would be independent of the position along the heated wall, due to the one-dimensional character of the heat conduction. After the onset of convection the thickness of the boundary layer is influenced by the history of the liquid and then depends on the position along the wall. The flow visualization technique used was not sufficiently sophisticated to detect this effect. Finally it can be noticed from Plate 4 that in the lower part of the container after $30\,s$ already eddies are developing, mainly in the centre, as a result of bottom heating.

Quasi-steady state   After about $90\,s$ the flow in the container is established and a quasi-steady state is achieved. In this quasi-steady state three flow regions can be distinguished namely an upward boundary layer flow at the wall, a downward core flow in the upper part and an eddy region in the lower part of the container (see Fig. 19 and Plate 4). This situation continues during the further heating period. However, the height of the eddy region reduces with time until an equilibrium height is achieved. The photographs of Plate 4 show that the upward moving boundary layer flow loses part of its liquid before reaching the top of the container. This liquid, which leaves the boundary layer, moves downward with the core flow. As a result the boundary layer is peeled off. This phenomenon of flow reversal, caused by the thermally stratified core, has already been discussed extensively in Section 3.3. This phenomenon could be detected with the 75 % glycerol solution too. Dye that was injected in the lower corner of the container, rapidly moved upwards with the boundary layer flow. Some dye, however, left the boundary layer before reaching the top and moved into the core.
The downward core flow is mainly fed by liquid flowing just below the free liquid surface from the wall to the centre. In the lower regions some liquid is added that leaves the boundary layer. The downward laminar core flow is disturbed when it meets the eddy region. Dye injections in the 75 % glycerol solution showed the core flow to become incorporated in the eddy region. In the eddy region a slow net liquid transport to the sidewall exists, to such an extent that the boundary flow can be fed from it. From dye injections in the eddy region it was found that no liquid from the eddy region penetrates into the laminar core.
Plate 4 shows that the height of the eddy region reduces to an equilibrium value (of about 25 % of the liquid height), reached after about 10 minutes. During heating temperatures were measured on four different levels in the liquid in the half cylindrical container. From these measurements the axial temperature
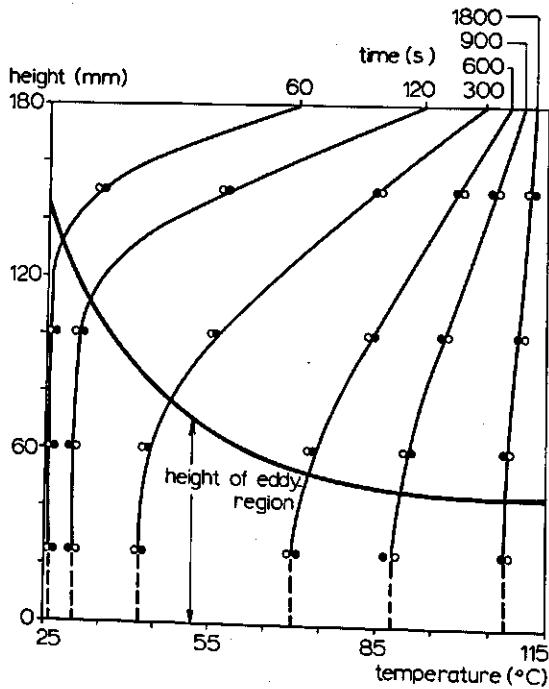
Fig. 22. Axial temperature profiles for silicone fluid F111/100, heated in the half-cylindrical container. The two dots at any time and height are successive runs. Total liquid height is 180 mm. The visually observed height of the eddy region is projected on the axial temperature profiles.

profiles shown in Fig. 22 were derived. The visually observed decreasing height of the eddy region is projected on these temperature profiles. It can be seen that the height of the eddy region corresponds with the bend in the axial profiles. Fig. 23 shows the temperature fluctuations as recorded by the thermocouples in the eddy region. The most pronounced fluctuations were recorded by the thermocouple next to the bottom. It can be seen that the fluctuations decrease with time. The fluctuations arise because warmer ascending liquid and colder descending liquid successively pass the thermocouples. At larger distance from bottom the fluctuations become smaller. Temperature differences between ascending and descending liquid parcels reduce at higher levels, since on their way the parcels gradually exchange matter and heat with each other.

The situation in the lower part of the container corresponds to some extent with that for Bénard convection, where a horizontal liquid layer is heated from below. Most investigations on Bénard convection are concerned with very thin liquid layers (from 1 mm to 2 cm). The subject of most investigations in this area is the value of the Rayleigh number for the onset of convection, see Somerscales & Dougherty (1970) and Hoard et al. (1970). Nielsen & Sabersky (1973) have described the flow patterns for natural convection in a horizontal liquid layer heated from below, for a wide range of Rayleigh numbers. From the study of Nielsen & Sabersky (1973) it should be concluded that in my study with a

46

temperature (°C)

x=150 mm
x=100 mm

x=25 mm
x=60 mm

time (s)
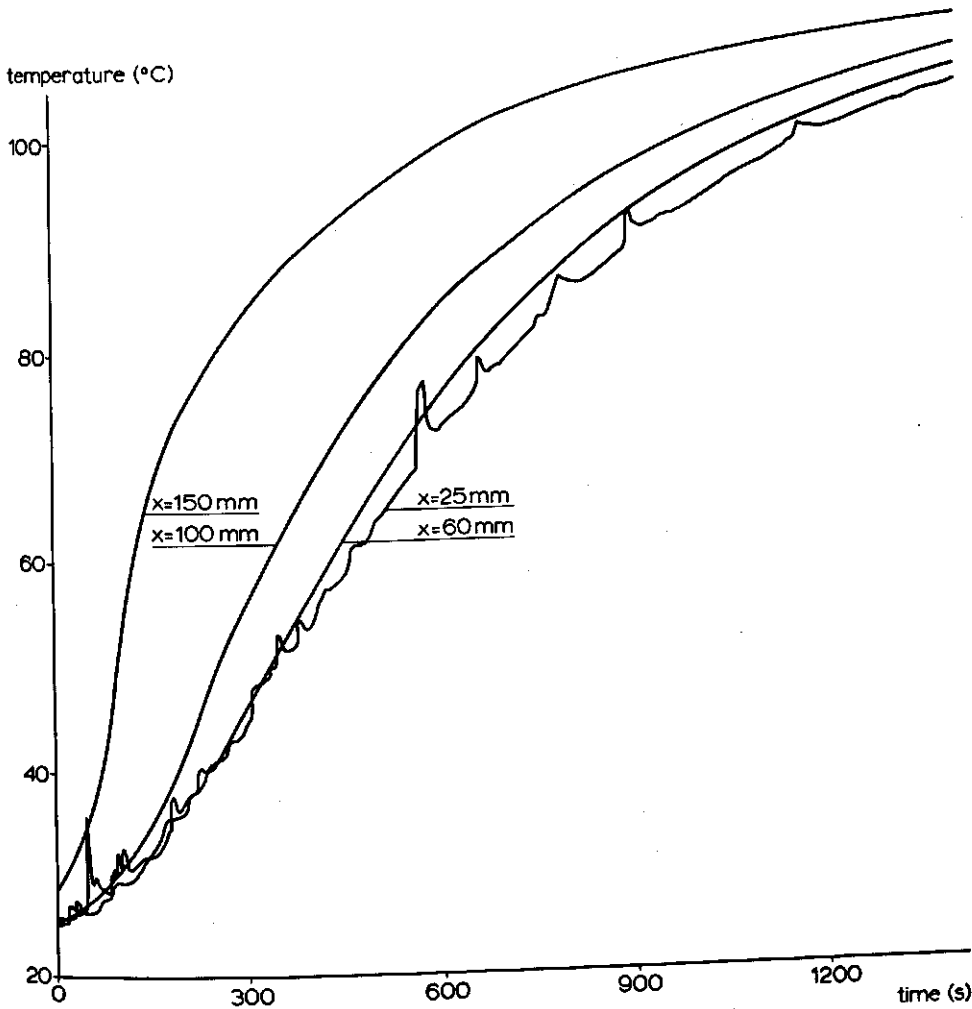
Fig. 23. Temperature courses recorded at four different levels (x) in silicone fluid F111/100, heated in the half-cylindrical container. Total liquid height 180 mm, initial temperature ca. 25° C and steam temperature 115° C.

Rayleigh number of 10^7 the flow will even be turbulent. The turbulent flow patterns as observed by Nielsen & Sabersky agree rather well with the results from our flow visualization.

We still have to discuss the correspondence of flow patterns in a half cylinder, as used in our flow visualization, with those in a complete cylinder. The desired correspondence was expected to be warranted by the special construction of the half-cylindrical container as described in Section 4.1.2. In the half-cylindrical container some observations were made which could give an indication of the pursued correspondence. First, as well as in the complete cylinder, some radial temperature profiles were determined. Here too these profiles were essentially flat. Furthermore, some infrared photographs of the free liquid surface were made

47

during heating of silicone fluid F111/100. A photograph of such a thermal picture is given in Plate 5. On this photograph the free liquid surface is visible as a crescent moon within a dark half circle. The dark line at the left is the boundary of the forewall. Outside the half circle (caused by a somewhat colder gasket) part of the heated frame of the half-cylindrical container is seen. This picture shows that at the liquid surface the temperature is decreasing from wall to centre. From the form of the isotherms (lines of equal darkness) we may assume cylinder symmetry to prevail. (The dark lines in radial direction are thermocouples above the liquid.) The foregoing supports the supposition that complete correspondence exists between the flow patterns in the half and in the full cylinder.

4.3.3 Laser-doppler measurements

From the photographs of Plate 4 the thickness of the boundary layer flow and the liquid velocities can be estimated. In the upper part of the container the thickness of the boundary layer flow was estimated on 4 to 5 mm. From the length of the streaks in the downward core flow an estimate can be made of the average
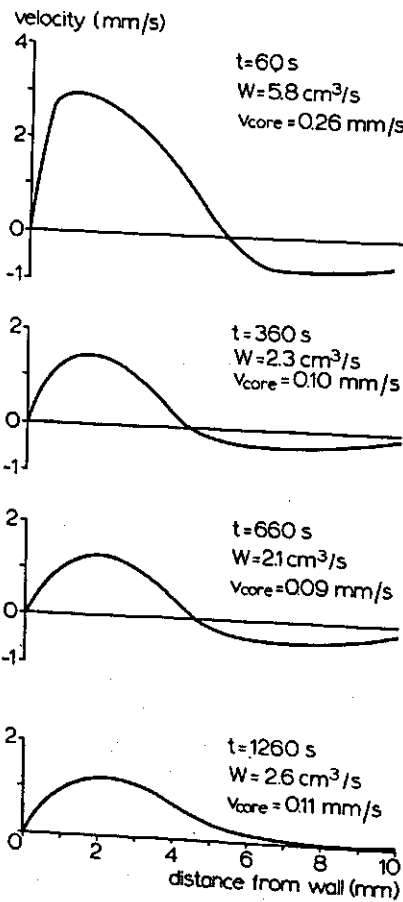
Fig. 24. Velocity profiles measured with laser-doppler velocimeter in silicone fluid F111/100 at sidewall at height $x = 100$ mm. Velocity profiles are shown at four different times after start of heating. Total liquid height 180 mm, initial temperature 30° C and steam temperature 107° C.

48

liquid velocity in the boundary layer by using Equation (33).

After 300 s: $\bar{v}_c = 0.2$ mm/s and $\bar{v}_{bl} = 2$ mm/s
After 1800 s: $\bar{v}_c = 0.1$ mm/s and $\bar{v}_{bl} = 1$ mm/s.

These velocities are much smaller than those reported for the initial period. This can be understood from the much larger temperature differences in the initial period.

The thickness of the boundary layer and the velocities in it were studied in more detail with a laser-doppler velocimeter. The readout of the laser-doppler meter showed that the boundary layer flow was essentially laminar. Rayleigh numbers were calculated to be of the order of 10^7 to 10^8. Fig. 24 gives the velocity profiles at the sidewall at a height of 100 mm at 4 different times after start of heating. Fig. 25 represents the velocity profiles measured at height $x = 50$, 100 and 160 mm at time $t = 360$ s. In Fig. 24 and 25 also are indicated the total boundary layer flow rate (assuming a full cylinder), W, obtained by graphical integration, and the downward velocity in the core as calculated from Equation (33). At $x = 50$ mm there is no regular boundary layer flow; comparison with the flow visualization experiments shows that this is still in the eddy region. Thus bottom heating plays an important role, which results in eddies causing the irregular profiles. At $x = 100$ and 160 mm more regular velocity profiles were observed.

In isothermal surroundings the boundary layer flow rate should increase with increasing distance from the bottom (Eckert, 1966 and Ostrach, 1953). However, due to the non-isothermal core here a flow reversal occurs (see Section 3.3). This will cause a decrease of the growth of the boundary layer. From $x = 50$ mm to

velocity (mm/s)

x = 160 mm
W = 2.6 cm³/s
v_{core} = 0.11 mm/s

x = 100 mm
W = 2.3 cm³/s
v_{core} = 0.10 mm/s

x = 50 mm
W = 5.8 cm³/s

distance from wall (mm)
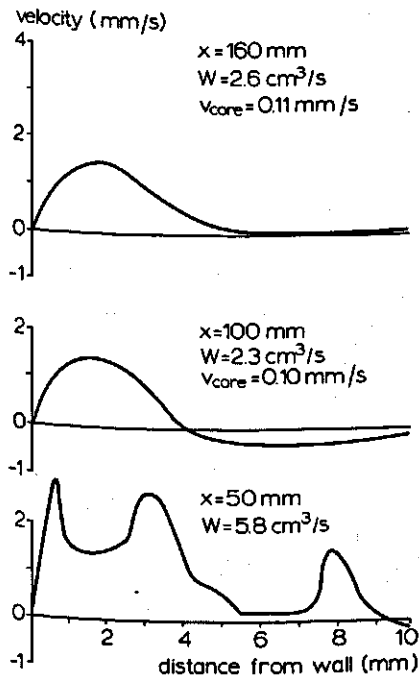
Fig. 25. Velocity profiles measured with laser-doppler velocimeter in silicone fluid F111/100 at sidewall at three different heights, 360 s after start of heating. Total liquid height 180 mm, initial temperature 30° C and steam temperature 107° C.

49

$x = 100$ mm there is a strong decrease of the boundary layer flow rate, between $x = 100$ mm and 160 mm the growth is negligible. In this connection we have to remember, that at $x = 50$ mm there is no real boundary layer flow, the upward flow rate here originates from bottom heating. From Fig. 24 we conclude that at $x = 100$ mm initially the boundary layer flow rate decreased rather strongly, while after about 360 s the flow rate remained roughly constant. From Fig. 24 and 25 a boundary layer thickness of about 5 mm is observed. The downward velocities in the core, which were calculated assuming plug flow, are smaller than the measured downward velocities. However, we think not too much importance must be attached to this fact, because the accuracy of the measurements is of the same magnitude as the downward velocities. Likewise the flow rates in Fig. 25 from $t = 360$ s to 1260 s were not considered to differ significantly, the differences in W being of the same magnitude as the accuracy of the measurements.

If we compare the estimations of flow velocity and boundary layer thickness made from flow visualization, with the values measured by the laser-doppler method, we see a rather good agreement.

4.3.4 Influence of liquid height

In the previous sections flow patterns and temperature profiles were described for a liquid height of 180 and 200 mm. Some measurements were done at other liquid heights too. Fig. 26 shows isochronic axial temperature profiles at four different times for three different total liquid heights. For smaller liquid heights the uniform temperature region in the lower part of the container is smaller. This is most marked at earlier stages, later on the differences decrease. Further it is seen that the smaller the liquid height the steeper the temperature gradient in the upper part of the container.

For a better comparison the axial temperature profiles are redrawn in dimensionless form in Fig. 27. The dimensionless temperature has been plotted along the horizontal axis and the dimensionless height above the bottom along the vertical axis. The shape of the dimensionless temperature profiles is not much influenced by the liquid height. The temperature profiles for the lower liquid heights are somewhat shifted to higher temperatures. This means that heating rate increases when the liquid height is reduced. This effect is caused by the increase of the ratio between heated surface and liquid volume at decreasing liquid height (see Eqn 5.) Or interpreting Fig. 26, we see that about the same bottom heating rate is available to heat a much smaller eddy region.

Plate 6 shows flow patterns for a liquid height of 100 mm. Essentially these flow patterns correspond with those of Plate 4 for a liquid height of 180 mm. In Plate 6 especially at later times the flow reversal in the boundary layer at the sidewall can be seen clearly. In Fig. 28 the height of the eddy region is plotted as a function of time for a liquid height of 180 mm and 100 mm. At a liquid height of 100 mm the equilibrium height is reached somewhat earlier than at a liquid height of 180 mm. This tendency agrees with the effect of faster heating, observed earlier, for lower liquid heights. Strikingly the ultimate equilibrium height is almost equal for both cases. This can be understood by assuming that the eddy region is mainly heated

50
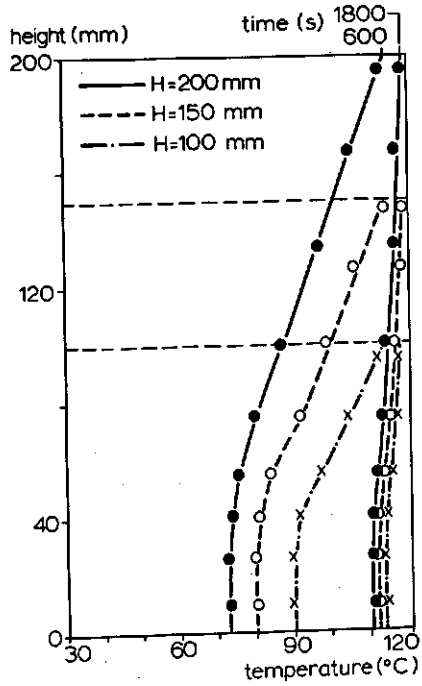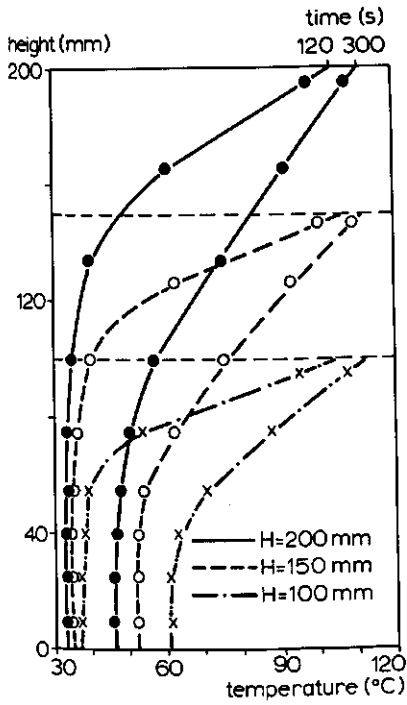
Fig. 26. Axial temperature profiles for silicone fluid F111/100 for three different total liquid heights at four times. Times are indicated at upper horizontal axis. The indicated times also hold for the axial temperature profiles presented for $H = 150$ mm and 100 mm.
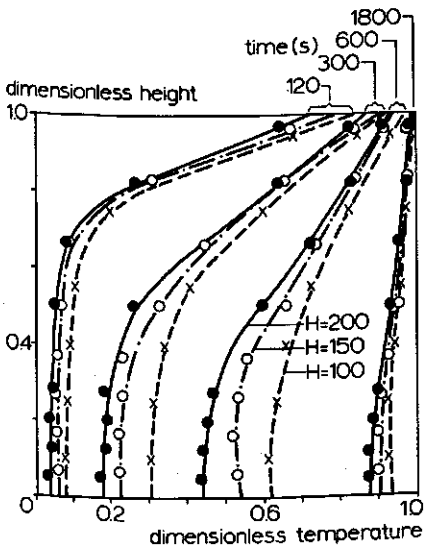
Fig. 27. Dimensionless axial temperature profiles for silicone fluid F111/100 for three different total liquid heights at four times. Dimensionless height $= x/H$, dimensionless temperature $= (T - T_0)/(T_a - T_0)$, $T_0 = 30°$ C, $T_a = 120°$ C.

51

height of eddy region (mm)
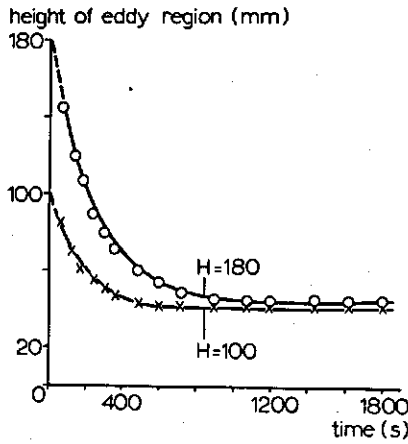
Fig. 28. Height of eddy region as function of time for two different total liquid heights, for silicone fluid F111/100.

from the bottom, while the stratified core in the upper part of the container is mainly heated as a result of boundary layer heating at the sidewall (see Section 4.2). If the liquid height in the container is reduced the ratio between bottom heating and sidewall heating will be increased. This will result in the eddy region forming a larger part of the container contents. In Chapter 6 more attention will be paid to this phenomenon.

4.3.5 Influence of initial temperature difference

I also investigated the influence of the initial temperature difference $\Delta T_0 = T_w - T_0$ on the temperature profiles. Two initial temperature differences were used, $\Delta T_0 = 90°$ C and $\Delta T_0 = 60°$ C. In both cases the steam temperature was 120° C. In Fig. 29 the dimensionless axial temperature profiles are drawn for both
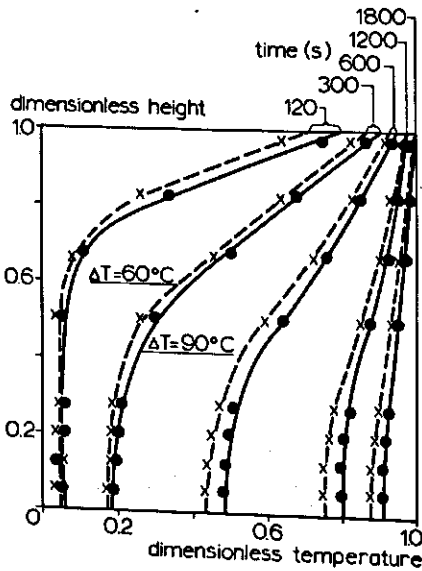
Fig. 29. Dimensionless axial temperature profiles for silicone fluid F111/100 for two initial temperature differences. Steam temperature 120° C. Dimensionless height $= x/H$, dimensionless temperature $= (T - T_0)/(T_s - T_0)$.

52

temperature differences, for a liquid height of 200 mm. The shape of the profiles shows a good correspondence. From the profiles one concludes that for $\Delta T_0 = 90°$ C the heat transfer to the liquid per unit of temperature difference (K) is a little bit higher than for $\Delta T_0 = 60°$ C. This means a somewhat larger heat transfer coefficient from the wall to liquid. This would be in accordance with the assumption that the Nusselt number is governed by the Rayleigh number:

$$Ra = \frac{(\tfrac{1}{2}D)^3 g \beta \, \Delta T_0}{\nu^2} \cdot \frac{\nu}{\alpha} = Gr \, Pr$$

Inserting ΔT_0 and the physical properties at the average temperature $\tfrac{1}{2}(T_w + T_0)$ we obtain

ΔT_0 (°C)	Ra —
90	1.02×10^8
60	0.77×10^8

The same effects were found for liquid heights of 100 and 150 mm.

4.4 Flow patterns and temperature profiles for water

In Plate 7 photographs of the flow patterns of water are shown. The first photograph shows the flow pattern after 15 s, clearly we are still in the initial period here. An upward boundary layer flow can be seen at the sidewall. Below the free liquid surface in the centre a plume of heated liquid shows up. In this plume the flow is unstable and inclines to turbulence. Such a liquid plume in the centre, was also reported by Schwind & Vliet (1964). Below this plume a region is to be seen with a slow laminar downward flow.

On the second photograph, 45 s after the start of heating, the flow in the core is unstable and hardly any difference can be seen between downward core flow and the eddy region. A boundary layer flow could only be indicated on the first photograph, it does not appear on the next pictures. Visual observations of the flow however, showed the existence of a boundary layer flow. The thickness was estimated on about 4 mm and the liquid velocities to vary from 3 cm/s initially to about 1 cm/s towards the end. Between boundary layer flow and core eddies could be observed. The photographs do not show a regular downward flow in the core, the flow tends to be turbulent. As heating proceeds the flow in the core establishes and gradually shifts to a more uniform downward flow. The Rayleigh number was calculated to be 10^9 to 10^{10}. According to Cheesewright (1968) the flow should then be of the 'transitional' type. Indeed the core flow shows the characteristics of this type of flow, that could be indicated as 'unquiet laminar'.

By using the laser-doppler method velocity profiles in the boundary layer at the sidewall were determined. From the velocity fluctuations it was concluded that the boundary layer flow was turbulent. By smoothing the fluctuations the velocity profiles of Fig. 30 and 31 were obtained. In these figures are also given the total flow rate of the boundary layer (assuming a full cylinder), W, obtained from

53
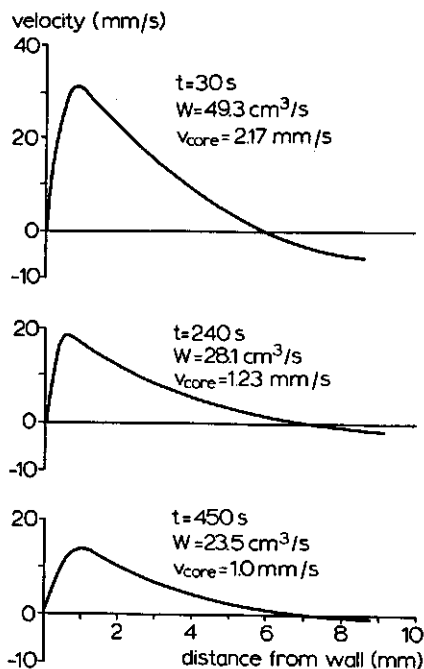
Fig. 30. Velocity profiles measured with laser-doppler velocimeter in water at sidewall at height $x = 100$ mm. Velocity profiles are shown for three different times after start of heating. Total liquid height 180 mm, initial temperature 30° C and steam temperature 107° C.
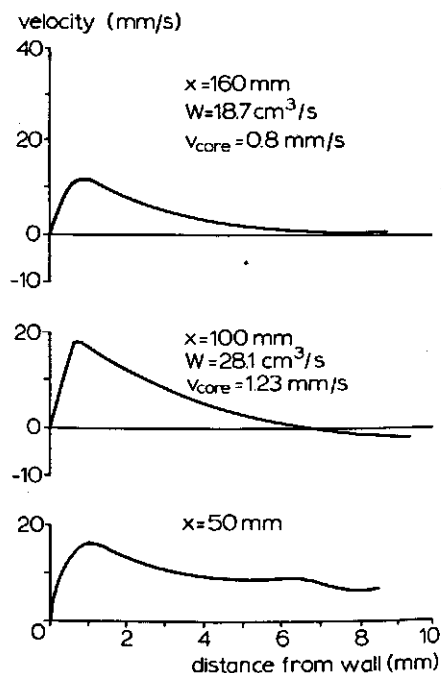
Fig. 31. Velocity profiles measured with laser-doppler velocimeter in water at sidewall at three different heights, 240 s after start of heating.

graphical integration of the velocity profiles, and the downward velocity, v_c, calculated from Eqn (33). Fig. 30 and 31 are mainly analogous to those for silicone fluid F111/100, presented in Fig. 24 and 25. Fig. 31 again shows that in the eddy region at $x = 50$ mm no regular boundary layer flow exists. Between $x = 100$ and 160 mm the boundary layer flow rate, W, reduces considerably, obviously caused by a flow reversal due to the temperature gradient in the core (see Fig. 32). From Fig. 30 a decrease of the boundary layer flow rate with time can be noted. Especially initially this decrease is rather strong. From Fig. 30 and 31 a boundary layer thickness of about 6 mm can be estimated, this is more than was visually observed. However, due to the turbulent nature of the flow it is difficult to make a reliable visual estimation of the boundary layer thickness. The thickness of the boundary layer is of the same order as for silicone fluid F111/100. Because the Prandtl number for silicone fluid is much higher, the hydrodynamic boundary layer for water should be smaller than for silicone fluid, if the flow were laminar in both cases (Ostrach, 1953). However, as observed by Cheesewright (1968) for turbulent flow the thickness of the hydrodynamic boundary layer is

54

larger than for the laminar case. From this the nearly equal thickness of the boundary layer for both liquids in our situation can be understood.

As done for silicone fluid F111/100, radial and axial temperature profiles were determined. It was found that here too the radial temperature profiles were essentially flat. From flow visualization the downward core flow can be supposed to be more or less plug flow, in spite of its unstable nature. On account of this a flat temperature profile is expected, see Section 4.3.1. Axial isochronic temperature profiles were determined for three different liquid heights. Fig. 32 shows the axial temperature profiles at four different times. The shape of the profiles is similar to those reported for silicone fluid. The temperature gradient in the upper part, however, is less steep than for silicone fluid. For water the liquid velocity in the boundary layer flow is much higher than for the much more viscous silicone fluid. Therefore, with water, the liquid leaving the boundary layer on top is less heated than in the former example. As liquid is continuously piled up in the core a less pronounced temperature gradient is built for water. Moreover, as a result of lower viscosity and consequently less pure plug flow in the core, some additional heat exchange may occur by axial mixing.

If the axial isochronic temperature profiles for the three different liquid heights are plotted in dimensionless form, like in Fig. 27 for silicone fluid F111/100, they are again essentially similar for all three heights.
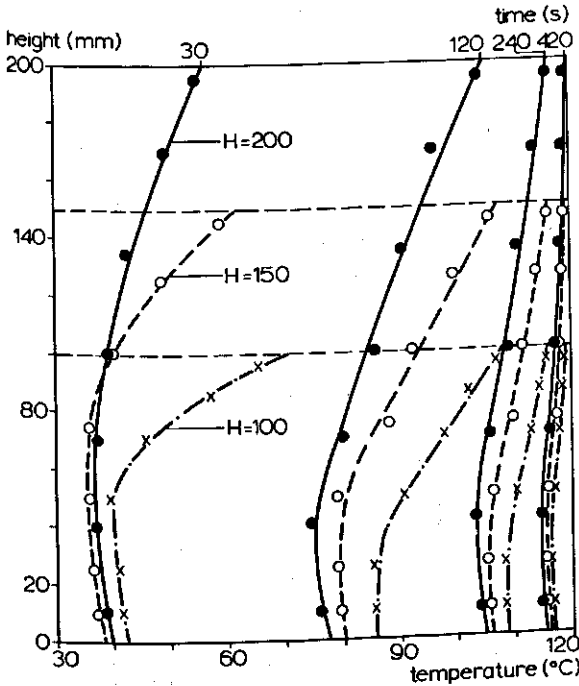
Fig. 32. Axial temperature profiles for water for three different total liquid heights. Times are indicated at upper horizontal axis. The indicated times also hold for the axial temperature profiles presented for 150 mm and 100 mm.

55

4.5 Flow patterns and temperature profiles for very viscous silicone fluid

The silicone fluid studied, silicone fluid F111/10000, had a kinematic viscosity of about 10^{-2} m²/s at 25° C (see also Appendix C). The heating of this liquid proceeds rather slowly. In Fig. 33 flow patterns are given for three different times during heating. These pictures were traced from a series of photographs. The photographs are not reproduced, as they were of poor quality. The silicone fluid was somewhat turbid, while at a later stage of heating a large number of air bubbles at the front glass wall disturbed the picture. From the length of the streaks on the photographs an estimate was made of the flow velocity. To get streaks of sufficient length the exposure times of the photographs were 20 to 40 s. After 120 s the boundary layer flow at the sidewall had a thickness of about 25 mm and a mean velocity of about 0.5 mm/s. During heating the thickness of the boundary layer decreases and stabilizes at about 15 mm. From Eqn (33) it could be calculated that at:

$t = 600$ s $\qquad \bar{v}_{bl} = 0.35$ mm/s $\qquad \bar{v}_c = 0.15$ mm/s

$t = 1800$ s $\qquad \bar{v}_{bl} = 0.25$ mm/s $\qquad \bar{v}_c = 0.10$ mm/s

These velocities are so small that practically no motion can be detected by visual observation.

Up to about 600 s the flow pattern is similar to that for silicone fluid F111/100. From then a rather strong flow to the centre can be seen just below the liquid surface. At the centre this flow goes in a downward direction. On the photographs in the centre just below the liquid surface the formation of a bulge can be observed. Probably this anomaly is caused by the combination of very high viscosity and the disturbing influence of the flat front wall. At the bottom there is no real eddy region here. Only incidentally does an eddy of considerable size rise from the bottom, preferably in the centre. Such eddies reach a height of about 40 % of the total liquid height. The flow velocities in these eddies are of the same magnitude as those in the boundary layer flow. In Fig. 34 the temperature courses

t = 180 s   t = 480 s   t = 1800 s
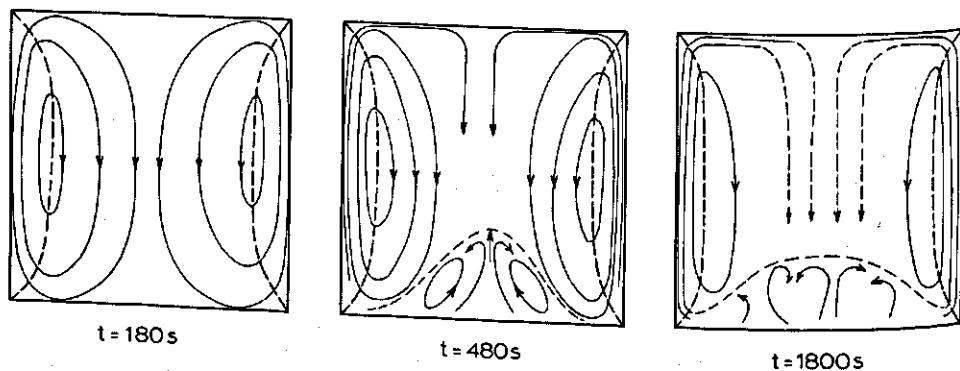
Fig. 33. Flow patterns for silicone fluid F111/10000 for three different times. The pictures are reproduced from photographs of the flow patterns. Total liquid height 180 mm.
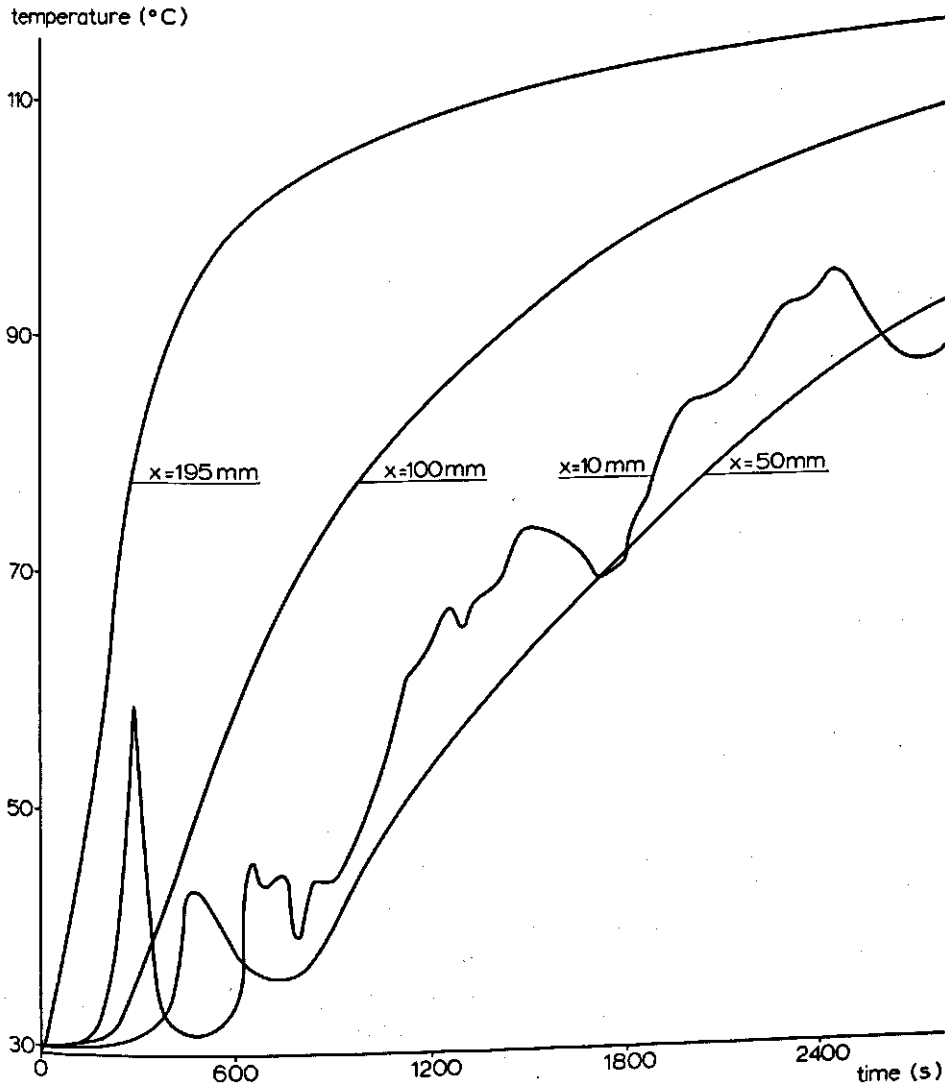
Fig. 34. Temperature courses recorded at four different levels (x) on the central axis for silicone fluid F111/10000, heated in the half-cylindrical container. $H = 180$ mm, $T_0 = 30°$ C and $T_a = 115°$ C.

at four different heights along the vertical axis are shown. The thermocouple 10 mm from the bottom recorded considerable temperature fluctuations. These fluctuations correspond with the occurrence of eddies. In Fig. 35 axial isochronic temperature profiles are shown at four different times. The temperature courses measured by the thermocouples in the lower part of the container (see Fig. 34) were smoothed to get the axial temperature profiles.

In the lower part of the container, from Fig. 35, the existence of a kind of cold point could be deduced. On the vertical axis a minimum temperature is found at
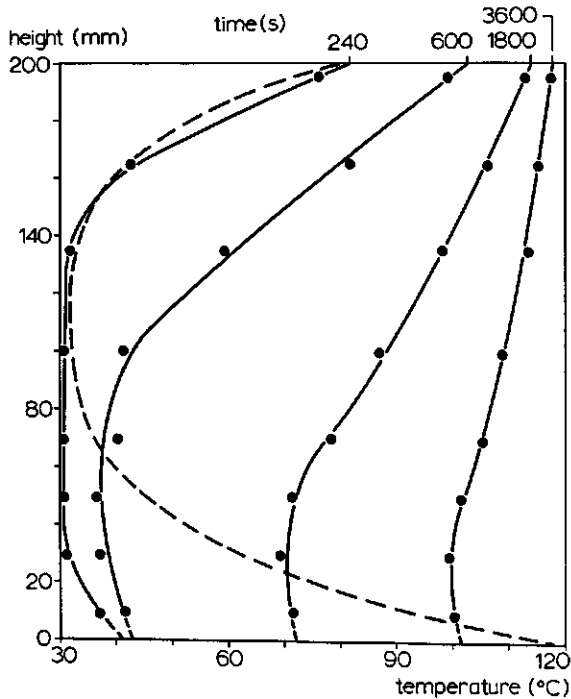
Fig. 35. Axial temperature profiles for heating silicone fluid F111/10000 at four different times. Calculated axial temperature profile for pure conduction heating at $t = 3600\,s$ is added for comparison (broken curve).

about 20 to 30 mm from the bottom. This suggests that the influence of eddies is much less important than for lower viscous liquids. This corresponds with our observation of the flow pattern. In Fig. 35 for $t = 3600\,s$ the axial isochronic temperature profile for conduction heating is also drawn. This axial temperature profile was calculated with the method indicated in Appendix D. It is obvious that, though the flow velocities are very small, convection plays the major role in heating this very viscous liquid. The liquid is mainly heated at the sidewall, which results in the stratification observed in the upper part of the container. It can be calculated from the estimated flow velocities that in 3600 s all the liquid passed the boundary layer at the heated sidewall about two times. The whole liquid was then heated to above 100° C. It can be expected that after about three circulations the liquid was nearly heated to the wall temperature.

Like for the other liquids the axial temperature profiles were determined for three different total liquid heights and two initial temperatures. By plotting these profiles in dimensionless form they again appeared to be similar for all cases.

4.6 Discussion and conclusions

From a comparison of simultaneous bottom and sidewall heating with only sidewall heating, it can be concluded that the influence of bottom heating is very

58

important. With only sidewall heating a boundary layer flow at the wall and a stratified core can be distinguished in the container. As a result of additional heating via the bottom, the core is divided in a stratified region in the upper part and an unstratified region in the lower part of the container. The stratified region corresponds with the downward laminar core flow, while the unstratified region corresponds with the eddy region. The eddy region has a nearly uniform temperature due to rigorous mixing by eddies, originating from the heated bottom. It can be observed how the flow pattern and the temperature distribution mutually affect each other. Further the flow pattern has a transient character. Initially the ratio between the height of stratified and unstratified region is changing. After some time, however, an equilibrium is achieved. During the remainder of the heating process the ratio between both remains unchanged. As will be shown in Chapter 6 the volume-ratio of stratified and unstratified region during this quasi-steady state is roughly proportional to the area-ratio of sidewall and bottom.

From the flow visualization results, especially for silicone fluid F111/100, I conclude there is a flow reversal in the boundary layer flow. This reversal is caused by the stratified core. This is in agreement with the analytical studies on natural convection in a thermally stratified environment, referred to in Section 3.3.

The boundary layer velocity profiles, determined with the laser-doppler velocimeter do confirm the visually observed flow phenomena. However, due to problems when using the laser-doppler method in a transient, non-isothermal system, the results of the laser-doppler measurements are rather qualitative than quantitative. Difficulties in using the laser-doppler method are described in Appendix B. Yet a comparison was made between the measured velocity profiles and velocity profiles for similar situations found in literature. Only very few experimentally determined velocity profiles of boundary layers for natural convection in a stratified environment are known. As far as I know only Fujii (1974) did some experiments in water, while Cheesewright (1968) reported more extensively on a number of experiments in air. I compared the velocity profiles, measured in water, with some velocity profiles from Fujii. Fujii reported a good agreement between experimental and calculated velocity profiles. In Fig. 36 our experimental velocity profiles at $t = 30$ s and $t = 450$ s for a height of 100 mm from the bottom (see Fig. 30) are compared with the velocity profile calculated by Fujii for heating water under similar conditions. However, the experiments of Fujii were done at a lower temperature level: $T_w = 32°$ C and $T_0 = $ ca. 22° C. Therefore he assumed for water a Prandtl number of 6.5. I applied $T_w = 107°$ C and $T_0 = 30°$ C, so I assumed a Prandtl number of 2.0 to 2.5 (based on mean temperature). From Fig. 36 it can be seen that the experimental thickness of the hydrodynamic boundary layer is about twice that predicted analytically by Fujii. Now it must be noticed that Fujii made his analysis for laminar conditions. But in our experiments, as already mentioned in Section 4.4, the boundary layer flow tended to be turbulent. More precisely, according to Cheesewright (1968), the boundary layer flow here should be of the transitional type. Based on the results for air, reported by Cheesewright, it can be expected that turbulence causes a broadening of the boundary layer flow. From these considerations the difference between the velocity profiles in Fig. 36

59
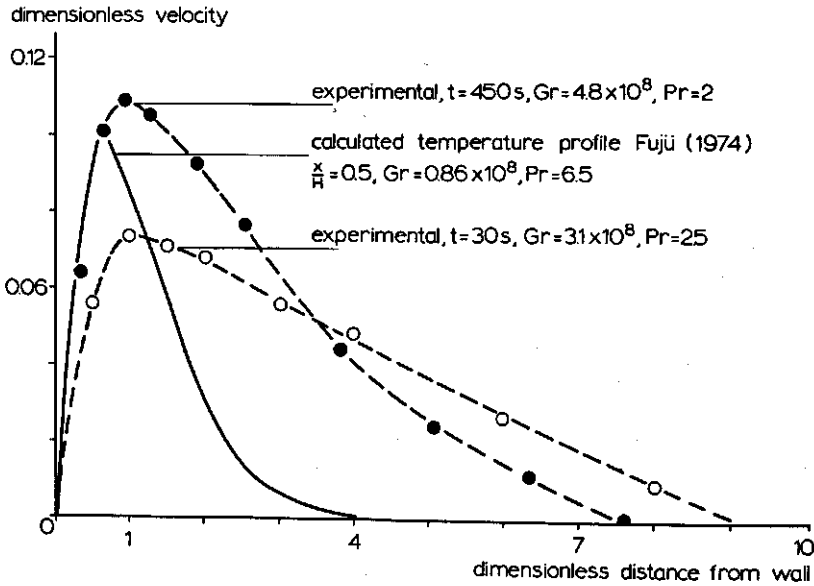
Fig. 36. Comparison of dimensionless velocity profiles for water at $x = 100$ mm, measured with laser-doppler velocimeter, with calculated temperature for water from Fujii (1974).

could be understood. It must be pointed out, however, that the maximum velocities of the profiles are of the same magnitude.

For liquids with a Prandtl number as high as for silicone fluid F111/100, as far as I know, no experiments under similar conditions are reported in literature. Analytical velocity profiles reported for natural convection in a stratified environment are restricted to a Prandtl number as high as 10. Therefore I compared velocity profiles measured for silicone fluid F111/100 (Pr ca. 300) with those predicted analytically by Ostrach (1953) for $Pr = 100$ and $Pr = 1000$, for natural convection in an isothermal environment. It appeared that the agreement between the measured profiles and those given by Ostrach was rather poor. The measured maximum velocity was about four times less than predicted by Ostrach, while the thickness of the boundary layer from Ostrach was much larger than in my results. Obviously the stratified core has a considerable influence on the boundary layer flow for large Prandtl numbers. For a better understanding of this phenomenon an extensive study should be made, both analytically and experimentally, of natural convection boundary layers in non-isothermal surroundings for high Prandtl numbers. As this was beyond the scope of this thesis the discrepancies between my experiments and the analytical results of Ostrach are not discussed further.

5 Experimental determination of heat transfer rate

For a rapid calculation of heating times (e.g. for design purpose), heating rates of liquids in containers may be conveniently characterized by heat transfer coefficients. Relevant data, however, are scarce. In Section 3.1 the parameters governing the heat transfer rate, were determined from a dimensional analysis. This resulted in:

$$\dot{Nu} = f\left(\frac{H}{D}, Gr, Pr, \tau\right) \qquad Pr > 1 \tag{34}$$

In Section 2.3.3 (Fig. 5) dimensionless correlations for heat transfer to liquids in containers, found by different authors, were discussed. All authors, quoted there, considered a quasi-steady state, during which the heat transfer coefficient was essentially constant. They therefore gave correlations which were not time dependent. Furthermore, all quoted authors stated that, by choosing an appropriate characteristic length in the Grashof number, the height to diameter ratio of the container can be omitted in the final relation. An objection to the work quoted above is that it covers only the H/D ratio range from 0.75 to 2.0. Another objection specifically to the work of Evans & Stefany (1966) is that completely filled containers heated at all sides were considered. Thus heat transfer through the top cover cannot be neglected as usual.

In my investigation I have tried to cover the H/D range from 0.25 to 2.0 which corresponds with commonly used food containers. The Prandtl number ranged from 5 to 80000, covering liquids with strong diverging viscosities and the Grashof number was chosen so as to correspond with practical heating conditions.

5.1 Method for determination of heat transfer coefficient

A heat transfer coefficient from container wall to liquid may be defined by the following equation:

$$hA_c(T_w - T) = V_c\rho c_p \frac{dT}{dt} \tag{35}$$

This can be rewritten as:

$$h = -\frac{V_c\rho c_p}{A_c} \cdot \frac{d \ln \dfrac{T_w - T}{T_w - T_0}}{dt} \tag{36}$$

If $\ln\{(T_w - T)/(T_w - T_0)\}$ is plotted versus time, the heat transfer coefficient can be

derived from the slope of the curve. If we use this method the temperature of the liquid, T, should be defined as the bulk (i.e. calorimetric mean) temperature. Now the problem arises how to measure the bulk temperature or a representative temperature that corresponds with it. Evans & Stefany (1966) used a technique first applied by Schmidt (1956) to totally-filled spheres. In this technique the container is connected to a small-diameter glass expansion tube. The thermal expansion of the liquid is used to indicate its averaged temperature, the container is effectively the bulb of a liquid-filled thermometer. A disadvantage of this method is that the container has to be filled completely, thus no head space is present. That means that: (a) the liquid in the container contacts the top cover of the container, causing an enhanced heat transfer from top cover to liquid, so the common supposition that heat transfer through the top can be neglected, is not valid here; (b) the liquid flow is influenced by the non-free liquid surface, which could also affect the heat transfer. Jowitt & Mynott (1974) used the same method as Evans & Stefany, but eliminated the first objection by soldering an inverted empty can to the top of the test can, thus simulating an insulating headspace. The possible influence of the non-zero shear stress at the liquid surface, however, still exists.

Now it is questionable whether we really need the exact bulk temperature for a determination of the heat transfer coefficient. For conduction heating of an object at a constant ambient temperature, the logarithmic dimensionless temperature plotted versus time gives straight lines that run parallel for different positions in the body. This also applies to the plot of the calorimetric mean temperature of the body, see e.g. Jakob (1958). So for conduction heating the heat transfer coefficient can be simply determined from the slope of the graph of logarithmic dimensionless temperature versus time for any arbitrary position in the body. If this was also valid for convection heating too, then it would suffice to measure the temperature course at any position in the liquid, e.g. at the geometric centre of the container. For the extreme situation of a perfectly mixed liquid this is obviously true. However, for moderate convection heating, where considerable temperature gradients exist in the liquid, there is no clear evidence for the validity of such an assumption. Jowitt & Mynot (1974) determined both the bulk temperature course as well as the temperature course in the geometric centre and in the supposedly slowest heating zone, for heating water and a 60 % sucrose solution. The bulk temperature rose logarithmically for most of the heating period. The logarithmic dimensionless temperature curves at geometric centre and slowest heating zone diverged initially and converged as the container contents approached the retort temperature. The lines for the bulk temperature and the geometric centre temperature ran parallel for most of the heating period. This would justify the heat transfer coefficient being estimated from the slope of the line for the geometric centre.

I tested this assumption for the actual problem too. In Chapter 4 radial and axial temperature profiles are described for heating silicone fluid F111/100 and water. The radial temperature profiles are flat except in the vicinity of the wall. If we neglect this contribution of the boundary layer the bulk temperature of the liquid in the container can be obtained by integrating the axial temperature

62

profiles. In Fig. 37 for silicone fluid F111/100 the logarithmic dimensionless temperature is plotted against time for four different positions in the container; the same is done for the mean temperature obtained from graphical integration of the profiles of Fig. 21. Fig. 37 shows that the lines for the different positions are not entirely straight and diverge somewhat. The lag in the earliest stage of heating depends on the position in the container. This can be understood from the fact that heated liquid flowing downward in the core, first arrives at $x/H = 0.83$, where it causes a rapid change of temperature from then onwards. At lower positions somewhat more time has to pass before the first temperature rise begins. The lines for $x/H = 0.05$ and $x/H = 0.20$ practically coincide because these points are both located in the eddy region, thus in a region of a more or less uniform temperature. The same graphs were drawn for water in Fig. 38. Here lines are given for three different positions in the container and for the mean temperature obtained from graphical integration of Fig. 32.

From Fig. 37 and 38 it can be concluded that in contrast to conduction heating, the lines for the different positions do not run parallel. Because the heating mechanisms for convection heating and conduction heating are quite different this is not surprising. Actually there are no theoretical arguments that a result valid for pure conduction heating also holds true for convection heating. For conduc-
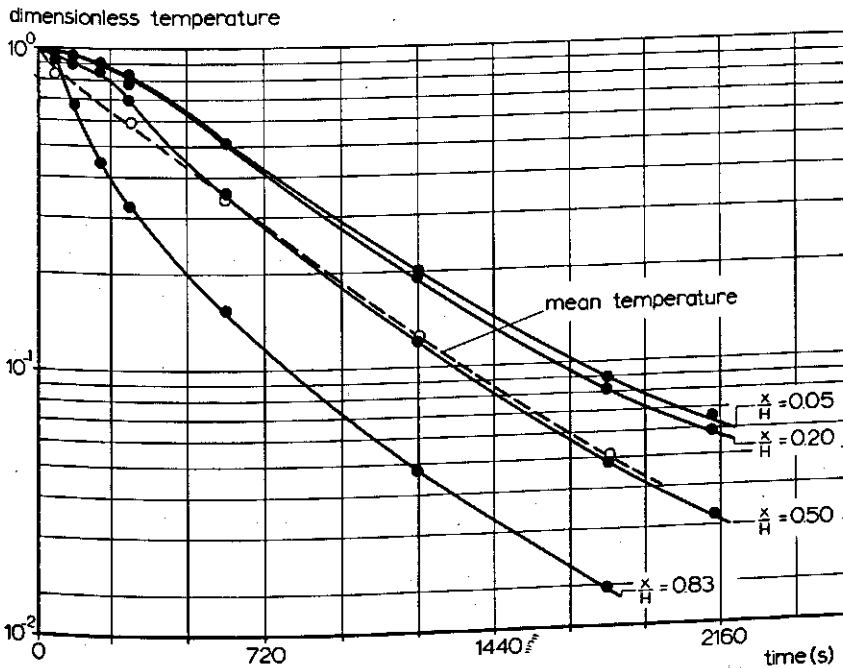
Fig. 37. Logarithmic dimensionless temperature $(T_a - T)/(T_a - T_0)$ versus time, at four different heights, for silicone fluid F111/100. The calorimetric mean temperature line obtained from graphical integration of the axial temperature profiles of Fig. 21, is also presented. $H = 200$ mm, $T_0 = 30°$ C and $T_a = 120°$ C.
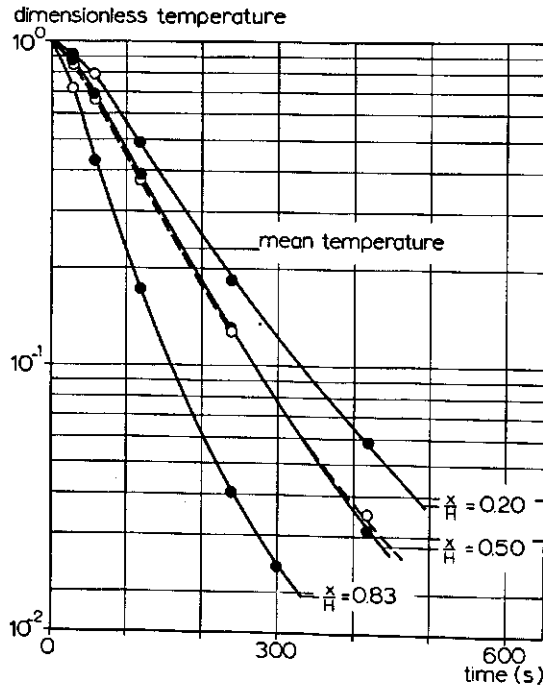
Fig. 38. Logarithmic dimensionless temperature $(T_a - T)/(T_a - T_0)$ versus time, at three different heights, for water. The calorimetric mean temperature line, obtained from graphical integration of the axial temperature profiles of Fig. 32, is also presented. $H = 200$ mm, $T_0 = 30°$ C, $T_a = 120°$ C.

tion heating usually a constant and uniform thermal diffusivity is supposed. However, if convection heating should be translated into a pure conduction heating problem, an effective thermal diffusivity has to be introduced. This diffusivity, however, is neither constant nor uniform, because the convection currents are dependent on time and position.

Fortunately in Fig. 37 and 38 the bulk (mean) temperature line mainly coincides with that for the geometric centre. If we look at the shape of the radial and axial temperature profiles, we can easily imagine that the bulk temperature may be represented by the temperature of a point close to the geometric centre. Thus it looks acceptable to use the geometric centre temperature instead of the bulk (mean) temperature for practical calculations.

If we neglect in Fig. 37 and 38 the initial heating stage and the stage for which the dimensionless temperature is less than 0.05, then the line for the geometric centre temperature (mean temperature) can be fairly well approximated by a straight line. Then this heating stage can be characterized by a constant value of the heat transfer coefficient (see Eqn 36). In food technology literature nearly always a constant f value is reported. If the material properties ρ and c_p are assumed to be constant this corresponds with a constant heat transfer coefficient (see Section 2.1).

64

5.2 Experimental procedure

A series of experiments was performed to determine the overall heat transfer coefficient from steam to liquid. Four differently sized containers and seven test liquids were used. The dimensions of the containers and the most important physical properties of the test liquids are presented in Appendix C. The geometric ratio H/D was varied by varying the liquid height in a container in the different experiments. The experiments covered the H/D range from 0.25 to 2.00. The containers were heated in a retort with condensing steam. The experimental set-up was the same as that described in Section 4.1.2. Before heating, the container with liquid was brought to the initial temperature of 20° C, 30° C or 60° C in a water bath. The heating temperature (= steam temperature) was 105° C, 114° C or 120° C. During heating the steam temperature and the temperature in the geometric centre were recorded with iron-constantan thermocouples. In a limited number of experiments the wall temperature was also measured with thin copper-constantan thermocouples which were soldered in the wall and led through sleeves in the wall over a distance of 150 mm.

For an estimation of the heat transfer from the bottom of the container some measurements were done with the laser-doppler velocimeter. In water and in silicone fluid F111/100, in the half-cylindrical container, vertical flow velocities in the eddy region at a distance of 10 mm from bottom were determined (see Section 4.1.2). From these flow velocities and from temperature fluctuations measured at the same distance from the bottom, a rough estimate of the heat flux from the bottom could be made.

5.3 Results

5.3.1 Dimensionless correlation for overall heat transfer coefficient

Following the procedure outlined in Section 5.2, I calculated a heat transfer coefficient from the temperature course in the geometric centre. Only the interval in which the curve for the dimensionless temperature versus time could be approximated by a straight line, was taken in consideration. Under practical conditions always the steam temperature will be measured and not the wall temperature. By using the steam temperature in Eqn (36), the overall heat transfer coefficient is obtained. Now the overall heat transfer coefficient is composed as follows:

$$\frac{1}{U} = \frac{1}{h_{\text{out}}} + \frac{d_w}{\lambda_w} + \frac{1}{h_{\text{in}}} \tag{37}$$

The outside heat transfer coefficient depends on the type of steam condensation. Film condensation was assumed and h_{out} was estimated at 12000 W/m² · K. For water the experimental value of U was about 1200 W/m² · K, for silicone fluid F111/100 U was about 100 W/m² · K and for silicone fluid F111/10000 about 30 W/m² · K. Obviously the heat resistance of the container wall ($\lambda_w = 120$ W/mK and $d_w = 2$ mm) can be fully neglected. According to the above mentioned data

65

for silicone fluid the heat resistance at the outside of the container can be neglected there too. But for water the outside heat resistance is about 10 % of the total heat resistance, which means that h_{in} is about 10 % higher than U. However, the overall heat transfer coefficient is of more practical interest than the partial inside heat transfer coefficient. Therefore I judged it most practical to use the overall heat transfer coefficient for further considerations.

In the calculations, the bottom of the container and the area of the sidewall in contact with the liquid were considered as the heated surface, A_c. This implies that heat transfer through the head space can be completely neglected. This, however, is not entirely correct. Due to effects of radiation and convection and conduction in the head space, a certain heat transfer from top cover to liquid surface can be expected. An estimate of the magnitude of these effects was made in Appendix E. The calculated heat transfer coefficient from the sidewall and the bottom was adjusted for the heat transfer through the head space.

Since the physical properties of the liquids used are temperature dependent, we have to decide at what temperature the physical properties should be taken. In transient processes like here, a reference temperature which is valid for the whole temperature traject is rather difficult to define. Usually in such situations the wall temperature is chosen because it is well defined, see Japikse (1973) and Pollard & Carlson (1969). I chose the steam temperature, as it is a well defined constant temperature that corresponds reasonably with the wall temperature.

For a large number of experiments, performed at the Department of Food Science, Wageningen by Schure (1972) and Holwerda (1973) a correlation of the form

$$Nu = c(Gr\, Pr)^a (H/D)^b \tag{38}$$

was tried, in which:

$$Nu = \frac{U \cdot \frac{1}{2}D}{\lambda} \quad \text{and} \quad Gr\, Pr = \frac{(\frac{1}{2}D)^3 g\beta(T_a - T_0)}{\nu\alpha} \tag{39}$$

First a regression analysis was applied to all experiments for which $H/D = 1$. This resulted in:

$$Nu = 0.31(Gr\, Pr)^{0.269} \tag{40}$$

Usually for laminar natural convection 0.25 is found as exponent for $Gr\, Pr$. The experiments with water showed $Gr\, Pr$ to be 10^8 to 10^{10}, thus probably in the transition region from laminar to turbulent. In that region a higher heat transfer coefficient than for the laminar case is to be expected. Therefore not too much importance was attached to the deviation from 0.25. Next a regression analysis was applied to $\log(Nu/(Gr\, Pr)^{0.25})$ and $\log(H/D)$ to obtain the exponent of H/D. Only a slight correlation was found between these variables (correlation coefficient -0.145), while the exponent amounted to -0.027. Thus the dependency of Nu on H/D is weak and can be neglected for most practical purposes. Now for all experiments a regression analysis was applied to Nu and $Gr\, Pr$, thus omitting the influence of the parameter H/D. This resulted in the highly significant correlation (correlation coefficient 0.995):

66
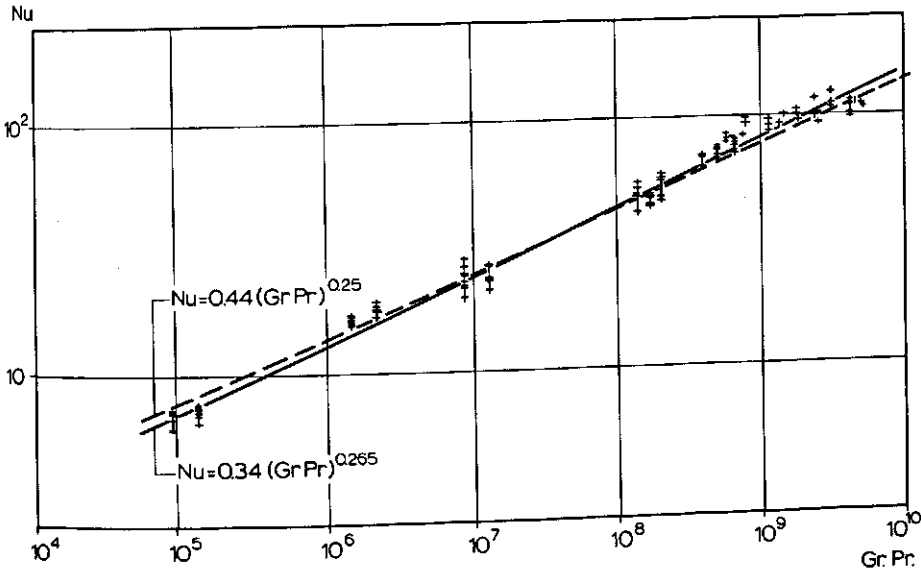
Fig. 39. Log Nu versus log $Gr\,Pr$ for all experimental runs.

$$Nu = 0.34(Gr\,Pr)^{0.265} \tag{41}$$

Fig. 39 is a logarithmic plot of Nu versus $Gr\,Pr$ for all 174 experimental runs. Fig. 39 shows the line corresponding with Eqn (41) and the line obtained if we assume an exponent for $Gr\,Pr$ of 0.25. From Fig. 39 it can be seen that my experimental results correspond reasonably well with

$$Nu = 0.44(Gr\,Pr)^{0.25} \tag{42}$$

5.3.2 Heat flux from the bottom

An estimate of the heat flux from the bottom was made from velocity fluctuations in the vertical flow in the eddy region measured with the laser-doppler velocimeter. In Fig. 40 a section of the velocity course is shown as measured in water, 10 mm above the bottom, about 40 mm behind the glass wall and 25 mm from the centreline. Smaller and more frequent fluctuations superimposed on the fluctuations shown in Fig. 40 were smoothed out. Another observation was made at which during heating the probe volume was moved from about 60 mm to about 20 mm behind the glass wall. The picture obtained was very similar to Fig. 40. From these observations it was concluded that the velocity fluctuation pattern is independent of position. By graphical integration of Fig. 40 a mean upward velocity, v_{up}, and a mean downward velocity, v_{down}, could be determined. Each integration was extended over a period of 120 s. In Table 2 the mean velocities obtained in this way for different periods, are presented.

During heating of silicone fluid F111/100 similar experiments were performed

67
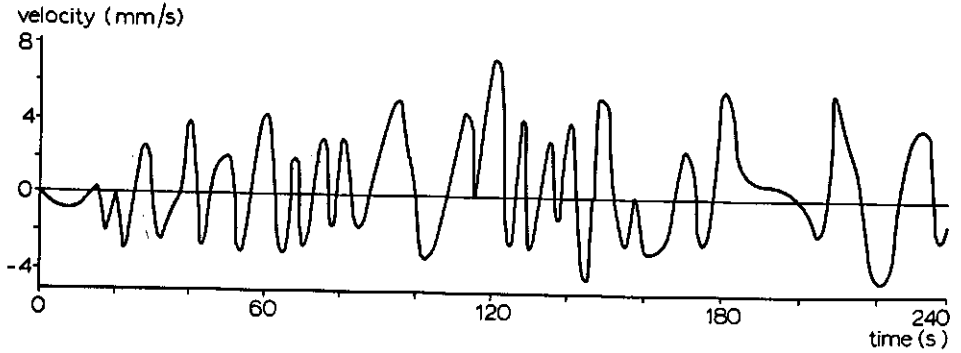
Fig. 40. Vertical flow velocities measured with laser-doppler velocimeter in the eddy region in water. Height above bottom 10 mm, 40 mm behind glass wall and 25 mm from centre line. $T_0 = 30°$ C and $T_a = 107°$C.

Table 2. Mean velocities obtained from graphical integration of flow velocities measured with laser-doppler velocimeter (Fig. 40 and 41) and comparison of heat fluxes obtained from Eqn (43) and those calculated from Eqn (44).

	Time (s)	v_{up} (mm/s)	v_{down} (mm/s)	$\bar{T}'_x$ (K)	$Gr\,Pr$	q_x (W/m²)	q_{OG} (W/m²)
Water	0–120	1.09	0.66	3.0	6×10^8	11000	27000
	120–240	1.31	0.89	2.5	6×10^8	11500	13000
	240–360	1.23	0.77	2.0	6×10^8	8400	6200
	360–480	0.61	0.79	1.5	6×10^8	4500	3600
Silicone fluid	0–540	0.49	0.14	5.0	4×10^7	2360	3910
	600–1140	0.49	0.07	2.5	4×10^7	1050	1070

as described above for water. In Fig. 41 the velocity course is shown for a period at which the probe volume was fixed. By graphical integration of Fig. 41 again a mean upward velocity and a mean downward velocity could be obtained. In Table 2 the results for the period of 0–540 s and 600–1140 s are presented.

From Table 2 it could be concluded that the upward flow rate should be larger than the downward flow rate. However, the accuracy of the laser-doppler measurements does not permit so definite a conclusion (see Appendix B).

From the observed velocity fluctuations and from observed temperature fluctuations at the same distance from the bottom an estimate of the heat flux from the bottom can be made. It can be derived (see Hinze, 1959, page 6 and Bird et al., 1960, page 375) that the mean heat flux through a level, x mm from the bottom, time smoothed over a period Δt, can be calculated from:

$$q_x = \frac{\rho c_p}{\Delta t} \int_0^{\Delta t} [v'_x(t)\, T'_x(t)]\, dt$$

(43)

68
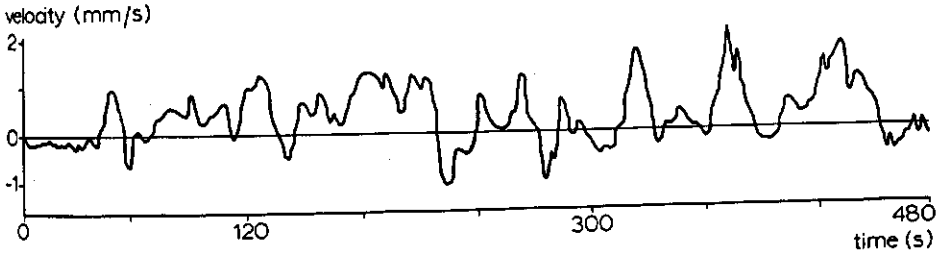
Fig. 41. Vertical flow velocities measured with laser-doppler velocimeter in the eddy region in silicone fluid F111/100. Position equal to that indicated in Fig. 40. $T_0 = 30°$ C and $T_z = 107°$ C.

in which $T'_x(t)$ and $v'_x(t)$ are the momentary temperature and velocity fluctuations, respectively. The velocity fluctuations can be obtained from Fig. 40 and 41 and the temperature fluctuations from graphs similar to Fig. 23. By evaluating Eqn (43) for the actual problem the results presented in Table 2 were obtained. It should be noted that the values of the heat flux q_x calculated from Eqn (43) are only estimates, since it is rather difficult to achieve exact values of the time-smoothed temperature fluctuations, due to the transient character of the heating process.

Finally the values of q_x obtained were compared with values for the heat flux density which were calculated from the relation of Onat & Grigull (1970), q_{oo}. They present a correlation for horizontal liquid layers heated from below:

$$Nu = 0.56(Gr\,Pr)^{0.25} \tag{44}$$

Except for the first periods the values of q_x and q_{oo} correspond rather well.

5.4 Discussion and conclusions

As shown in Fig. 37 and 38 the temperature differences decay approximately expo-nentially with time. This implies a constant overall heat transfer coefficient (Eqn 36). Evans & Stefany (1966) and Jowitt & Mynott (1974) reported similar observations. They pointed out that this result is rather surprising if, for these transient conditions, one starts from the generally accepted form of correlation for steady state natural convection. Because the continually decreasing temperature difference implies a continually decreasing $Gr\,Pr$, then the generally accepted type of correlation for steady state predicts a continually decreasing value for Nu. If the physical properties were to be evaluated at the mixed mean temperature $\frac{1}{2}(T_w + T)$ at each moment, $Gr\,Pr$ is still decreasing during the heating process, since the variation in physical properties does not compensate the decrease in temperature difference. Evans & Stefany (1966) and Jowitt & Mynott (1974) calculated the instantaneous values of both Nu and $Gr\,Pr$. Jowitt & Mynott concluded that from shortly after initiation of heating until the temperature difference decreased to about 7.5 K (initial temperature difference 84.5 K) the Nusselt number was constant and apparently independent of the Raleigh number, since the latter

69

decreased during this period. Thereafter Nu decreased proportionally to $(Gr\,Pr)^{\frac{1}{4}}$. Jowitt & Mynott suggested that this result is caused by the interaction between ascending and descending flows in the container. I think the cause can only be found in the momentary evaluation of temperature difference and physical properties. The heat transfer process is going on in the boundary layer, so the temperature difference and the physical properties should be concerned with the boundary layer and not with the bulk liquid.

When heating liquids in vertically orientated closed containers, we have to consider two differently orientated heated surfaces, namely the vertical sidewall and the horizontal bottom. For laminar natural convection at a vertical flat plate in isothermal surroundings it is generally stated (see Jakob, 1958) that

$$Nu = 0.55(Gr\,Pr)^{\frac{1}{4}} \tag{45}$$

Pollard & Carlson (1969) and Barakat & Clark (1966) reported the same proportionality from their experiments on heating of liquids in closed containers with sidewall heating only.

For natural convection in liquid layers heated from below correlations are presented by Onat & Grigull (1970) and Chu & Goldstein (1973). Chu & Goldstein reported that though the flow regime was turbulent the dependency of Nu to $Gr\,Pr$ was less than the one-third power. They found for $Gr\,Pr$ between 2.76×10^5 and 1.05×10^8:

$$Nu = 0.183(Gr\,Pr)^{0.278} \tag{46}$$

Onat & Grigull assumed laminar flow up to $Gr\,Pr = 10^8$ and stated the correlation already mentioned in Eqn (44). For $Gr\,Pr$ between 10^8 and 3×10^9 they assumed transitional flow and suggested a correlation:

$$Nu = 0.181(Gr\,Pr)^{0.31} \tag{47}$$

On account of the above it is not surprising to find for my experiments a Nusselt number proportional to the Raleigh number with a power of about 0.25.

A: $Nu = 0.77(Gr\,Pr)^{0.25}$ _van Santen (1969)
B: $Nu = 0.55(Gr\,Pr)^{0.25}$ _Evans and Stefany (1966)
C: $Nu = 0.0288(Gr\,Pr)^{0.4}$ _Kiis (1964)
D: $Nu = 0.119(Gr\,Pr)^{0.33}$ _Schmidt (1956)
E: $Nu = 0.34(Gr\,Pr)^{0.265}$ _(own experiments)
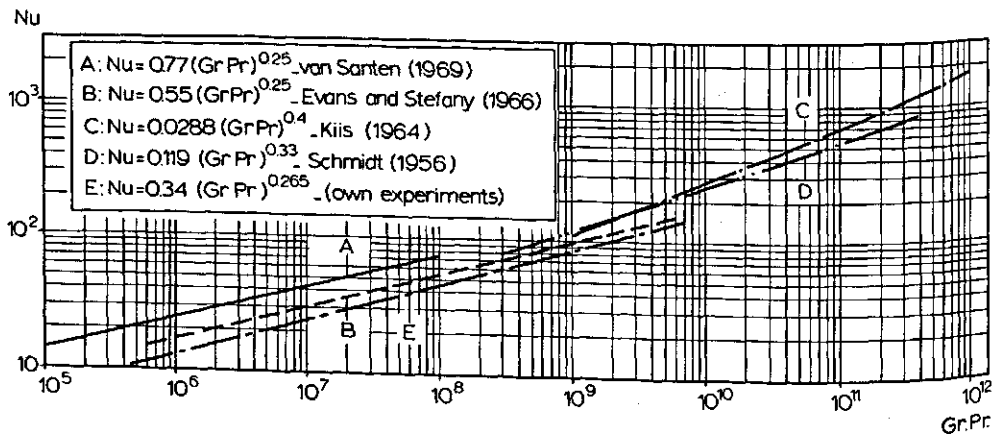
Fig. 42. Comparison of experimentally determined correlation for heat transfer coefficient, with those of other authors.

Since the Nusselt numbers and thus the heat transfer coefficients for the sidewall and the bottom do not differ much, the heat flux density will not be influenced much by changing the ratio of sidewall to bottom area, thus by changing H/D. From this it can be understood that the Nusselt number is only slightly dependent on the geometric ratio H/D.

In Fig. 42 the dimensionless correlation derived from my experiments, Eqn (41), is compared with other correlations published, dealing with heating of liquids in closed containers. The different levels of the lines can be explained from the different reference temperatures used for evaluating the physical properties and from the different definitions of the characteristic length.

6 Simplified model

In this chapter a simplified model is developed, to describe the heating of a liquid in a closed container. In Chapter 3 we investigated whether a numerical solution of the differential equations governing the actual problem was possible. But, this method did not provide reasonable results for situations where a considerable part of the heat transfer occurs through the bottom of the container. Therefore, using observed flow patterns and temperature profiles I developed a simplified model of the heating process. In this simplified model the flow pattern is considered to be known in its schematized form. The model is based on heat balances which give approximate temperature stratification profiles.

In Chapter 3 we indicated how Evans et al. (1968) and Matulevicius (1970) succeeded in developing a stratification model for sidewall heating only. For simultaneous bottom and sidewall heating, with uniform and adjustable heat fluxes at the sidewall and the bottom, a simplified analysis was provided by Vliet (1966). Vliet considered two regions, an upper thermally stratified region with an assumed time-invariant axial temperature profile and a lower unstratified region of spatially uniform temperature. The bottom heat flux is assumed to distribute homogenously over the unstratified region while the boundary layer flow at the vertical sidewall convects the energy flux from the sidewall into the thermally stratified region. For the boundary layer flow Vliet used the exact solution of Sparrow & Gregg (1958) for laminar natural convection in isothermal surroundings at a vertical wall with a uniform heat flux. From his stratification model an asymptotic unstratified layer height is predicted, which was in agreement with his experimental results. The development of the simplified model was similar to the method of Vliet (1966). However, I was concerned with a uniform temperature at the sidewall and the bottom instead of uniform heat flux. On the other hand I did not assume a time-invariant axial temperature profile since such an assumption would be contradictory to the observations given in Chapter 4. I tested the validity of the simplified model by comparing calculated temperature profiles with experimental results for water and silicone fluid F111/100.

Finally I used the results of the simplified model for an estimation of the lethality of the heating process. In process evaluation the effect of liquid movement was included. The lethality calculated in this manner was compared with the lethality calculated from a conventional, single-point, method.

6.1 Analysis of the simplified model

According to the observed temperature profiles and flow patterns in Chapter 4, it seems reasonable to distinguish between three regions within the liquid in the container. First a boundary layer flow in an upward direction at the sidewall, second a region with temperature stratification in the upper part of the container and third a region of uniform temperature in the lower part of the container.

The region of boundary layer flow is thin compared with the diameter of the container, which implies that the liquid volume of the boundary layer can be neglected in comparison with the volume of the core. Experimental data described in Chapter 4, see Fig. 22, reveal that during the heating process the height of the unstratified region reduces to an asymptotic value. In the stratified region plug flow downwards (x direction) is assumed with a velocity v_c. If the effect of thermal conduction in x direction can be neglected in comparison with the convective flow ($\alpha\, \partial^2 T/\partial x^2 \ll v_c\, \partial T/\partial x$) the thermal energy balance reduces to:

$$\frac{\partial T_c}{\partial t} + v_c \frac{\partial T_c}{\partial x} = 0 \tag{48}$$

An energy balance over the unstratified region results in:

$$\frac{q_b}{\rho c_p} - X \frac{dT_b}{dt} = 0 \tag{49}$$

The net growth of the thermally stratified region (Fig. 43) is a result of both a downward shift of the stratified liquid in the core due to boundary layer flow, and the heating of the unstratified region from the bottom. It is assumed that the vertical shift of the interface between stratified and unstratified region is determined by the requirement that the temperature at this interface at the side of the unstratified region is always equal to that (at the interface) in the stratified region.
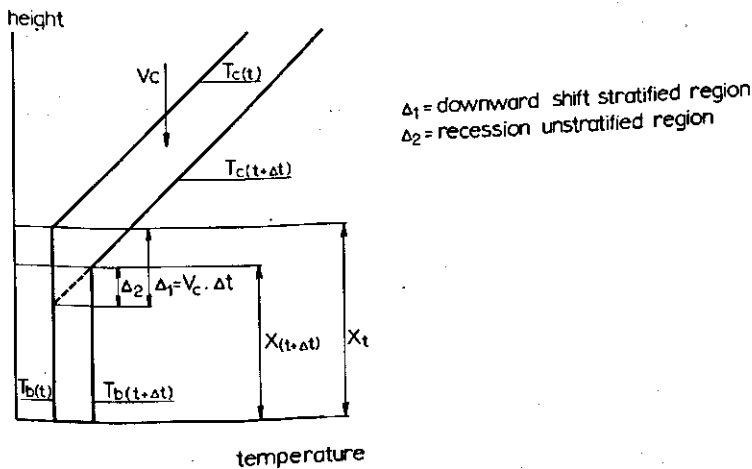
Fig. 43. Schematic temperature profiles in stratified and unstratified region at t and $t + \Delta t$. Vertical axis indicates distance from bottom, horizontal axis indicates temperature.

73

The mechanism can be understood as follows. The uniform temperature (unstratified) region in the lower part of the container is caused by the mixing activity of eddies rising from the bottom. These eddies do not penetrate in the stratified region, because they would experience here a negative buoyancy force from an environment with higher temperature. Due to the downward shift of liquid in the stratified region the temperature at the upper side of the interface between both regions will rise. At the underside of the interface the temperature rises due to heating of the unstratified region from the bottom. If the heating rate at the stratified side of the interface is smaller than at the unstratified side the eddies will be able to travel to a higher level than in the initial situation. This will cause an upward shift of the interface and succeedingly a smaller heating rate of the unstratified region. If, however, the heating rate of the unstratified region is smaller than in the stratified region, a downward shift of their common interface will occur. If the heating rates are equal the interface will be stagnant.

The increase of the stratified region during a small time increment Δt, if no bottom heating would take place, is given by the equation (see Fig. 43):

$$\Delta_1 = v_c \, \Delta t \tag{50}$$

while the decrease of the stratified region during the same time increment, if no flow in the core would occur, is given by:

$$\Delta_2 = \frac{\Delta T_b}{\Delta T_c} \Delta_1 \tag{51}$$

The net shift of the height of the unstratified region, X, in the time increment Δt would have been:

$$X_t - X_{t+\Delta t} = \Delta_1 - \Delta_2 = v_c \, \Delta t - \frac{\Delta T_b}{\Delta T_c} \, v_c \, \Delta t \tag{52}$$

So taking the limit $\Delta t \rightarrow 0$ this results in:

$$\frac{dX}{dt} = -v_c + v_c \frac{dT_b}{\partial T_c} = -v_c + \frac{dT_b}{dt}\left(\frac{v_c}{\partial T_c/\partial t}\right) \tag{53}$$

Because we assume that the temperature profile in the stratified region is linear, with slope $\partial T_c/\partial x = $ constant, then according to Eqn (48)

$$\frac{v_c}{\partial T_c/\partial t} = -\frac{1}{\partial T_c/\partial x} = \kappa$$

By introducing Eqn (49), Eqn (53) results in:

$$\frac{dX}{dt} = -v_c + \kappa \frac{q_b}{X \rho c_p} \tag{54}$$

6.1.1 Solution for constant parameter A

Eqn (54) is made dimensionless by introducing a dimensionless height, a dimensionless time and a constant parameter A:

74

$$Z = \frac{X}{H} \qquad \tau = \frac{v_c t}{H} \qquad A = \frac{\kappa q_b}{v_c H \rho c_p} \tag{55}$$

Now Eqn (54) results in the dimensionless differential equation:

$$\frac{dZ}{d\tau} + 1 - \frac{A}{Z} = 0 \tag{56}$$

We impose the initial condition:

$$\text{at} \quad \tau = 0, \quad Z = 1 \tag{57}$$

The solution for the differential equation is as follows:

$$\left. \begin{array}{ll} 1 - Z + A \ln \left(\dfrac{1-A}{Z-A} \right) = \tau & (A \neq 1) \\[2mm] Z = A & (A = 1) \end{array} \right\} \tag{58}$$

For $A > 1$ the solution has no physical significance since only values of $Z \leqslant 1$ are possible. The interpretation is, that for $A > 1$ the bottom heat flux completely predominates over the sidewall heating, so stratification cannot develop at all. So on physical grounds we have to add to the solution as presented in Eqn (58)

$$\text{If } (A \geqslant 1), \quad Z = 1 \quad \text{for all } \tau \tag{58a}$$

By Eqn (58) an asymptotic height of the unstratified region is predicted. The asymptotic value of Z is obtained by putting $dZ/d\tau = 0$ in Eqn (56) and solving for A:

$$(Z)_{\tau \to \infty} = A \tag{59}$$

In Fig. 44 the dimensionless height, Z, is given as a function of the dimensionless time, τ, for different values of the dimensionless parameter A. For each value of A an asymptotic dimensionless height of the unstratified region $Z = A$ is reached
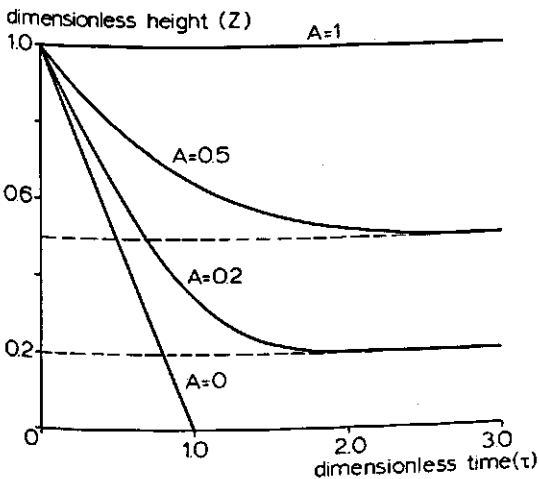
Fig. 44. Graphical representation of Eqn (58) for different values of the parameter A.

when τ approaches infinity. The value of A is proportional to the ratio of bottom heat flux to sidewall heat flux. The latter quantity enters into that ratio via v_c. The asymptotic behaviour of the height of the unstratified region agrees very well with experimental findings as reported in Chapter 4, Fig. 28.

6.1.2 Solution for variable parameter A

In practice the value of parameter A will not be constant during the whole heating process, because v_c, q_b and κ all change during heating. Thus the dimensionless height does not exactly follow a curve for constant A in Fig. 44, but crosses the curves for different A values. We will now discuss this situation in more detail.

The quantities v_c and κ are a result of the natural convection boundary layer flow at the sidewall. However, an analysis of the boundary layer flow would be difficult, because of the shape of the temperature profile existing in the core. The temperature gradient in the stratified region in the upper part of the core influences the boundary layer flow at the sidewall, a phenomenon that was discussed at length in Section 3.3. In the stratified region therefore a boundary layer analysis should be made for natural convection in non-isothermal surroundings. On the other hand, in the unstratified region a boundary layer analysis for isothermal surroundings should be applied. Obviously such a procedure will be rather complex.

For my simplified model I assumed that a natural convection boundary layer develops in the unstratified region, like in isothermal surroundings at a flat plate. For the stratified region a constant boundary layer thickness was assumed. These assumptions are confirmed to some extent by the flow visualization studies discussed in Chapter 4. I took the boundary layer flow rate in the stratified region as equal to the boundary layer flow rate at the top of the unstratified region.

The natural convection boundary layer for a constant bulk liquid temperature was analysed by Eckert (1966). He assumed a boundary layer velocity profile:

$$u = u_1 \frac{y}{\delta}\left(1 - \frac{y}{\delta}\right)^2 \tag{60}$$

with:

$$u_1 = \frac{27}{4} u_{max} \tag{61}$$

while:

$$u_{max} = 0.766 \nu (0.952 + Pr)^{-\frac{1}{2}}\left(\frac{g\beta(T_w - T_0)}{\nu^2}\right)^{\frac{1}{2}} x^{\frac{1}{2}} \tag{62}$$

The boundary layer thickness calculated with these equations is:

$$\delta = 3.93 \times Pr^{-\frac{1}{2}}(0.952 + Pr)^{\frac{1}{4}}Gr^{\frac{1}{4}} \tag{63}$$

The boundary layer flow rate follows by integration of the velocity profile over the boundary layer thickness:

$$W = \pi D \int_0^\delta u \, dy = \frac{27}{48} \pi D u_{max} \delta \qquad (64)$$

Since the boundary layer is very thin compared with the diameter of the container, the velocity in the core is related to W by

$$v_c = \frac{4W}{\pi D^2} \qquad (65)$$

. Strictly the analysis of Eckert is only correct for an equal thickness of the thermal and hydrodynamic boundary layer, so for a Prandtl number near 1. However, as I used this analysis for water, $Pr \simeq 3$, not too large deviations are expected here. According to Eckert the local Nusselt number is given by

$$Nu_x = 0.508 Pr^{\frac{1}{2}}(0.952 + Pr)^{-\frac{1}{4}} Gr^{\frac{1}{4}} \qquad (66)$$

In the model the temperature of the liquid leaving the boundary layer on top was calculated from the equation for heating a liquid flowing in plug flow along a heated flat plate:

$$T_{out} = T_w - (T_w - T_{in}) \exp\left(-\frac{hH}{W \rho c_p}\right) \qquad (67)$$

In Eqn (67) we used the flow rate, W, as calculated from Eqn (64) at the top of the unstratified region. Further we used for the heat transfer coefficient, h, interpreted as an averaged heat transfer coefficient in this example, the value of the overall heat transfer coefficient, calculated from Eqn (41).

Based on the above information a simulation model was developed. In this simulation model the heating of the liquid in the container was schematized as follows (see Fig. 45): The boundary layer is assumed to act like a heat exchanger (I), the liquid leaving this heat exchanger enters the core on top. The core is divided in two parts, an upper stratified region in which the liquid flows downwards more or less in plug flow (II) and a lower unstratified region in which perfect mixing is assumed (III). During the heating process the interface between
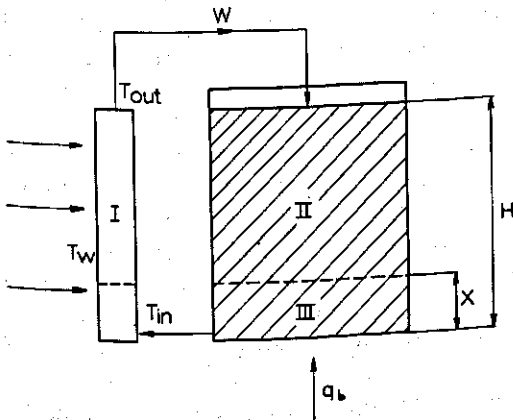
Fig. 45. Schematized model of heating of a liquid in a closed container by natural convection. I—heat exchanger, II—upper stratified region with downward flow, III—lower unstratified region with perfect mixing.

(II) and (III) is shifting, according to the model earlier described. The heat exchanger (I) is fed with liquid from the perfectly mixed region (III).

By using the appropriate equations for each region the heating of a liquid in a container can be simulated numerically. For such a simulation the x coordinate is divided in increments Δx. By using sufficiently small increments Δx, plug flow in the core can be simulated. By choosing a more or less coarse grid (large increments Δx) the effect of axial dispersion on temperature profiles can be estimated. In the latter situation the volume between two grid points in the vertical direction corresponds with one perfectly mixed tank. As usual the number of tanks in series is a reasonable, though not exact, measure for the degree of axial dispersion. The computational procedure used for the simulation is outlined in Appendix F.

The heating of water in a cylindrical container was simulated with the model. The dimensions of the container, the initial temperature and the wall temperature were chosen according to my experiments. The diameter of the container amounted to 180 mm and the total liquid height to 200 mm. The initial liquid temperature was 30° C and the wall temperature 120° C. The heat transfer coefficient from steam to liquid, calculated from Eqn (41), amounted to 1200 W/m² · K. By using a very small grid size, $\Delta x = 5$ mm, downward plug flow in the stratified region was simulated. Temperature profiles calculated from the simulation model were compared with experimental ones. However, experimental and calculated temperature profiles had a different shape. Especially initially differences were considerable. In the simulation model the stratified region became heated too fast while the unstratified region lagged behind. Further the experimentally determined unstratified region height was smaller than predicted.

From the flow visualization studies, reported in Chapter 4, it appeared that part of the liquid of the boundary layer leaves the boundary layer before reaching the liquid top surface. An attempt was made to incorporate this phenomenon in the simulation model to get better agreement between experimental and calculated temperature profiles. Therefore the boundary layer flow rate was divided into two parts, a part flowing upwards towards the liquid top surface and entering the core from above, and a part entering the stratified region radially from the boundary layer. It was supposed that the latter part was distributed equally over the stratified region and that there was perfect mixing in a radial direction. Heating of water was simulated for different ratios of boundary layer liquid entering the core from above to liquid entering the core radially. A comparison between calculated and experimental temperature profiles showed that introduction of a radial liquid flow from boundary layer to stratified region gave no improvement of the correspondence between calculated and experimental temperature profiles. In the stratified region the calculated temperature profiles showed an S shape, which was most pronounced at early times, and a large radial flow rate. This S shape was also found in experiments reported by Schwind & Vliet (1964) and Tatom & Carlson (1966) for sidewall heating only with very high heat flux levels. At these high heat flux levels transition to turbulence occurred, causing a considerable exchange of liquid between boundary layer and core.

It is likely that in the core during heating, axial dispersion plays a role. To

estimate the influence of such mixing, heating of water was simulated while the stratified region was represented successively by various numbers of perfectly mixed tanks. This was effected by using different grid sizes in the simulation model. In these simulations again no radial liquid flow from boundary layer to core was assumed. I used a grid size of $\Delta x = 10$ mm, of $\Delta x = 20$ mm and of $\Delta x = 40$ mm. For the third size, $\Delta x = 40$ mm, temperature distributions calculated from the simulation model are presented in Fig. 46. In this figure the experimentally found temperature profiles are also drawn. We see that the calculated temperatures correspond fairly well with the experimental temperature profiles. From the temperature profiles at $t = 30$ s and $t = 60$ s, it can be concluded that, in fact, axial dispersion will be more pronounced than when the assumption of five tanks in series, is applied.

Since we are concerned with a transient problem the effect of axial dispersion will decrease with time. Initially, when the driving force is largest, the tendency to turbulence in the core will be strongest and so will axial dispersion. For a better simulation the number of tanks in series should be adapted during the heating process. Fig. 46 shows that the calculated temperatures lag behind the experimental ones especially at intermediate time levels. This is because we used in Eqn (67) the overall heat transfer coefficient calculated from Eqn (41). The overall heat transfer coefficient from Eqn (41) was defined on the temperature difference $(T_a - T)$ in which T should be the mixed-mean temperature, see Section 5.1. However, the heat transfer coefficient to be used in Eqn (67) should be defined on $(T_a - \bar{T}_{bl})$, which could be evaluated as a logarithmic mean temperature difference. This latter temperature difference will be less than $(T_a - T)$ which implies a slower heating than would be expected from Eqn (36). When the temperature differences within the liquid have become small towards the end of the heating process, the
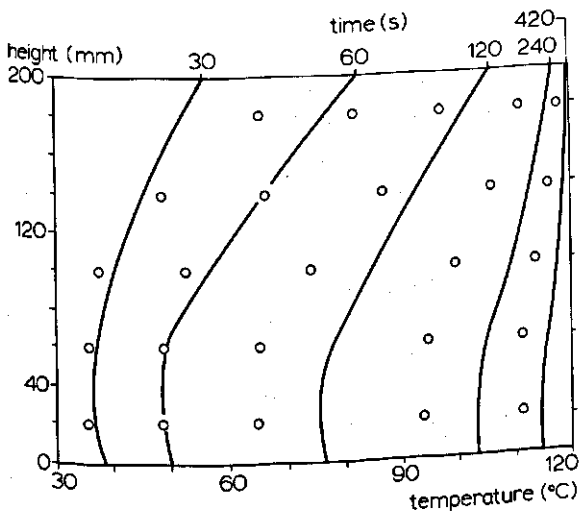
Fig. 46. Comparison of temperatures calculated (circles) from the simulation model for water, with experimental temperature profiles (lines), at five different times.

79
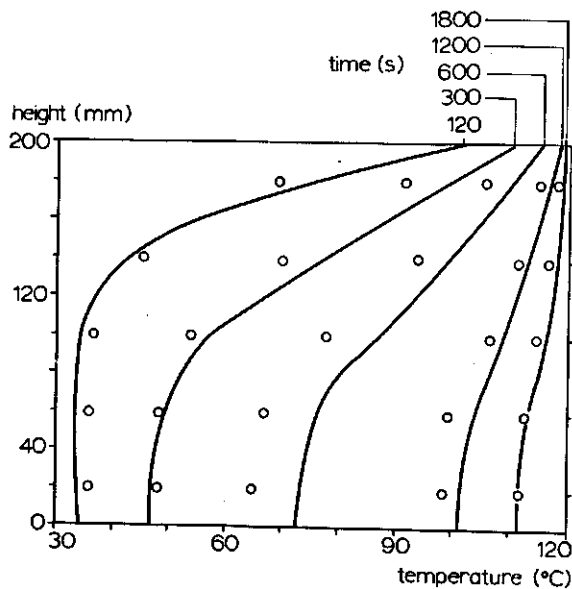
Fig. 47. Comparison of temperatures calculated (circles) from the simulation model for silicone fluid F111/100, with experimental temperature profiles (lines).

discrepancy between $(T_a - T)$ and the logarithmic mean temperature difference will become gradually less important. From this it can be understood that at moderate times the calculated temperatures lag behind while afterwards the differences become smaller again. The flow rate, W, calculated from Eqn (64) in the simulation was 70.7 cm³/s initially and became 14.7 cm³/s towards the end of the heating process. This corresponds fairly well with the experimental values reported in Section 4.4.

Heating of silicone fluid F111/100 was simulated with different grid sizes too. The boundary conditions were equal to those mentioned above for water. The overall heat transfer coefficient calculated from Eqn (41) and used in Eqn (67) amounted to 105 W/m² · K. Since an easy method to calculate the boundary layer flow rate for liquids with Prandtl numbers as high as for silicone fluid was not found, I used values for the boundary layer rate corresponding with those reported in Section 4.3.3. Again it appeared that a cascade of five tanks resulted in satisfactory temperature distributions. In Fig. 47 calculated temperatures are compared with experimental temperature profiles. Also initially a good agreement between both is seen. From the slope of the temperature profiles it can be concluded that in silicone fluid axial dispersion is less important than for water (compare Fig. 46), which can be understood from the different viscosities and rates of boundary layer flow.

80

6.2 Discussion of the simplified model

From the analysis of the simulation model it appears that axial dispersion in the core cannot be neglected. In the model I chose the number of tanks in series arbitrarily to force agreement with experimental data. A cascade of five tanks provided satisfactory results.

A more exact determination of the number of tanks in series should be based on measurements of residence time distributions. From the residence time distribution the number of tanks in series can be calculated by standard techniques. Collection of such information is not impossible in my experimental arrangement, but was beyond the scope of the original research programme.

From Eqn (59) in Section 6.1.1 an asymptotic height of the unstratified region is predicted $(Z)_{\tau \to \infty} = A$. The parameter A was defined as (see Eqn 55):

$$A = \frac{q_b \kappa}{v_c H \rho c_p} \tag{68}$$

If we assume a linear temperature profile in the stratified region and a constant κ (from Chapter 4, Fig. 26, we can see that this picture is value for not too long intervals of time), A can be written as:

$$A = \frac{\phi_{bottom}}{\phi_{sidewall}} \cdot \frac{(H-X)}{H} = \frac{h_{bottom} \Delta T_{bottom} \frac{1}{4}\pi D^2}{h_{sidewall} \Delta T_{sidewall} \pi D H} \cdot \frac{(H-X)}{H} \tag{69}$$

When, towards the end of the heating process, the convection currents and eddies have been damped out, it may be assumed that the heat flux density from the bottom is roughly equal to that from the sidewall. So a reasonable approximation will be:

$$(A)_{\tau \to \infty} = \frac{(H-X)}{H} \cdot \frac{D}{4H} \tag{70}$$

with

$$(Z)_{\tau \to \infty} = (A)_{\tau \to \infty} \tag{71}$$

this leads to:

$$(X)_{\tau \to \infty} = \tfrac{1}{4}D\{1/(1+D/4H)\} \tag{72}$$

From Eqn (72) it is seen that the asymptotic height of the unstratified region depends only weakly on the liquid height. Thus for different liquid heights in a container with diameter D, the ultimate height of the unstratified region (eddy region) should not differ much. This is in agreement with my experimental findings in Chapter 4. In Fig. 28 nearly the same ultimate eddy region height was found for two different liquid heights. For $H = 180$ mm the ultimate height amounted to about 45 mm and for $H = 100$ mm to about 40 mm. The asymptotic heights calculated from Eqn (72) were 36 and 31 mm, respectively.

In Fig. 48 the dimensionless height of the unstratified region, Z, is given as a function of the dimensionless time, τ, for two situations. Curve (I) is the
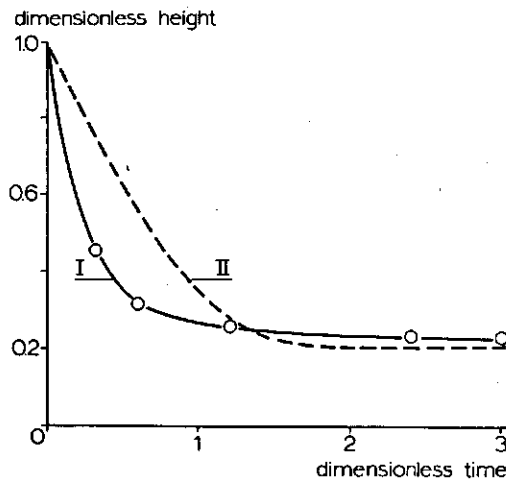
Fig. 48. Dimensionless height of unstratified region, Z, for water, as a function of dimensionless time, τ. Curve I, experimentally obtained for $D = 180$ mm, $H = 180$ mm. Curve II calculated from Eqn (58) for $A = 0.2$.

experimental eddy region height found for water for a total liquid height $H = 180$ mm $(D = 180$ mm$)$. Here an ultimate dimensionless height, $Z = 0.24$ is reached. Curve (II) in Fig. 48 was calculated from Eqn (58) for $A = 0.2$; this value of A is equal to the asymptotic dimensionless height of the unstratified region predicted from Eqn (72) for $H = 180$ mm and $D = 180$ mm. From Fig. 48 it is seen that the experimental curve descends faster than the calculated one. However, the experimental ultimate dimensionless height is somewhat higher than predicted. From this picture it should be concluded that in reality A varies during the heating process. From a comparison with Fig. 44 it should be concluded that initially A is considerably smaller than 0.2, but afterwards gradually increases to about 0.25. Such an increase of A during the heating process is not surprising since q_b, v_c and κ are changing during heating.

6.3 Use of the simplified model for process evaluation

By using the simulation model I was able to calculate lethality. As shown in Section 6.1 the heating of a liquid in a container could be simulated to a certain extent with the concept of a cascade of perfectly mixed tanks. The liquid, with micro-organisms suspended in it, flows through the cascade, each tank having a different temperature and consequently a different reaction rate for bacterial death. Now generally, see Hersom & Hulland (1964), bacterial death rate is assumed to be a first order reaction, thus:

$$\frac{dc_B}{dt} = -k_r c_B$$

(73)

where c_B is the concentration of bacteria and k_r a first-order reaction rate.

82

If the variation of k_r with temperature is known the death rate in each tank can be calculated. In food technology literature the death rate is defined in terms of decimal reduction time, DRT. DRT is the time required at a constant temperature to destroy 90 % of the population. By integration of Eqn (73) we can derive the relation between k_r and DRT:

$$k_r = \frac{\ln 10}{DRT} \tag{74}$$

The variation of DRT with temperature can be described by:

$$DRT = DRT(\text{ref}) \cdot 10^{(T_{ref} - T)/z_t} \tag{75}$$

in which DRT(ref) is the value of DRT at a reference temperature T_{ref} (commonly defined as 121.1° C) and z_t is the temperature coefficient of DRT, being the increase in temperature to achieve a ten times higher death rate.

For the calculations of process lethality, the liquid core was considered to be a cascade of continuous-flow, stirred-tank reactors. This concept corresponds with that used in the simulation of heating. For each tank (N) the change in concentration of bacteria can be calculated from a 'mass' balance over the bacteria in each tank. Accounting for flow into and out of the tank and bacterial death in the tank (neglecting the diffusion of bacteria) this 'mass' balance results in:

$$\frac{dc_{B,N}}{dt} = \frac{W}{V_r}(c_{B,N-1} - c_{B,N}) - k_r c_{B,N} \tag{76}$$

Equations (74) to (76) were incorporated in the simulation program, described in Section 6.1.2. By evaluating these equations at each time step in each tank the number of survivors at each moment can be calculated. In this procedure the unstratified (eddy) region was also considered to be a continuous-flow, stirred-tank reactor but with a volume, changing step-wise in time. No destruction of bacteria was assumed to occur in the boundary layer at the wall. This means, in other words, that the residence time of the liquid in the boundary layer was assumed to be zero.

By integrating the number of survivors over all tanks in the cascade the average over the whole container can be calculated. For comparison lethality calculations were also performed according to the single-point method. In this method the temperature history at one single point is used. Commonly the slowest heating point is selected for this purpose. In the latter method the effect of liquid movement through regions of different temperature is neglected. In such a method the number of survivors should be calculated from Eqn (73). The calculations for the single-point method were based on the temperature history in the unstratified region, because in my situation it was the 'slowest heating zone'.

Assuming $DRT = 12$ s and $z_t = 10$ K, I calculated lethality for the heating of silicone fluid F111/100, for which experimental and calculated temperatures are presented in Section 6.1.2, Fig. 47. In Table 3 fractions of survivors are shown for ten different times. Also presented are the average fraction of survivors if integrated over the whole container and the fraction of survivors indicated by the single-point method.

83

Table 3. Results of lethality calculations. The results obtained by using Eqn (76) and those obtained by using a single-point method are compared. It is assumed that $DRT(\text{ref}) = 12$ s, $z_t = 10$ K, $T_b = 30°$ C and $T_a = 120°$ C.

Time (s)	$T_{\text{unstratified}}$ region (°C)	Fraction of survivors in					Average fraction of survivors	Fraction of survivors with single-point method
		Tank 1	Tank 2	Tank 3	Tank 4	unstratified region		
300	48.9	0.99	1.00	1.00		1.00	1.00	1.00
600	66.1	0.71	0.90	0.97		1.00	0.91	1.00
900	82.2	0.22	0.34	0.67		0.91	0.61	1.00
1200	95.3	0.78×10^{-1}	0.26×10^{-1}	0.15	0.46	0.70	0.28	0.95
1500	105.0	0.15×10^{-1}	0.19×10^{-2}	0.24×10^{-2}	0.79×10^{-1}	0.20	0.59×10^{-1}	0.52
1800	110.9	0.19×10^{-3}	0.18×10^{-4}	0.36×10^{-5}	0.80×10^{-3}	0.31×10^{-2}	0.82×10^{-3}	0.21×10^{-1}
2100	114.4	0.69×10^{-8}	0.61×10^{-9}	0.97×10^{-10}	0.20×10^{-7}	0.11×10^{-6}	0.26×10^{-7}	0.22×10^{-5}
2250	115.6	0.18×10^{-11}	0.17×10^{-12}	0.26×10^{-13}	0.41×10^{-11}	0.25×10^{-10}	0.63×10^{-11}	0.10×10^{-8}
2340	116.2	0.40×10^{-14}	0.39×10^{-15}	0.64×10^{-16}	0.80×10^{-14}	0.53×10^{-13}	0.13×10^{-13}	0.32×10^{-11}
2400	116.6	0.42×10^{-16}	0.43×10^{-17}	0.72×10^{-18}	0.76×10^{-16}	0.54×10^{-15}	0.13×10^{-15}	0.43×10^{-13}

6.4 Discussion of results of lethality calculations

From Table 3 first we see that only at temperatures above 100° C are substantial death rates achieved. It can also be concluded that a single-point method, as commonly used, underestimates the lethality of the heating process. Towards the end of the heating process, the fraction of survivors calculated from the single-point method was about 100 times higher than that calculated with my method. It should be noted that in my example the sterilization effect of the boundary layer was neglected. In reality the residence time in the boundary layer will not be zero. Especially for viscous products this fact will contribute substantially to the sterilization and will cause an increase in the already found difference between our method and the single-point method.

For very low-viscous products, like water, the temperature differences within the liquid during the heating process are rather small. This will cause a smaller difference between our calculation method and the single-point method than in the example above for a rather viscous liquid.

It is somewhat surprising that in Table 3 the lowest fraction of survivors is found in the third tank, thus approximately in the centre of the container. In the upper part of the liquid (Tank 1) the temperature is highest. However, liquid from the unstratified region with a relatively high fraction of survivors is transported by the boundary layer flow towards Tank 1. While it takes some time before a substantial reduction is obtained this boundary layer flow will cause a rather high fraction of survivors in Tank 1. Tank 2, 3 and 4 are fed with liquid with decreasing concentrations but as the temperature is decreasing in the same direction the death rate is also decreasing. Due to the relatively low temperature in Tank 4 and in the unstratified region, here the high concentration is only slowly reduced. In Tank 4 the instantaneous fraction of survivors is mainly determined by the concentration of the output of Tank 3 some time before.

84

7 Effect of solid particles

As already remarked in Chapter 2 only some research has been done on the effect of solid pieces on convection heating. The work of Schmidt & Pflug (1966) was restricted to spheres of various sizes and only resulted in some qualitative conclusions about the effect of particle size on the heating rate of the liquid part in the container (see Section 2.1.5).

In analogy with the work described in the preceding chapters, where I heated liquid only, a study of flow patterns and temperature profiles should be made. However, since solid particles are seldom sufficiently transparent, a method for flow visualization as described in Chapter 4 cannot be applied. From my study of combined flow patterns and temperature profiles for liquid only, it appeared that a close relation exists between these phenomena. So I think that a study of temperature profiles only, should provide some insight into the heating process and the flow phenomena.

In this chapter temperature profiles as measured for heating water and silicone fluid with differently sized spherical particles are presented. Spherical particles were chosen because their geometry is the simplest of a large variety of possible shapes. From the measured temperature profiles conclusions were drawn about both the contribution of convection and conduction. Further attention was paid to the influence of particle size on the heat transfer coefficient from wall to liquid. Finally a mathematical model was suggested to describe the process of temperature stratification during heating. This stratification model is essentially similar to that presented in Chapter 6.

This chapter is based on the work of Zwijgers (1974) and van Boxtel (1975), who prepared their Masters thesis under my supervision. More details are to be found in these references.

7.1 Methods and materials

The experiments were performed in two differently sized containers, corresponding with Container 1 and 2 of Table C.1. (Appendix C). Heating was performed with condensing steam ($T_a = 120°$ C) in the retort described in Section 4.1.2. The initial temperature of container and contents was 30° C. The test liquids were water, silicone fluid F111/100 and silicone fluid F111/10000 (see Table C.2 Appendix C). In the experiments referred to here, the following solid particles were used: steatite spheres with diameters of 3, 6, 10, 18 and 26 mm and glass spheres with a diameter of 3 mm. In Table 4 the relevant material properties of the spheres are given.

Table 4. Some physical properties of test spheres.

	ρ_s(kg/m^3)	λ_s(W/m $\cdot$ K)	c_{ps}(J/kg $\cdot$ K)
Steatite spheres	2750	2.42	865
Glass spheres	2600	0.80	800

Axial and radial temperature profiles were determined in Container 2 by inserting thermocouples at different positions. A detailed description of this technique is given in Section 4.1.2. Temperature profiles for the following combinations were observed: (a) 3-mm glass spheres in water, (b) 3-mm glass spheres in silicone fluid F111/100 and (c) 18-mm steatite spheres in silicone fluid F111/100.

In Container 1 some experiments were performed to establish the effect of particle size on the heat transfer coefficient from steam to liquid. For the experiments with water a thermocouple was placed on the centre line 70 mm from the bottom, while the total liquid height was 147 mm. For the experiments with solid spheres in silicone fluid ($H = 147$ mm) three thermocouples were placed on the centre line 20, 70 and 125 mm from the bottom. From the temperature course of the container contents, a heat transfer coefficient can be calculated in a way similar to that indicated in Chapter 5. Here the overall heat transfer coefficient U can be defined as:

$$U = -\frac{(\rho c_p)_{bed}}{A_c} \cdot \frac{d \ln \left(\frac{T_a - T}{T_a - T_0} \right)}{dt} \tag{77}$$

in which $(\rho c_p)_{bed}$ is the heat capacity of the total container contents (liquid + solids). The overall heat transfer coefficient U can be derived from the slope of the curve obtained by plotting $\ln \{(T_a - T)/(T_a - T_0)\}$ versus time. For water T was assumed to be represented by the temperature measured by the thermocouple 70 mm from the bottom. For silicone fluid T was assumed to be the weighted mean of the three measured temperatures, by using:

$$T = 0.27 T_{20} + 0.43 T_{70} + 0.30 T_{125} \tag{78}$$

The numerical coefficients were derived by assuming T_{20} being representative for 0–40 mm from the bottom, T_{70} for 40–103 mm from the bottom and T_{125} for 103–147 mm from the bottom.

7.2 Results and discussion

7.2.1 Temperature profiles

Glass spheres of 3 mm in water Experimental radial temperature profiles for three different times are presented in Fig. 49. In Fig. 50 the axial temperature profiles are given. The curves of Fig. 49 and 50 show some similarity with

86
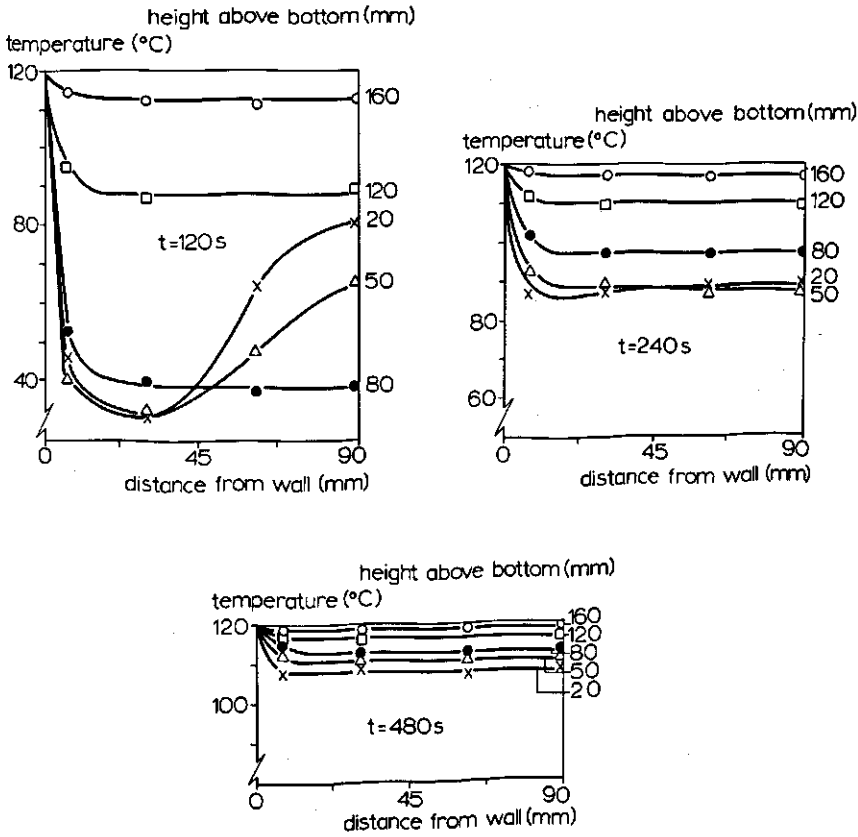
Fig. 49. Experimental radial temperature profiles for water with 3 mm glass spheres ($\varepsilon = 0.37$), at three different times. $H = 170$ mm, $T_0 = 30°$ C and $T_s = 120°$ C.
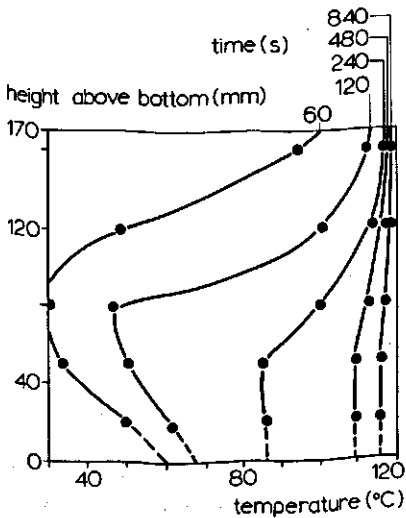
Fig. 50. Experimental axial temperature profiles for water with 3 mm glass spheres. Measuring points on central axis (see Fig. 49).

87

corresponding temperature profiles for heating water without spheres (see Section 4.4). In Fig. 49 a steep temperature gradient at the heated sidewall is to be noticed, while in the core at $t = 240$ s and $t = 480$ s nearly flat temperature profiles are found. At $t = 120$ s the radial temperature profiles in the upper part of the container are flat, but at 20 and 50 mm from the bottom they show a somewhat surprising shape, the temperature being at maximum at the central axis. This latter phenomenon is also responsible for the very pronounced characteristic shape of the axial temperature profiles. I think Fig. 49 and 50 confirm the existence of 'core stratification'. Just as with pure liquid, it results from boundary layer heat transfer at the sidewall. The ascending boundary layer flow at the wall
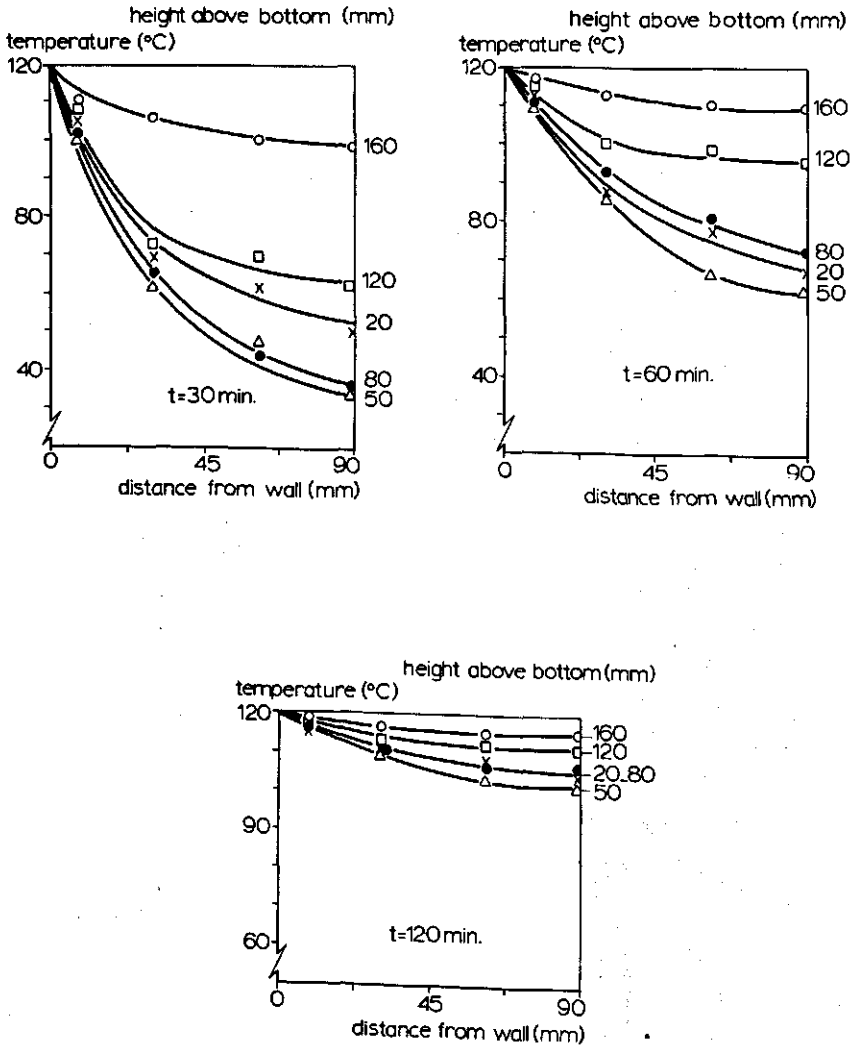
Fig. 51. Experimental radial temperature profiles for silicone fluid F111/100 with 3-mm glass spheres ($\varepsilon = 0.37$), at three different times. $H = 170$ mm, $T_0 = 30°$ C and $T_s = 120°$ C.

causes a downward flow in the core, and so core stratification. The radial temperature profiles at 20 and 50 mm from bottom at $t = 120$ s suggest an influence of the glass spheres on the rise of eddies from the bottom. One can imagine that the spheres restrict the upward flow from the bottom, which prevents the genesis of a perfectly mixed region that extends up to the stratified region. It must be concluded that obviously eddies preferably rise towards the centre line of the container. This would explain the existence of a 'slowest heating ring' in the early stage of heating, about 20 to 50 mm from bottom and about 70 mm from the centre line (see Fig. 49).

Glass spheres of 3 mm in silicone fluid F111/100   In Fig. 51 and 52 the radial and axial temperature profiles are shown. If compared with temperature profiles for the similar situation of heating the same silicone fluid F111/100 without spheres (see Section 4.3), some differences appear. Fig. 51 does not show the familiar picture of a steep temperature gradient at the sidewall and a flat profile in the core. The radial temperature profiles of Fig. 51 are characteristic for conduction heating. However, the sequence of the radial temperature profiles from top to bottom in Fig. 51 and the shape of the axial temperature profiles in Fig. 52 indicate that convection heating is not negligible. Specifically the temperature increase from bottom to top suggests clearly a temperature stratification in the upper part of the container. This temperature stratification would not be present for pure conduction heating, then a continuously decreasing temperature from bottom to top would have been found. From Fig. 51 it can be concluded that the stratification in the upper part of the container proceeds in time. It can also be concluded that the presence of solid particles strongly reduces the convection heating rate. While for a liquid without particles about 30 minutes were sufficient to accomplish heating of the container contents (see Section 4.3), here about 3 hours were necessary for a corresponding degree of heating.

The conclusion from the above mentioned observations is that for a moderately
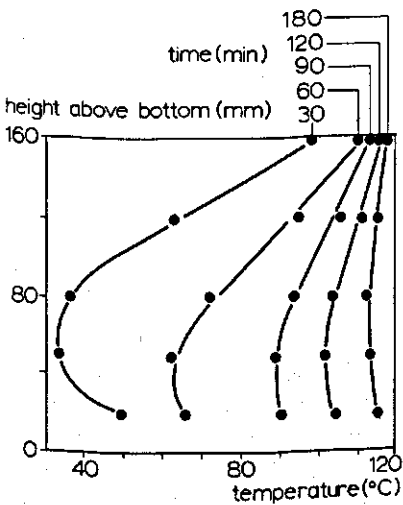
Fig. 52. Experimental axial temperature profiles for silicone fluid F111/100 with 3-mm glass spheres. Measuring points on central axis (see Fig. 51).

viscous fluid, addition of small (diameter 3 mm) spheres suppresses convection heating considerably. However, convection is not completely excluded.

Steatite spheres of 18 mm in silicone fluid F111/100 To get an impression of the influence of the spherical particle size on convection heating, I repeated the determination of radial and axial temperature profiles for silicone fluid F111/100 with 18-mm steatite spheres. Axial temperature profiles are shown in Fig. 53. The radial temperature profiles showed the familiar shape for convection heating, a steep temperature gradient at the wall and a flat profile in the core, compare Section 4.3.1 and Fig. 49. The shape of the axial profiles and the time required to accomplish heating are also indicative for predominant convection heating (compare Fig. 53 and 52). The shape of the axial temperature profiles in Fig. 53 is somewhat different from the axial temperature profiles for heating pure liquid. For pure liquid a uniform temperature region just above the bottom was found, which corresponded with the occurrence of the eddy region. In Fig. 53 no uniform temperature region is seen. Obviously the buoyancy of the eddies is quickly interrupted by the solid particles, even with these relatively large spheres.

From the temperature profiles for heating water and silicone fluid F111/100 with solid spheres of different size, we conclude that especially small particles in a rather viscous liquid are able to suppress convection almost completely. The presence of larger particles in a liquid of moderate viscosity does not considerably reduce convection. In a liquid of low viscosity this effect of small particles is restricted to much smaller particle sizes. In the experiments cited above I found no reduction. However it is well known in technology and soil physics that a substantial reduction occurs for particle sizes of some mm or less (see also Section 7.2.2 and Table 5).
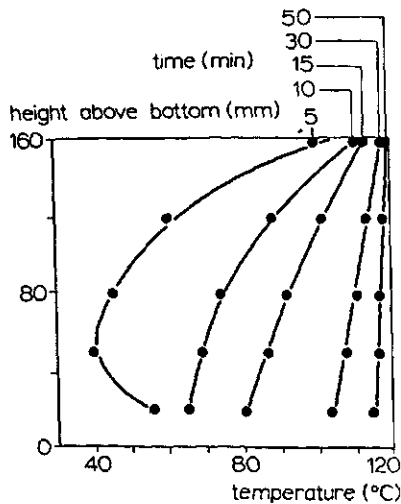
Fig. 53. Experimental axial temperature profiles for silicone fluid F111/100 with 18-mm steatite spheres ($\varepsilon = 0.41$). $H = 170$ mm.

90

Table 5. Overall heat transfer coefficients (U in W/m² · K) for liquids with steatite spheres of different diameter.

Diameter (mm)	Porosity	U		
		water	silicone fluid F111/100	silicone fluid F111/100000
3	0.39	842±28	56.6±0.4	50.7±0.4
6	0.41	1269±32	62.0±0.5	
10	0.43	1297±94	62.0±1.1	
18	0.46	1071±21	79.6±1.3	
26	0.50	1054±58	73.1±0.7	
Liquid without particles		1270±61	92.0±4.0	29.2±2.6

7.2.2 Influence of particle size on heat transfer rate

An interesting point, especially for practical calculations, is the influence of particle size on the heat transfer from heating medium to the liquid in the container. The heat transfer coefficient can be calculated from experiments by Eqn (77). In Table 5 the results are shown of measurements on heat transfer coefficients for different combinations of liquids and particles. The porosity and the standard deviation are also indicated.

For water with differently sized steatite spheres it is obvious from Table 5 that convection heat transfer predominates. Further an effect of particle size on the heat transfer coefficient can be seen. We can distinguish three regions: (a) at a small particle size (3 mm) we see a heat transfer coefficient which is considerably smaller than for pure water, (b) at moderate particle sizes (6 and 10 mm) we see heat transfer coefficients which are nearly equal to that for pure water, (c) at large particle sizes (18 and 26 mm) we see a somewhat reduced heat transfer coefficient compared with the situation for pure water. There is no simple physical explanation for this effect. For that purpose the exact behaviour of the boundary layer flow at the wall should be carefully reconsidered for different diameters of the flow disturbing particles. Primarily one would expect a decrease of the heat transfer coefficient with increasing flow friction, i.e. a smaller diameter of the spheres and a lower porosity. Qualitatively this holds true, except for the larger diameters (18 and 26 mm). Supposedly the observed effect of particle size must be attributed to an influence of particles on the boundary layer flow. A possible explanation is as follows. The flow rate of the boundary layer will always be reduced by the presence of solid particles. However, for decreasing diameter (from 26 to 10 mm) the turbulent liquid renewal in the boundary layer might progressively compensate for the negative effect of flow reduction. Finally this effect of liquid renewal may even overcompensate for the flow reduction effect. Obviously, for very small particles the flow rate is so strongly reduced that no turbulence exists. Heat transfer is again decreased (diameter 3 mm). For ex-

tremely small particles heat transfer will even reduce to the limit of pure conduction.

For silicone fluid F111/100 with differently sized steatite spheres a similar effect is seen. Here a maximum value in the heat transfer coefficient was measured for a diameter of 18 mm.

From the experimental temperature profiles for silicone fluid F111/100 with 3 mm (glass) spheres, quoted earlier in Section 7.2.1, I concluded that conduction heating was the dominating factor. For conduction heating also, an overall heat transfer coefficient from heating medium to heated object can be defined, by introducing a mean temperature of the object. This overall heat transfer coefficient can be calculated from (see Appendix G):

$$U_{cond} = \frac{\alpha_{eff}(\rho c_p)_{bed} V_c}{A_c} \left(\frac{5.7831}{\frac{1}{4}D^2} + \frac{2.4674}{H^2} \right) \tag{79}$$

For a calculation of the effective heat diffusivity for a packed bed of steatite spheres in silicone fluid, the method indicated in Appendix G was used. By using
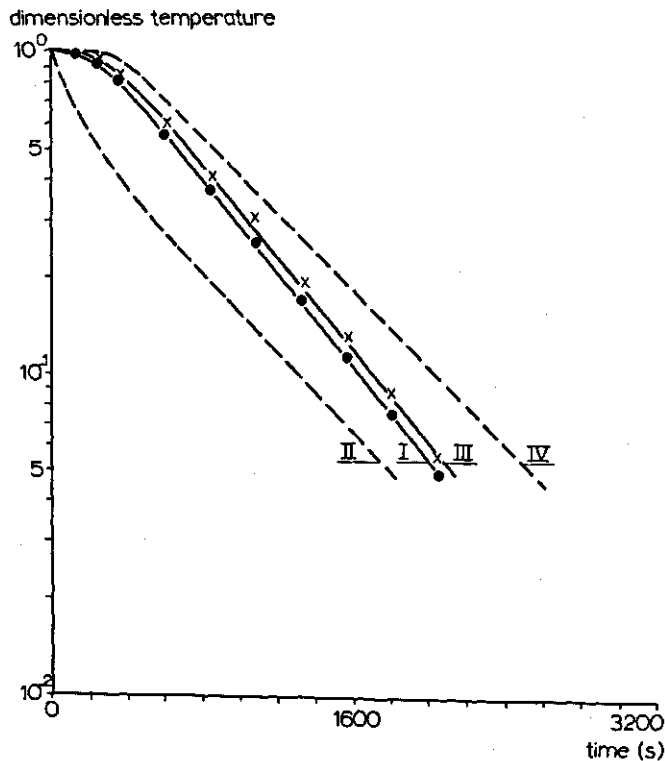
Fig. 54. Dimensionless logarithmic temperature course for silicone fluid F111/100 with 3-mm steatite spheres ($\varepsilon = 0.39$). $D = 75$ mm, $H = 147$ mm, $T_0 = 30°$ C and $T_a = 120°$ C. I—experimental weighted mean temperature, II—calculated mean temperature for conduction heating, III—experimental temperature on central axis 70 mm from bottom, IV—calculated temperature for conduction heating on central axis 70 mm from bottom.

92

Eqn (79) for silicone fluid with 3-mm steatite spheres, a $U_{cond} = 47.2$ W/m² · K was found. This is less than experimentally determined. Therefore, as already concluded from the temperature profiles (Fig. 51 and 52), convection cannot be fully neglected in this situation. For larger particles U_{cond} remains almost unchanged, so that we may conclude from Table 5 that convection becomes more and more important. In Fig. 54 experimental and calculated temperature-time plots are compared for the smallest particles. The overall heat transfer coefficient can be derived from the slope of the curves. Now we see that in the experiments it does not matter whether we take the weighted mean temperature (Eqn 78) or the temperature measured 70 mm from the bottom. The difference in heat transfer coefficient between calculated conduction heating and the experimental case is demonstrated by the different slopes of the heating curves.

Finally, at first sight it is somewhat surprising that for the very viscous silicone fluid F111/10000 with 3-mm steatite spheres, where convection is expected to be negligible, the experimental heat transfer coefficient is much higher than the value found for convection heating of the pure liquid (see Table 5). This is caused by the heat conductivity of steatite being much higher than for silicone fluid, which causes a more rapid heating by conduction. Comparing calculated values from Eqn (79), amounting to 47.2 W/m² · K, and experimental values of the heat transfer coefficient, we can conclude that indeed here the role of convection practically can be neglected.

7.3 Simplified model for heating liquids with solid spheres

Bimbenet & Duquenoy (1974) and Bimbenet & Michiels (1974) developed a model for the simulation of heating during sterilization of cans filled with liquid and cylindrical or spherical solids. They assumed the liquid part in the container to have a uniform temperature. If the overall heat transfer coefficient from heating medium to liquid and the heat transfer coefficient from liquid to solids are known, then the temperature course in the liquid and in the solids can be simulated easily.

The assumption of a uniform temperature in the liquid part is reasonable for cans agitated during heating. However, in this situation of non-agitated cans, considerable temperature differences in the liquid were found (see Section 7.2). Therefore I tried to develop a simplified simulation model in which experimental temperature profiles such as were found, are involved. As we concluded from Section 7.2 that the convective phenomena for heating a liquid with solid spheres are similar to those for heating a liquid without solids, a model analogous to that in Chapter 6 was developed for a pure liquid.

In this model I distinguished a boundary layer flow at the sidewall, a stratified core in the upper part of the container with downward flow and an eddy region in the lower part of the container. If the effect of heat conduction in axial direction is neglected, and a downward cross-sectional mean flow rate, $\bar{v}_c$, in the core is assumed the heating of the liquid in the core is given by:

$$\rho_f c_{pf} \varepsilon \frac{\partial T_l}{\partial t} + h_s S(T_l - \bar{T}_s) = \rho_f c_{pf} \bar{v}_c \frac{\partial T_l}{\partial x}$$

(80)

93

while the heating of the solid spheres can be calculated from:

$$\frac{\partial \bar{T}_s}{\partial t} = \frac{h_s S}{c_{ps} \rho_s (1-\varepsilon)} (T_\ell - \bar{T}_s) \tag{81}$$

For the eddy region essentially the same approximation can be used as for the pure liquid (see Section 6.1), which results in the following energy balance:

$$q_b = X \rho_\ell c_{p\ell} \varepsilon \frac{dT_\ell}{dt} + h_s S X (T_\ell - \bar{T}_s) \tag{82}$$

The term on the left is the heat flux from the bottom, those on the right are the accumulation of heat in the liquid and the heat transferred from liquid to solid particles. The heating of the solid fraction in the eddy region can again be calculated from Eqn (81). The cross-sectional mean flow rate in the core results from the boundary layer flow rate. The relation between both is given by:

$$\bar{v}_c = \frac{4W}{\pi D^2} \tag{83}$$

With these equations, in the same way as described in Chapter 6, the heating of the liquid with solid spheres can be simulated. However, for application of the simulation model the following additional information is required:
1. The flow rate of the boundary layer. It will be obvious that the packed bed of spheres restricts the flow in the core and in the boundary layer. This could be concluded also from the heat transfer coefficients reported in Section 7.2. For a proper application of the simulation model an analysis of natural convection boundary layer flow at a heated wall in a packed bed should be made. However, as far as I know there is no such analysis and the development of it was beyond the original scope of this study. For a first approximation, just like for pure liquid, the analysis of Eckert (1966) could be used, in which an empirical constant is introduced, which is a measure for the reduction of the boundary layer flow rate due to the presence of the solid particles. This constant could be determined experimentally from a measurement of the downward flow rate in the core.
2. Behaviour of the eddy region. As already concluded in Section 7.2 from the shape of the temperature profiles, the upward flow from the bottom is restricted by the presence of the solid particles, that prevents a perfectly mixed region in the lower part of the container. Thus the assumptions for the unstratified region as made in Chapter 6 do not hold for this situation. Therefore in the simulation model an additional expression should be introduced, that accounts for the flow restriction from the bottom.
3. Heat transfer coefficient at the sidewall and the bottom. If the simulation model is to be used for a prediction of the heating process, the heat transfer coefficient should be obtained from a mathematical analysis or from a generally accepted semi-empirical correlation. Since such data are not available, again for a first approximation heat transfer coefficients could be obtained as indicated in Section 7.2.
4. Heat transfer from liquid to solid particles. For an evaluation of the temperature of a solid sphere in a packed bed the following situations could be distin-

guished. First the assumption could be made that the thermal diffusivity of the solid is so high in comparison with the outside heat transfer, that a uniform temperature in the sphere may be assumed. In this situation the outside heat transfer coefficient from liquid to solid sphere could be evaluated from correlations, for example, given in Bird et al. (1960), page 411. However, these correlations are not valid for very small Reynolds numbers. Therefore, for low liquid velocities like for silicone fluids, as used in my experiments, I think for a first approximation it is reasonable to use a correlation of the form (see Kronig & Bruijsten, 1951):

$$Nu = 2 + \tfrac{1}{2}P\acute{e} + 0.303 P\acute{e}^2 \qquad (P\acute{e} < 3) \tag{84}$$

This correlation holds for heating one sphere in a liquid for Reynolds numbers where Stokes' law applies to the flow field (Soo, 1967). Since we do not have one single sphere but a packed bed a somewhat better agreement can be obtained by using λ_{eff} instead of λ_t in the Nusselt number (see Appendix G).

For the situation that both the internal heat resistance of the solid and the external heat resistance play a role, a procedure suggested by Kramers (1953) could be used. Then the overall heat transfer coefficient can be calculated from the first eigenvalue in the series expansion for the temperature in the sphere (as function of time and radial position). If we assume that the outside heat transfer coefficient leads to $Bi = 1$, the first eigenvalue amounts to $\tfrac{1}{2}\pi$. Then the overall heat transfer coefficient becomes:

$$U_s = \frac{\pi^2}{6} \frac{\lambda_s}{d_p} \tag{85}$$

The supposition $Bi = 1$ seems not too unreasonable for this rough approximation since $Bi = (\lambda_t/\lambda_s)Nu$ and according to Eqn (84) Nu is not much larger than 2. For the sake of completeness we add that for $Bi = 5$ the numerical factor in (85) becomes 2.202 instead of $\pi^2/6$.

On the basis of the above mentioned assumptions, a computational procedure was developed similar to that in Chapter 6 and heating of water and silicone fluid with solid spheres was simulated (see van Boxtel, 1975). In this simulation, arbitrary values were chosen for the boundary layer flow rate, the behaviour of the eddy region and the heat transfer coefficients. The correspondence of the calculated results with the experimental results was only fair. However, to give such a simulation model more predictive value further work should be done on the natural convection boundary layer flow at a wall in a packed bed, on the suppression of the flow from the bottom and on heat transfer coefficients.

8   Final discussion

This study was started to obtain a better insight in the physical phenomena that occur during the sterilization of canned liquid food. Therefore I studied flow phenomena and heat transfer experimentally as well as theoretically.

The most important results of the experimental study were recognition of the transient character of the flow patterns and temperature profiles, and the important effect of bottom heating on the flow phenomena. Further the flow patterns observed during heating silicone fluid F111/100 confirm experimentally the existence of a reverse shear layer, a phenomenon predicted analytically by several authors (see Section 3.3). Simultaneous heating of the bottom and the sidewall, which were the actual boundary conditions I applied, seriously limits the validity of a numerical solution of the equations of energy and motion, governing this problem. The numerical method developed by Barakat & Clark (1966) for sidewall heating only, is not applicable because convective heat transfer from the bottom is not accounted for. It would be very interesting to try and apply perturbation techniques to the actual problem as Charlson & Sani (1970) did for horizontal liquid layers heated from below.

From my study of flow patterns and temperature profiles, a better estimation can be made of the value to be given to the slowest heating point. In food technology literature for convection-heated products usually a slowest heating point is assumed somewhere between bottom and geometric centre; see for example Hersom & Hulland (1969). However, I did not observe a well defined slowest heating point. For low viscous liquids of intermediate viscosity a uniform temperature region was found in the lower part of the container, so really one can only talk about a 'slowest heating region'. Only for the highly viscous silicone fluid F111/10000 and for liquids containing solid particles do temperature profiles suggest a more pronounced 'slowest heating point'. In these situations eddies from the bottom are strongly suppressed, either by the high viscosity or by the presence of solid particles, so preventing a well mixed eddy region from developing. For a good understanding we may add that (a) the 'slowest heating point' does not persist in a fixed position during heating and (b) that there is no stagnant liquid that continuously stays at this 'slowest heating point'.

As already noticed by Fagerson & Esselen (1950), the liquid movement causes a discrepancy between the lethality calculated from a conventional single-point method and the actual lethality of the heating process applied. As far as I know only Stevens (1972) tried to incorporate product movement in process evaluation. However, due to shortcomings in his model he could only conclude qualitatively that a single-point method gives rise to overprocessing. My calculations, which

were based on a more realistic model, clearly show that a single-point method underestimates the lethal effect of the heating process. As my calculations are in turn conservative because I omitted the extra sterilization effect in the boundary layer, differences as shown in Table 3 between the single-point method and my method might in the actual heating process be somewhat larger. However, from Table 3 it also can be concluded that once a temperature of about 120°C is reached, further reduction of the number of survivors by a factor 100 only takes some minutes. Only at low reaction rates would my calculation method predict a substantial reduction in process time compared with common practice.

The most important conclusion from these calculations, I think, is that the conventional single-point methods are certainly safe. On the other hand application of these methods leads to stronger quality degradation than strictly necessary. With this model also the quality degradation due to the heating process could be estimated, provided that the reaction kinetics of the degradation processes are known.

Clearly my simplified model was only a beginning. For a wider application a more complete study should be made of the physical problems of boundary layer flow and axial dispersion in the core. Application of this model to liquids with solid particles leads to additional problems such as the effect of the solid particles on boundary layer flow, the suppression of the eddy region by the particles and how to obtain a realistic estimation of the heat transfer.

Summary

The aim of this work was to develop a better understanding of the mechanism of heat transfer within a liquid heated in a closed container. This goal originates from special interest in heat sterilization of canned liquid food. The study of the transport phenomena of heat and momentum should provide the information for a mathematical treatment of the heating process. The mathematical model can then be used for an evaluation of lethality and quality conservation in sterilization of canned food.

From the literature reviewed in Chapter 2 it was concluded that food technologists have paid much attention to convection heating of products and especially to factors affecting the rate of heating. However, most of this work was only qualitative. From a literature study of flow patterns and temperature profiles, it was concluded that the understanding of the mechanism of natural convection heating is incomplete, because: (a) the interaction between flow patterns and temperature profiles has been analysed insufficiently, (b) the flow pattern is mostly, but not rightly so, described as a steady state, (c) the study of flow patterns was restricted to non-viscous liquids like water, (d) mostly flow visualization studies were limited to conditions that were not very representative for food sterilization. A review of the methods available for calculating convection heating of liquids in containers revealed that often over-simplified, and therefore unrealistic, physical models have been used. Similar problems have also been extensively studied in other fields of technology, viz. the problem of storage of cryogenic fluids, such as liquid natural gas. Although the majority of these studies is concerned with boundary conditions different from those common in heat sterilization of foods, the results of these basic studies are valuable for application in food technology.

Chapter 3 discusses the different ways to describe the heating of a liquid in a closed container mathematically. Although it is relatively simple to formulate the governing differential equations and their corresponding boundary conditions, an analytical solution of these equations seems beyond the present scope of science. Barakat & Clark (1966) succeeded in obtaining a numerical solution of the momentum and energy equations for a similar problem. The results I obtained with a numerical model similar to that of Barakat & Clark, but adapted to the boundary conditions I applied were not satisfactory. The streamline patterns and temperature profiles for simultaneous bottom and sidewall heating were very similar to those obtained by Barakat & Clark for sidewall heating only. This was in contrast with experimental findings. For simultaneous bottom and sidewall heating considerable convective heat transport from the bottom occurs, which

cannot be accounted for by the numerical method. As could be expected, the numerical method only refers to conductive heat transport from the bottom.

In Chapter 4 I described experimental flow patterns and temperature profiles for three different liquids. During heating a boundary layer flow develops at the vertical sidewall of the container. At the top this boundary layer flow spreads inwards over the free liquid surface and then slowly moves downwards causing a thermally stratified core. In the lower part of the container an unstable region (eddy region) is found due to bottom heating. Initially the height of this eddy region decreases, but after some time an equilibrium height is reached that remains essentially constant during the remainder of the heating process.

The radial temperature profiles were essentially flat in the core, but revealed a steep gradient in the boundary layer near the wall. The axial temperature profiles showed a nearly uniform temperature in the lower part of the container, which corresponds with the eddy region, and a temperature increasing towards the liquid surface in the upper part of the container, which corresponds with the stratified core. A close connection between flow phenomena and these temperature profiles was demonstrated. From the flow visualization studies it was concluded that, due to core stratification, a flow reversal in the outer portion of the boundary layer flow occurs. A more detailed study of the thickness and the liquid velocities in the boundary layer flow was made with a laser-doppler velocimeter. From a study of combined flow patterns and temperature profiles for a very viscous silicone fluid ($\nu = 10^{-2}$ m²/s) I concluded that, in spite of the relative weakness of the convection currents in the liquid, convection was still the most important factor contributing to heat transfer.

From a great number of experiments covering the range of H/D ratios from 0.25 to 2.00 and Prandtl numbers from 5 to 80000, a dimensionless correlation for heat transfer to a liquid in a closed container was determined (Chapter 5). An overall heat transfer coefficient was calculated from the temperature measured in the geometric centre. The geometric centre temperature was found to represent the cup-mixing temperature rather well. Within certain limits the heat transfer coefficient was found to be constant. Ultimately it was found that Nu was approximately proportional to $Ra^{\frac{1}{4}}$, which is in agreement with well known relations in laminar natural convection.

In Chapter 6 a simplified model developed for practical calculations is discussed. The model is based on the assumption of the existence of a natural convection boundary layer flow near the wall, a stratified region in the upper part of the container and a perfectly mixed, unstratified, region in the lower part of the container. From the energy equations, the behaviour of the height of the unstratified region was derived. An asymptotic value of this unstratified region height was predicted, which corresponds rather well with experimental findings. The asymptotic height depends mainly on the ratio of bottom heat transfer to sidewall heat transfer. The model in which pure plug flow was assumed in the core did not satisfy the experimental temperature profiles. A model in which axial dispersion was accounted for by discretization of the core flow to a cascade of tanks in series, gave better agreement with experimentally observed temperature profiles. Since no quantitative data about the magnitude of the axial dispersion

were available, the number of tanks in series had to be assigned arbitrarily. This is a serious drawback of the model, that restricts its predictive value. Further work should be directed towards measurement of residence time distributions in the core flow.

Results of the simplified model were used to estimate the lethality of a heating process. In the process evaluation the effect of product movement, due to convective flow was included by assuming the container to be composed of a cascade of continuous-flow, stirred-tank reactors. From the lethality calculations it was concluded that the conventional 'single-point' method, sometimes underestimates the lethality of the heating process.

Chapter 7 describes a study of the effect of solid particles on convection heating. Experimental temperature profiles were reported for heating water and silicone fluids with spherical particles of different diameter. For heating water with solid spheres (diameter 3 to 26 mm) the predominant heat transfer mode is convection. For heating highly viscous silicone fluids I found that for a small particle size (diameter 3 mm) convection is strongly suppressed, resulting in much longer heating times than for pure liquid. The presence of larger particles in silicone fluid does not considerably reduce convection. For both water and silicone fluid an effect of particle size on the heat transfer coefficient was found. If the particle size increased from 3 to 10 mm, there was an increase of the heat transfer coefficient to a value nearly equal to that for the pure liquid. However, for a further increase of the diameter (10 to 26 mm) again a somewhat reduced heat transfer coefficient was found.

Résumé

On a étudié la convection naturelle à l'intérieur d'un récipient cylindrique chauffé par le fond et la paroi latérale. Le but de cette recherche était d'examiner le comportement des aliments liquides en boîte au cours de la stérilisation. Durant ce processus, bien entendu, l'échauffement par le haut est considérablement limité par la couche d'air au-dessus du liquide. Des travaux théoriques et expérimentaux ont été effectués sur les phénomènes physiques qui se déroulent pendant la stérilisation. Les résultats peuvent dès lors s'appliquer au calcul numérique de la létalité dans les aliments en conserve et à l'évaluation théorique de la conservation de leur goût et de leur qualité.

La littérature traitant de l'échauffement des aliments par convection, et en particulier de l'efficacité de cet échauffement, est abondante. Elle a été résumée au chapitre 2. Toutefois, les auteurs de la plupart de ces études se sont bornés à une recherche qualitative. Alors on est mené à conclure que la compréhension des phénomènes physiques de l'écoulement et du transfert de chaleur est insuffisante. C'est à dire: (a) l'interaction entre l'écoulement et la distribution des températures n'a que peu retenu l'attention jusqu'à présent; (b) on considère le plus souvent l'écoulement en régime permanent, quoique le régime de la température soit transitoire; (c) on s'est borné aux liquides de faible viscosité, comme l'eau; (d) si l'écoulement dans un liquide chauffé a parfois été observé par des méthodes visuelles, les résultats obtenus jusqu'à présent ne sont pas convenables pour une application à la stérilisation des aliments. D'autre part les méthodes mathématiques de calcul proposées dans la littérature se réfèrent à des modèles physiques qui manquent de rigueur. Hormis les ouvrages spécialisés du génie industriel alimentaire, la littérature présente beaucoup de travaux sur des problèmes similaires, comme le stockage des liquides cryogènes, tel par exemple le gaz naturel liquide. Bien que la plupart de ces études ne soient pas tout à fait appropriées au problème en question, l'approche et les résultats qu'elles présentent ont contribué à la présente recherche.

Au chapitre 3 on a étudié les méthodes mathématiques permettant d'analyser l'échauffement d'un liquide dans un récipient clos. Quoiqu'il soit relativement aisé d'établir les équations différentielles et les conditions aux limites définissant la répartition des températures et des vitesses, il semble que l'état actuel de la science ne fournisse pas de solution analytique rigoureuse. Une solution numérique a été proposée par Barakat et Clark (1966), qui ont étudié un problème analogue, où le cylindre était chauffé par la paroi latérale. On a repris ce calcul après l'avoir adapté aux conditions spécifiques de la présente recherche, c'est à dire en tenant compte d'un échauffement supplémentaire par le fond.

101

Pourtant, les résultats de ce calcul numérique s'avéraient peu différents de ceux de Barakat et Clark qui avaient supposé une isolation parfaite par le fond. Cette issue ne concorde pas avec les résultats expérimentaux, pour lesquels le récipient a été chauffé simultanément par le fond et la paroi latérale. Ces expériences, en effet, démontrent que la convection contribue de façon importante à la transmission de chaleur par le fond. Or, avec la méthode numérique de Barakat et Clark on ignore forcément la contribution de cette convection verticale dans la partie inférieure du récipient.

Le chapitre 4 est consacré aux expériences concernant l'écoulement et la distribution des températures pour trois liquides de viscosité différente. Durant l'échauffement, le liquide monte le long de la paroi verticale en couche limite laminaire. Arrivé à la surface supérieure du liquide, l'écoulement s'y répand et redescend ensuite lentement sur toute sa largeur. Il en résulte une région centrale thermiquement stratifiée qui occupe la partie supérieure du récipient. Dans la partie inférieure apparaît simultanément une région de turbulence dont les tourbillons sont dus à l'échauffement par le fond. La hauteur de cette région de turbulence décroît au début pour atteindre après quelque temps un équilibre qui ne variera plus durant le processus.

Les profils des températures radials apparaissent nettement uniformes, sauf dans la couche limite où la température monte brutalement vers la paroi. Quant au profil axial, on trouve en bas une partie correspondant à la région de turbulence où la température est uniforme; dans la partie supérieure la temperature s'accroît vers le haut, ce qui correspond à la région stratifiée. L'interaction entre cette distribution des températures et l'écoulement a été démontrée.

On a examiné plus en détail l'écoulement dans la couche limite au moyen d'une méthode visuelle et en mesurant la vitesse locale du liquide par l'effet Doppler. On trouve dans la partie extérieure de la couche limite une inversion partielle de l'écoulement par suite de la hausse de la température dans la partie centrale thermiquement stratifiée. Les résultats des expériences réalisées avec un liquide de haute viscosité ($\nu = 10^{-2}\,\mathrm{m^2/s}$) permettent de conclure que l'échauffement par convection est encore toujours dominant, bien que l'écoulement soit relativement faible.

On a ressemblé au chapitre 5 un grand nombre de résultats expérimentaux valables pour $0,25 < H/D < 2,00$ et $5 < Pr < 8 \cdot 10^4$. Il en résulte une relation empirique (en nombres adimensionnels), valable pour le transfert de chaleur à un liquide dans un récipient fermé. Le coefficient global de transmission de chaleur a été calculé en partant de l'évolution quasi-logarithmique de la température dans le centre géométrique du récipient. Cette température du centre géométrique paraît nettement représentative de la température moyenne du liquide. Avec certaines restrictions, le coefficient global de transmission de chaleur qui résulte de ces calculs demeure constant durant le processus. Enfin, nous avons établi que la relation entre le nombre de Nusselt et celui de Rayleigh peut être présentée par une loi exponentielle. L'exposant de cette loi se situe avec assez de précision aux environs de $\frac{1}{4}$, puissance qui revient fréquemment dans le domaine de la convection naturelle laminaire.

On a également élaboré un modèle simplifié de calcul pratique au service de

l'industrie alimentaire (voir chapitre 6). On part de l'hypothèse de l'existence de trois régions: (1) une couche de faible épaisseur, près de la paroi avec un écoulement ascendant par convection naturelle; (2) une région stratifiée, dans la partie supérieure du récipient; (3) une région où le liquide est parfaitement mélangé, dans la partie inférieure. Partant des équations d'énergie, on déduit une relation mathématique pour le comportement de la hauteur de la région de turbulence. La hauteur asymptotique calculée était en accord avec les résultats expérimentaux. Elle dépend principalement du rapport entre les flux de chaleur transmis respectivement par le fond et par la paroi latérale.

Le modèle avec la partie supérieure en régime d'écoulement-piston simple ne s'accorde pas avec les données expérimentales. Après l'introduction dans ce modèle d'une dispersion axiale, représentée par une cascade de mélangeurs parfaitement agités, on obtient de meilleurs résultats. Cependant, n'ayant pas de données quantitatives concernant la dispersion axiale, le choix du nombre de mélangeurs en série doit être arbitraire. Ceci signifie une restriction importante des possibilités d'application du modèle. Des travaux additionnels seront nécessaires, notamment en ce qui concerne la distribution des temps de séjour dans la région stratifiée.

Les résultats obtenus au moyen de ce modèle simplifié ont été appliqués pour estimer la létalité du processus. Dans ce calcul l'effet du mouvement par convection du produit a été représenté par la substitution du récipient par une cascade de mélangeurs agités en série. Considérant les résultats du calcul on est mené à conclure, que la méthode conventionnelle du point unique sous-estime dans certains cas la létalité réelle du processus.

Au chapitre 7 on a étudié l'effet de la présence de particules solides sur l'échauffement par convection. Des profils de température ont été établis pour l'échauffement de l'eau et de l'huile de silicones en présence de particules sphériques de diamètre différent. Si l'échauffement de l'eau s'effectue en présence de particules sphériques solides ayant de 3 à 26 mm de diamètre, le transfert de chaleur par convection l'emporte sur la conduction.

Cependant, on a trouvé que, dans les huiles de silicones de haute viscosité, la convection est considérablement réduite par la présence de particules de petit diamètre (3 mm), de sorte que la hausse de la température se produit beaucoup plus lentement que celle d'un liquide sans l'addition de particules. La présence de particules de diamètre plus important dans l'huile de silicones ne réduit pas la convection de manière appréciable.

Que le liquide en question soit de l'eau ou une huile de silicones, la transmission de chaleur est fonction du diamètre des particules. Si celui-ci varie de 3 à 10 mm le coefficient global de transmission de chaleur va croissant: lorsque ce diamètre atteint 10 mm le coefficient est à peu près égal à celui du liquide sans particules. Enfin, pour ce qui est des diamètres plus importants (de 10 à 26 mm) le coefficient global de transmission de chaleur diminue graduellement.

Samenvatting

Het doel van dit onderzoek was te komen tot een beter inzicht in het gedrag van vloeibare levensmiddelen die na het afvullen in bussen of potten door verhitting gesteriliseerd worden. Vanuit deze doelstelling werd een modelstudie gemaakt van de temperatuurvereffening door vrije convectie in verticaal opgestelde cylindrische bussen die uitwendig met stoom verhit werden. Er werd zowel theoretisch als experimenteel onderzoek gedaan aan de fysische transportverschijnselen tijdens de opwarming. De resultaten van het experimentele deel van dit onderzoek vormden de basis voor de ontwikkeling van een vereenvoudigd wiskundig model. Het vereenvoudigde model kon vervolgens gebruikt worden voor een berekening van de sterilisatiewaarde van het opwarmingsproces.

De literatuur die betrekking heeft op de opwarming van produkten van het convectietype is samengevat in hoofdstuk 2. Vooral de factoren die de opwarmsnelheid mogelijkerwijs beïnvloeden, hebben in de literatuur veel aandacht gekregen. Het grootste deel van deze studies was echter kwalitatief van aard. Op grond van een literatuurstudie over stromingspatronen en temperatuurprofielen werd geconcludeerd dat de kennis van het mechanisme van de temperatuurvereffening door convectie leemten vertoont: (a) de interactie tussen stromingspatronen en temperatuurprofielen is onvoldoende geanalyseerd, (b) het stromingspatroon wordt meestal, ten onrechte, beschreven als een stationair proces, (c) studies van stromingspatronen werden over het algemeen alleen maar gemaakt bij niet-visceuze vloeistoffen, zoals water, (d) in de meeste gevallen vonden deze studies plaats onder omstandigheden die niet erg representatief zijn voor die tijdens het steriliseren van levensmiddelen. De in de literatuur voorgestelde berekeningsmethoden voor temperatuurvereffening door vrije convectie bleken, op een enkele uitzondering na, te sterk vereenvoudigd te zijn en fysisch niet altijd realistisch. Tenslotte bleek dat er uitvoerig en diepgaand onderzoek is gedaan aan soortgelijke problemen buiten het terrein van de levensmiddelentechnologie. Te denken valt hierbij aan de opslag van cryogene vloeistoffen in tanks, bijvoorbeeld vloeibaar aardgas. Hoewel bij deze problemen de randvoorwaarden meestal verschillen van die bij hitte-sterilisatie van levensmiddelen, ziet het er naar uit dat de resultaten van deze studies waardevol zijn bij de bestudering van het onderhavige probleem.

In hoofdstuk 3 zijn de mogelijkheden van een analytische beschrijving van de opwarming van een vloeistof in een gesloten vat nader onderzocht. Hoewel het tamelijk eenvoudig is de desbetreffende differentiaalvergelijkingen met bijbehorende randvoorwaarden op te stellen, lijkt een volledig analytische oplossing van dit stelsel op dit moment onmogelijk. Bestudeerd werd het werk van Barakat

& Clark (1966), die erin slaagden de vergelijkingen voor een soortgelijk geval numeriek op te lossen. De resultaten verkregen met een numeriek model verwant aan dat van Barakat & Clark, aangepast aan onze randvoorwaarden, waren niet bevredigend. In dit geval, waarbij zowel de bodem als de zijwand van het vat verwarmd werden, werden soortgelijke stromingspatronen en temperatuur- profielen verkregen als Barakat & Clark verkregen voor alleen zijwandverwar- ming. Dit is in strijd met experimentele waarnemingen waarbij zowel de bodem als de zijwand verwarmd werden. Bij gelijktijdige bodem en zijwand verwarming vindt een aanzienlijk convectief warmtetransport vanaf de bodem plaats. In het numerieke model verwaarloost men echter dit convectieve warmtetransport vanaf de bodem.

Hoofdstuk 4 geeft een overzicht van experimenteel bepaalde stromingspatro- nen en temperatuurprofielen voor drie vloeistoffen met sterk verschillende vis- cositeiten. Tijdens de opwarming ontwikkelt zich aan de zijwand van de bus een grenslaagstroming. Bovenin aangekomen verspreid de grenslaagstroming zich over het vrije vloeistofoppervlak en stroomt vervolgens langzaam naar beneden. Deze neerwaartse stroming gedraagt zich min of meer als propstroming en veroorzaakt een temperatuurgradiënt in het bovenste deel van de bus. Onderin de bus onstaat, tengevolge van de verwarming van de bodem, een zone waarin de stroming sterk instabiel is (wervelzone). Aanvankelijk neemt de hoogte van deze wervelzone af, na enige tijd echter wordt een evenwichtshoogte bereikt, die dan gedurende het verdere verloop van de opwarming niet meer verandert.

De horizontale temperatuurprofielen bleken in de kern van de vloeistof nagenoeg vlak te zijn, in de grenslaag aan de zijwand vertoonden deze profielen echter een sterke gradiënt. De verticale temperatuurprofielen gaven onderin de bus een uniforme temperatuur te zien, overeenkomend met die van de wervel- zone, terwijl in het bovenste deel van de bus naar het vloeistofoppervlak toe de temperatuur steeg. Uit het stromingsbeeld werd geconcludeerd dat, tengevolge van de verticale temperatuurgradiënt in de kern, een stromingsomkering plaats vond in het buitenste gedeelte van de grenslaag. Een meer gedetailleerde studie van de dikte van en de stroomsnelheden in de grenslaag aan de wand werd gemaakt met behulp van een laser-doppler snelheidsmeter. Uit een studie van strömings- en temperatuurprofielen voor een zeer visceuze siliconenolie ($v = 10^{-2}$ m²/s) bleek dat, ondanks de zeer geringe vloeistofsnelheden, de warm- teoverdracht door convectie bepalend was.

Uit een groot aantal experimenten voor H/D verhoudingen van 0.25 tot 2.00 en Prandtl-waarden van 5 tot 80000, werd een dimensieloos verband voor de warmtedoorgangscoëfficiënt van stoom naar vloeistof afgeleid (hoofdstuk 5). De warmtedoorgangscoëfficiënt werd berekend uit het temperatuurverloop in het geometrisch centrum van de vloeistof in de bus. De temperatuur in het geome- trisch centrum bleek de gemiddelde temperatuur van de vloeistof goed weer te geven. Uiteindelijk werd een relatie gevonden waarin Nu evenredig was met $Gr\,Pr$ tot de macht $\frac{1}{4}$, hetgeen overeenkomt met de gangbare relaties voor laminaire vrije convectie.

In hoofdstuk 6 is een vereenvoudigd wiskundig model voor de opwarming ontwikkeld. In dit model werden onderscheiden: een grenslaagstroming aan de

105

zijwand, een zone met een temperatuurgradiënt in het bovenste deel van de bus en een perfect gemengde zone van uniforme temperatuur in het onderste deel van de bus. Uit de energievergelijkingen voor dit systeem kon het verloop van de hoogte van de wervelzone voorspeld worden. De evenwichtshoogte die na enige tijd bereikt werd, bleek voornamelijk af te hangen van de verhouding tussen de warmtetoevoer via de bodem en de warmtetoevoer via de zijwand. De versie van het model waarbij propstroming in de kern verondersteld werd, leverde resultaten op die niet in overeenstemming waren met de experimenteel bepaalde temperatuurprofielen. De versie van het model waarin rekening gehouden werd met axiale menging, door de kern onder te verdelen in een aantal mengers in serie, gaf betere resultaten. Helaas waren er geen kwantitatieve gegevens beschikbaar omtrent de grootte van het effect van axiale menging, de keuze van het aantal mengers in serie was daarom arbitrair. Dit is een ernstige tekortkoming in het model, waardoor de voorspellende waarde ervan beperkt wordt. Om aan dit bezwaar tegemoet te komen zou onderzoek gedaan moeten worden aan de spreiding in de verblijftijd in de neerwaartse kernstroming.

De resultaten verkregen met het vereenvoudigd model werden gebruikt voor een schatting van de sterilisatiewaarde van het opwarmingsproces. In deze berekening werd het effect van vloeistofstroming tengevolge van convectie betrokken, door aan te nemen dat de bus is samengesteld uit een cascade van perfect geroerde tankreactoren. Uit de procesberekeningen bleek dat een methode waarbij uitgegaan wordt van het temperatuurverloop in één enkel punt (koudste punt) in bepaalde gevallen een onderschatting geeft van de werkelijke sterilisatiewaarde. Bovengenoemde berekeningsmethode, waarbij uitgegaan wordt van het vereenvoudigde model, kan ook gebruikt worden voor een schatting van de kwaliteitsachteruitgang tengevolge van de verhitting, als tenminste de reactiekinetiek van de verschillende afbraakprocessen bekend is.

In hoofdstuk 7 is een studie gemaakt van het effect van vaste deeltjes op de opwarming door convectie. Er zijn temperatuurprofielen gemeten tijdens de opwarming van water en siliconenoliën met daarin bolletjes van verschillende afmetingen. Uit deze experimenten werd geconcludeerd dat bij de opwarming van water met bolletjes (diameter 3 tot 26 mm) convectie de belangrijkste faktor is. Bij de opwarming van de veel visceuzere siliconenoliën werd gevonden dat kleine deeltjes (3 mm) de convectie sterk onderdrukken, hetgeen resulteert in een veel langzamer opwarming dan in het geval van alleen vloeistof. Grotere deeltjes veroorzaakten geen sterke afname van de convectie. Zowel voor water als siliconenolie werd gevonden dat de aanwezigheid van vaste deeltjes de warmteoverdrachtscoëfficiënt beïnvloedt. Bij toenemende deeltjesdiameter, van 3 tot 10 mm, werd een toename geconstateerd. Bij 10 mm was de waarde van de warmteoverdrachtscoëfficiënt nagenoeg gelijk aan die voor het geval van alleen vloeistof. Voor grotere diameters (10 tot 26 mm) werd bij toenemende deeltjesdiameter weer een geleidelijke afname gevonden.

References

Adrian, R. J., 1971. Analysis of a Laser-Doppler anemometer. J. of Physics E: Sci. Instrum. 4: 505–511.

Bailey, T. E. & R. F. Fearn, 1963. Analytical and experimental determination of liquid-hydrogen temperature stratification. Adv. cryogen. Engng 9: 254–263.

Ball, C. O. & F. C. W. Olson, 1957. Sterilization in Food Technology. McGraw Hill.

Barakat, H. Z. & J. A. Clark, 1966. Analytical and experimental study of the transient laminar natural convection flows in partially filled liquid containers. Proceedings Third International Heat Transfer Conference Vol. II: 152–162.

Bigelow, W. D., G. S. Bohart, A. C. Richardson & C. O. Ball, 1920. Heat penetration in processing canned foods. Bull. Natn. Cann. Ass. 16-L.

Bimbenet, J. J. & A. Duquenoy, 1974. Simulation mathématique de phénomènes intéressant les industries alimentaires. 1. Transferts de chaleur au cours de la stérilisation. Ind aliment agric. 4: 359–375.

Bimbenet, J. J. & L. Michiels, 1974. Transferts de chaleur par convection au cours de la stérilisation des conserves. Fourth International Congress of Food Science and Technology, Madrid.

Bird, R. B., W. E. Stewart & E. N. Lightfoot, 1960. Transport Phenomena. Wiley and Sons, Inc., New York, London, Tokyo.

Blaisdell, J. L., 1963. Natural convection heating of liquids in unagitated food containers. Ph. D. thesis. Michigan State University.

Board, P. W., 1966. Principles and practice of heat sterilization in canning. Food Preserv. Quart. 26: 26–31.

Boxtel. L. B. J. van, 1975. Opwarming van een vast bed van bollen in vloeistof in een gesloten bus. M.Sc. thesis, Wageningen. Available at Agriculatural University, Department of Food Science.

Carslaw, H. S. & J. C. Jaeger, 1959. Conduction of heat in solids. At the Clarendon Press, Oxford.

Charlson, G. S. & R. L. Sani, 1970. Thermoconvective instability in a bounded cylindrical fluid layer. Int. J. Heat Mass Transfer 13: 1479–1496.

Charm, S. E., 1963. The fundamentals of food engineering. Avi Publishing Co., Inc. Westport Connecticut.

Cheesewright, R., 1967. Natural convection from a plane, vertical surface in non-isothermal surroundings. Int. J. Heat Mass Transfer 10: 1847–1859.

Cheesewright, R., 1968. Turbulent natural convection from a vertical plane surface. J. Heat Transfer 90: 1–8.

Chu, T. Y. & R. J. Goldstein, 1973. Turbulent convection in a horizontal layer of water. J. Fluid Mech. 60: 141–159.

Eckert, E. R. G., 1966. Einführung in den Wärme- und Stoffaustausch. Springer Verlag. Berlin.

Ede, A. J., 1967. Advances in free convection. Adv. Heat Transfer 3: 1–64.

Eichhorn, R., 1969. Natural convection in a thermally stratified liquid. Prog. Heat Mass Transfer 2: 41–53.

Evans, L. B., E. S. Matulevicius & P. C. Pan, 1971. Reduction of thermal stratification by nonuniform wall heating. A.I.Ch.E. Jl 17: 752–753.

Evans, L. B. & N. E. Stefany, 1966. An experimental study of transient heat transfer to liquids in cylindrical enclosures. Chem. Engng Prog. Symp. Ser. 64, 62: 209–215.

Evans, L. B., R. C. Reid & E. M. Drake, 1968. Transient natural convection in a vertical cylinder. A.I.Ch.E. Jl 14: 251–259.

Fagerson, I. S. & W. B. Esselen, 1950. Heat transfer in commercial glass containers during thermal processing. Food Technol. 4: 411–415.

Fagerson, I. S., W. B. Esselen & J. L. Liciardello, 1951. Heat transfer in commercial glass containers during thermal processing. II Distribution in foods heating by convection. Food Technol. 5: 261–262.

Fujii, T., M. Takeuchi & I. Morioka, 1974. Laminar boundary layer of free convection in a temperature stratified environment. Fifth International Heat transfer Conference III: 44–48.

Goodman, J., 1973. Ambient temperature stratification effects in laminar free convection. Int. J. Heat Mass Transfer 16:1949–1950.

Groeber, H., S. Erk & U. Grigull, 1963. Die Grundgesetze der Wärmeübertragung. Springer Verlag, Berlin.

Handbook of Chemistry and Physics, 1971. 52nd edition. The Chemical Rubber Company. Cleveland, Ohio.

Hauf, W. & U. Grigull, 1970. Optical methods in heat transfer. Adv. Heat Transfer 6: 133–366.

Haug, R. I., W. M. Stevenson & E. R. F. Winter, 1968. An interferometric study of thermal stratification by natural convection in a contained liquid. Wärme- und Stoffübertragung 1: 251–254.

Hayakawa, K. I. & C. O. Ball, 1971. Theoretical formulas for temperatures in cans of solid food and for evaluating various heat processes. J. Food Sci. 36: 306–310.

Held, E. F. M. van der, 1954. Straling in holle ruimten. Voordrachten van de vacantieleergang voor verwarmingstechniek: 5–10.

Hellums, J. D. & S. W. Churchill, 1961. Dimensional analysis and natural circulation. Chem. Engng Prog. Symp. Ser. 32, 57: 75–80.

Hersom, A. C. & E. D. Hulland, 1969. Canned Foods. J. & A. Churchill Ltd., London.

Hinze, J. O., 1959. Turbulence. McGraw-Hill Book Company, Inc. New York.

Hoard, C. Q., C. R. Robertson & A. Acrivos, 1970. Experiments on the cellular structure in Bénard convection. Int. J. Heat Mass Transfer 13: 849–856.

Holwerda, E., 1973. Temperatuurvereffening bij vrije convectie in gesloten bussen. M.Sc. Thesis, Wageningen. Available at Agricultural University, Department of Food Science.

Jackson, J. M. & F. C. W. Olson, 1940. Thermal processing of canned foods in tin containers. Food Res. 5: 409–421.

Jakob, M., 1958. Heat Transfer. John Wiley & Sons, Inc. New York.

Japikse, D., 1973. Advances in thermosyphon technology. Adv. Heat Transfer 9: 1–111.

Jen, Y., J. E. Manson, C. R. Stumbo & J. W. Zahradnik, 1971. A procedure for estimating sterilization of and quality factor degradation in thermally processed foods. J. Food Sci. 36: 692–698.

Jones, D. E. A., 1931. Heat penetration by convection. Food Technol. 1: 63–65.

Jones, W. B., 1971. Fluid velocity sensor. General Physics Laboratory, Report no. 71-C-105.

Jowitt, R. & A. R. Mynott, 1974. Some factors affecting natural convective heat transfer to canned foods. Dechema-Monogr. 77: 153–164.

Kiis, A., 1964. The sterilization of tins heated by convection. Estonskaya Sel'skokhoz, Akad. Sbom. Nauch Trudov 38: 276–279.

Kitson, J. A., 1962. Syrup stratification in canned fruit slows heat processing. Food Can. 22: 34–36.

Kopelman, I. J. & S. Mizrahi, 1972. Dimensional analysis of the temperature response parameter f. Symposium on Heat and Mass Transfer Problems in Food Engineering, Wageningen.

108

Kramers, H., 1953. Grondslagen van de stroming, warmte- en stofoverdracht in vaste en gefluidiseerde systemen van korrelig materiaal. College fysische technologie. Bijzondere Onderwerpen. Technological University Delft.

Krischer, O., 1956. Die wissenschaftlichen Grundlagen der Trocknungstechnik. Springer Verlag, Berlin.

Kronig, R. & J. Bruijsten, 1951. On the theory of the heat and mass transfer from a sphere in a flowing liquid at low Reynolds numbers. Appl. sci. Res. A2: 439–446.

Kunii, D. & J. M. Smith, 1960. Heat transfer characteristics of porous rocks. A.I.Ch.E. Jl 6: 71–77.

Magoon, C. A. & C. W. Culpepper, 1921. A study of the factors affecting temperature changes in the container during the canning of fruits and vegetables. U.S. dep. Agr. Bull.: 1–55.

Matulevicius, E. S., 1970. Thermal stratification in enclosed fluids due to natural convection. Sc.D. Thesis, Massachusetts Institute of Technology, Cambridge.

McAdams, W., 1954. Heat Transmission. McGraw-Hill, London.

Meel, D. A. van & H. Vermij, 1961. A method for flow visualization. Appl. sci. Res. AX: 109–117.

Merrill, D. G., 1948. Heating rates of food in glass containers. Ind. Engng Chem. 40: 2263–2268.

Mulvaney, T. R., R. C. Nicholas & I. J. Pflug, 1960. Product-induced stratification of covering syrups. Food Technol. 14: 207–211.

Nicholas, R. C. & I. J. Pflug, 1961. Heat processing characteristics of fresh cucumber pickle products. Mich. agr. Exp. Sta. Q. Bull. 43: 522–531.

Nicholas, R. C., I. J. Pflug & T. R. Mulvaney, 1960a. Convection in syrup-packed products. Food Technol. 14: 205–206.

Nicholas, R. C., I. J. Pflug & T. R. Mulvaney, 1960b. Convection heating studies of water-syrup layered systems. Food Technol. 14: 212–214.

Nielsen, R. C. & R. H. Sabersky, 1973. Transient heat transfer in Bénard convection. Int. J. Heat Mass Transfer 16: 2407–2420.

Okada, M., 1940. Natural convection in can-shaped space, referred to the laws of similitude. Jap. Soc. sci. Fish. Bull. 8: 324–327.

Oldengarm, J., A. H. van Krieken & H. J. Raterink, 1973. Laser-doppler velocimeter with optical frequency shifting. Opt. Laser Technol, 5: 249–252.

Olson, F. C. W., 1947. Recent Japanese researches on canning technology. Food Technol. 1: 553–555.

Onat, K. & U. Grigull, 1970. Das Einsetzen der Konvektion in Flüssigkeiten über einer beheizten waagerechten Platte. Wärme- und Stoffübertragung 3: 103–113.

Ostrach. S., 1953. An analysis of laminar free-convection flow and heat transfer about a flat plate parallel to the direction of the generating body force. NACA Rep. 1111.

Ostrach, S., 1972. Natural convection in enclosures. Adv. Heat Transfer 8: 161–227.

Packer, G. J. K. & J. L. B. Gamlen, 1974. Calculation of temperature measurement errors in thermocouples in convection heating cans. J. Food Sci. 39: 739–743.

Pflug, I. J. & R. C. Nicholas, 1961a. Heating rates in glass containers as affected by heating medium and product. Mich. agr. Exp. Sta. Q. Bull. 44: 153–165.

Pflug, I. J. & R. C. Nicholas, 1961b. Heat processing characteristics of fresh cucumber pickle products. I. Heating rates of spears. Mich. agr. Exp. Sta. Q. Bull. 44: 407–414.

Pflug. I. J., J. L. Blaisdell & R. C. Nicholas, 1965. Rate of heating and location of the slowest heating zone in sweet fresh cucumber pickles. Food Technol. 19: 121–126.

Piau, J. M., 1974. Influence des variations des propriétés physiques et de la stratification en convection naturelle. Int. J. Heat Mass Transfer 17: 465–476.

Pollard, R. B. & W. O. Carlson, 1969. An experimental investigation of the effect of baffles on transient natural convection of a confined fluid. Prog. Heat Mass Transfer 2: 23–40.

Powe, R. E., S. H. Yin, J. A. Scanlan & E. H. Bishop, 1973. A technique for visualization of the very slow motion of water in enclosed spaces. J. Heat Transfer 95: 408–409.

Powers, J. J., D. E. Pratt & W. Norris, 1952. Comparative heating rates of bentonite suspensions in jars processed in boiling water and in steam of atmosferic pressure. Food Technol. 6: 246–250.

Rao, C. V. N. & P. V. Prabhu, 1971. Heat distribution patterns in canned prawns. Indian Food Packer 25: 20–24.

Reichert, J. E. & H. J. Bielig, 1973. Sterilisationsbedingungen zur Herstellung von Kartoffelkonserven. Confructa 18: 149–163.

Riedel, L., 1947. Zur Theorie der Hitzesterilisierung von Dosenkonserven. Mitt. kältetech. Inst. Karlsruhe.

Rudd, M. J., 1969. A new theoretical model for the laser-doppler meter. J. of Physics E: Sci. Instruments 2: 55–58.

Ruder, J. M., 1964. Stratification in a pressurized container with sidewall heating. A.I.A.A. Jl 2: 135–137.

Santen, N. van, 1969. De warmteoverdracht naar cylindervormige blikken M.Sc. thesis, Delft. Available at Technological University Delft.

Sarsten, J. A., 1972. LNG stratification and roll-over. Pipeline and Gas J., September 1972: 37–39.

Schmidt, E., 1956. Versuche zum Wärmeübergang bei natürlicher Konvektion. Chem. Ing. Technik 28: 175–180.

Schmidt, E. D. & I. J. Pflug, 1966. A study of the variables that affect heat penetration rates in glass containers. Mich. agr. Exp. Sta. Q. Bull. 48: 397–410.

Schultz, O. T. & F. C. W. Olson, 1938. Thermal processing of canned foods in tin containers. Food Res. 3: 647–651.

Schure, F. P., 1972. De invloed van vrije convectie op de opwarmsnelheid van vloeistoffen in conservenbussen. M.Sc. thesis, Wageningen. Available at Agricultural University, Department of Food Science.

Schwind, R. G. & G. C. Vliet, 1964. Observations and interpretations of natural convection and stratification in vessels. Proceedings of the Heat Transfer and Fluid Mechanics Institute: 51–68.

Siegel, R., 1958. Transient free convection from a vertical flat plate. Trans. Am. Soc. Mech. Eng. 80: 347–359.

Soehngen, E. E., 1969. Experimental studies on heat transfer at very high Prandtl numbers. Prog. Heat Mass Transfer 2: 125–150.

Somerscales, E. F. C. & T. S. Dougherty, 1970. Observed flow patterns at the initiation of convection in a horizontal liquid layer heated from below. J. Fluid Mech. 42: 755–768.

Soo, S. L., 1967. Fluid dynamics of multiphase systems. Blaisdell Publ. Co., Waltham, Massachusetts.

Sörenfirs, P., 1974. Determination of the temperature distribution in deep fat fried meat ball, by means of heat photography. Lebensmittel-Wiss. Technol. 7: 94–97.

Sparrow, E. M. & J. L. Gregg, 1956. Laminar free convection from a vertical plate with uniform surface heat flux. Trans. Am. Soc. Mech. Eng. 78: 435–440.

Stevens, P. M., 1972. Lethality calculations, including effects of product-movement, for convection heating and broken heating foods in still-cook retorts. Ph.D.-Thesis. University of Massachusetts.

Stumbo, C. R., 1953. New procedures for evaluating thermal processing for foods in cylindrical containers. Food Technol. 7: 309–315.

Tani, S., 1940. Natural convection in can-shaped space. Bull. Jap. Soc. Sci. Fish. 8: 76–78

Tatom, J. W. & W. O. Carlson, 1966. Transient turbulent free convection in close containers. Proceedings Third International Heat Transfer Conference. II: 163–170.

Tatom, J. W., W. H. Brown, L. H. Knight & E. F. Coxe, 1963. Analysis of therm stratification of liquid-hydrogen in rocket propellant tanks. Adv. cryogen. Engng ' 265–272.

110

Teixeira, A. A., J. R. Dixon, J. W. Zahradnik & G. E. Zinsmeister, 1969. Computer optimization of nutrient retention in the thermal processing of conduction-heated foods. Food Technol. 23: 845–850.

Thompson, G. E., 1919. Time-temperature relations in canned food during sterilization. Ind. Engng Chem. 11: 657–664.

Thorne, S. N. & R. Jowitt, 1972. Fluidized bed heating; the influence of the outside heat transfer coefficient on the sterilizing value of the process. Symposium Heat and Mass Transfer Problems in Food Engineering, Wageningen.

Torrance, K. E., 1968. Comparison of finite-difference computations of natural convection. J. Res. nat. Bur. Stand. 72B: 281–301.

Townsend, C. T., J. M. Reed, J. McConnel, M. J. Powers, W. B. Esselen, I. I. Somers, J. J. Duyer & C. O. Ball, 1949. Comparative heat penetration studies on jars and cans. Food Technol. 3: 213–226.

Vliet, G. C., 1966. Stratification with bottom heating. J. Spacecraft 3: 1142–1144.

Whitley, H. G. & R. I. Vachon, 1972. Transient laminar free convection in closed spherical containers. J. Heat Transfer 94: 360–366.

Wideff, K. J., P. G. Poschtoff & D. C. Koleff, 1963. Mathematische Ermittlung der Temperature in Konserven. Die Lebensmittel-Ind. 10: 283–285.

Yang, K. T., J. L. Novotny & Y. S. Cheng, 1972. Laminar free convection from a nonisothermal plate immersed in a temperature stratified medium. Int. J. Heat Mass Transfer 15: 1097–1109.

Zwijgers, A. J., 1974. Temperatuurvereffening bij vrije convectie in gesloten bussen met vaste deeltjes in de opgiet. M.Sc. thesis, Wageningen. Available at Agricultural University, Department of Food Science.

Appendix A

Numerical solution of the differential equations for natural convection in a closed cylindrical container

This appendix summarizes the numerical approach of Barakat & Clark (1966), as applied to my calculations. We start from the differential Eqns (18) to (21), as established in Section 3.1. The x component of the equation of motion (19) was differentiated with respect to r and the r component of the equation of motion (20) with respect to x. The resulting equations were subtracted and combined with the continuity Eqn (21). A stream function, Ψ', was introduced, which was defined as:

$$u = \frac{1}{r}\frac{\partial \Psi'}{\partial r} \qquad v = -\frac{1}{r}\frac{\partial \Psi'}{\partial x} \qquad (A.1)$$

Barakat & Clark also introduced a vorticity function, defined as:

$$\omega'' = \frac{1}{r}\left(\frac{\partial u''}{\partial r} - \frac{\partial v}{\partial x}\right) \qquad (A.2)$$

The three non-dimensionless transport equations obtained in this way, are made dimensionless by introducing the reduced quantities:

$$\left. \begin{array}{ll}
X = \dfrac{x}{H} & R = \dfrac{r}{\frac{1}{2}D} \\[2mm]
U = \dfrac{\frac{1}{4}D^2 u}{\alpha H} & V = \dfrac{\frac{1}{2}Dv}{\alpha} \\[2mm]
\tau = \dfrac{\alpha t}{\frac{1}{4}D^2} & \theta = \dfrac{(\frac{1}{2}D)^4 g\beta(T - T_0)}{H\nu\alpha} \\[2mm]
\omega = \dfrac{(\frac{1}{2}D)^4 \omega''}{\alpha H} & \Psi = \dfrac{\Psi'}{\alpha H}
\end{array} \right\} \qquad (A.3)$$

The above results in the Eqns (25), (26) and (27) of Section 3.2.

The boundary and initial conditions for the situation studied have already been pointed out in Chapter 3: see Section 3.4. Most investigators who tackled problems of natural convection in closed containers (Barakat & Clark, 1966 and Whitley & Vachon, 1972) found that for these problems explicit numerical methods were preferable. I also applied explicit finite difference approximations. The time derivates $\partial\theta/\partial\tau$ and $\partial\omega/\partial\tau$ are approximated by

112

$$\frac{\partial \theta}{\partial \tau} = \frac{\theta'_{i,j} - \theta_{i,j}}{\Delta \tau} \quad \text{and} \quad \frac{\partial \omega}{\partial \tau} = \frac{\omega'_{i,j} - \omega_{i,j}}{\Delta \tau} \tag{A.4}$$

where the primes refer to the time level $\tau + \Delta \tau$ and the unprimed variables to time level τ. The subscripts i and j refer to the location such that $X = i \cdot \Delta X$ and $R = j \cdot \Delta R$.

The non-linear terms

$$U \frac{\partial \theta}{\partial X}, \ V \frac{\partial \theta}{\partial R}, \ U \frac{\partial \omega}{\partial X} \quad \text{and} \quad V \frac{\partial \omega}{\partial R}$$

are linearized by considering the velocity components U and V to be known and equal to their values at time level τ.

These non-linear terms are thereupon approximated by forward differences if the velocity U or V is negative and by backward differences if U or V is positive.

Central differences are used to approximate the first order terms

$$\frac{1}{R} \frac{\partial \theta}{\partial R}, \frac{3}{R} \frac{\partial \omega}{\partial R} \quad \text{and} \quad \frac{1}{R} \frac{\partial \Psi}{\partial R}$$

At the centre line, where both R and $\partial \theta / \partial R$ are zero, $(1/R)(\partial \theta / \partial R)$ is replaced by the first non-zero term of its Taylor development:

$$\lim_{R \to 0} \frac{1}{R} \frac{\partial \theta}{\partial R} = \frac{\partial^2 \theta}{\partial R^2} \bigg|_{R=0} \tag{A.5}$$

Accordingly Eqns (25) to (27) of Chapter 3 can be approximated by finite differences as follows $(U \geq 0$ and $V \geq 0)$:

$$\frac{\theta'_{i,j} - \theta_{i,j}}{\Delta \tau} + U_{i,j} \frac{\theta_{i,j} - \theta_{i-1,j}}{\Delta X} + V_{i,j} \frac{\theta_{i,j} - \theta_{i,j-1}}{\Delta R}$$

$$= \frac{(\frac{1}{2}D)^2}{H^2} \cdot \frac{\theta_{i+1,j} - 2\theta_{i,j} + \theta_{i-1,j}}{(\Delta X)^2} + \frac{1}{R} \frac{\theta_{i,j+1} - \theta_{i,j-1}}{2 \Delta R} + \frac{\theta_{i,j+1} - 2\theta_{i,j} + \theta_{i,j-1}}{(\Delta R)^2} \tag{A.6}$$

$$\frac{\omega'_{i,j} - \omega_{i,j}}{\Delta \tau} + U_{i,j} \frac{\omega_{i,j} - \omega_{i-1,j}}{\Delta X} + V \frac{\omega_{i,j} - \omega_{i,j-1}}{\Delta R} = \frac{Pr}{R} \frac{\theta'_{i,j+1} - \theta'_{i,j-1}}{2 \Delta R}$$

$$+ Pr \left[\frac{(\frac{1}{2}D)^2}{H^2} \cdot \frac{\omega_{i+1,j} - 2\omega_{i,j} + \omega_{i-1,j}}{(\Delta X)^2} + \frac{3}{R} \frac{\omega_{i,j+1} - \omega_{i,j-1}}{2 \Delta R} + \frac{\omega_{i,j+1} - 2\omega_{i,j} + \omega_{i,j-1}}{(\Delta R)^2} \right] \tag{A.7}$$

$$\frac{(\frac{1}{2}D)^2}{H^2} \frac{\Psi_{i+1,j} - 2\Psi_{i,j} + \Psi_{i-1,j}}{(\Delta X)^2} - \frac{1}{R} \frac{\Psi_{i,j+1} - \Psi_{i,j-1}}{2 \Delta R} + \frac{\Psi_{i,j+1} - 2\Psi_{i,j} + \Psi_{i,j-1}}{(\Delta R)^2} = \omega_{i,j} \cdot R^2 \tag{A.8}$$

In this numerical model I used the same differential approximations for the boundary conditions as Barakat & Clark. Likewise the computational procedure for the values of the vorticity at the solid boundaries and the calculation method for the velocity components, were the same as those used by Barakat & Clark. For more details see their work.

The stability criteria were also equal to those used by Barakat & Clark. They are satisfied by using a time-step:

$$\Delta\tau = \frac{0.8}{\left(2 \cdot \frac{(\frac{1}{2}D)^2}{H^2} \cdot \frac{Pr}{(\Delta X)^2} + 2 \cdot \frac{Pr}{(\Delta R)^2} + \frac{|U_{max}|}{\Delta X} + \frac{|V_{max}|}{\Delta R}\right)} \tag{A.9}$$

The procedure of calculations was the same as that of Barakat & Clark, including the special iterative solution of Eqn (A.8).

The problem was programmed in Algol and executed on a CDC 6000 computer, at a grid size of 30×30. The program was made by Mr G. S. Stelling of the Mathematical Centre of the Agricultural University. A copy of the program and numerical results can be obtained on demand at the Department of Food Science of the Agricultural University, De Dreyen 12, Wageningen, the Netherlands.

114

Appendix B

The laser-doppler method

Several authors have described the principle of the laser-doppler velocimeter, see Adrian & Goldstein (1971), Jones (1971), Rudd (1969) and Oldengarm et al. (1973). An illustrative description is that based on the fringe model. If two laser beams intersect at a small angle ϕ (see Fig. B.1), this results in an interference pattern well known from optical interferometry. However, the theoretical picture of an interference pattern in a flat plane through the optical main axis of the system must be extended to a three dimensional one because of the finite thickness of the laser beam. Consequently we find in the situation of Fig. B.1 a fringe pattern that consists of light and dark planes, that is called the probe volume. A particle that crosses the probe volume with velocity v will scatter light during its passage. The frequency of the scattered light, as can be derived from Fig. B.1, can be presented by:

$$\nu_D = \frac{v \cdot \cos \beta}{d} = \frac{2 \sin \frac{\phi}{2} \cdot v \cos \beta}{\lambda_0} \tag{B.1}$$

where ν_D = doppler frequency

λ_0 = wavelength of the laser light

d = distance between two maxima.

1. laser beams
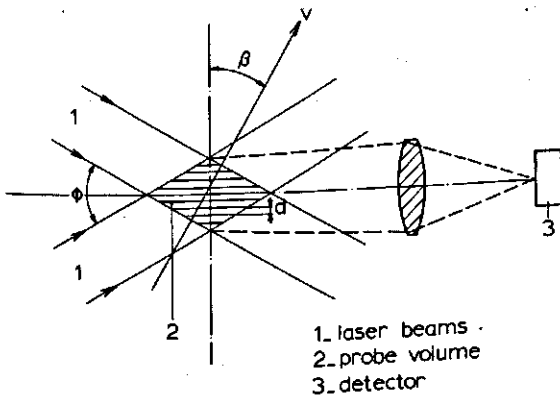2. probe volume
3. detector

Fig. B.1. Fringe pattern in probe volume. In the probe volume the interference lines with mutual distance d are indicated.

115

From theory of optical interferometry

$$d = \frac{\lambda_0}{2 \sin \frac{\phi}{2}}$$

(B.2)

Thus a linear relation exists between the doppler frequency ν_D and the velocity v. More sophisticated theory leads to the same result, as demonstrated by the authors quoted above. With a lens a part of the scattered light is focussed on a detector. The signal from the detector can be translated with a spectrum analyser or frequency tracker. This provides us with a value of the doppler frequency, that can be used in Eqn (B.1) to calculate the absolute value of v.

Experimental set-up   The experimental set-up developed by TPD-TNO/TH, was given in Fig. 18. The measurements were performed in the half-cylindrical container described in Section 4.1. The brass container wall was polished and used as a mirror to reflect the forwardly scattered light. The laser, together with a rotating grating and three lenses, was mounted on an optical bench, that could be translated along its optical axis, with a velocity of 0.05 mm/s. The laser beam was focussed on the grating, which was used as beam splitter. With a second lens the beams were made parallel and with a third lens they were focussed in the probe volume. The two beams were located in the vertical plane, while the angle between the beams was 8.74 degrees. The dimensions of the probe volume were about $300 \times 25 \times 25$ μm, with the largest dimension in the direction of the optical axis. The optical axis made an angle of 32.8 degrees with the normal on the glass window. The forward scattered light from the probe volume was reflected via the brass wall and with a lens focussed on the detector (photomultiplier). The signal from the photomultiplier was filtered and amplified and translated into an analogue signal by a frequency tracker. Then this signal could be registrated on a mV recorder.

The intrinsic accuracy of this laser-doppler arrangement in terms of velocity was estimated to be 0.2 to 0.3 mm/s. However, there were some other factors that lessened the accuracy of the measurements. First the brass wall of the container expands by heating, which causes a shift of the wall from the probe volume. Another serious problem was the variation of the refractive index of the liquid with temperature. If the laser beams pass regions with fluctuating temperatures like in the eddy region the probe volume continuously will shift due to fluctuations in the refractive index. Thus the distance from the probe volume to the wall will vary. In silicone fluid, where this problem was most serious, the accuracy of the indicated distance from the wall was estimated at 0.5 mm. In water this error will be less, due to the smaller fluctuations. Clearly the final accuracy here was determined by these other factors.

It must be pointed out that a time delay of 200 s exists between the moment at which the velocity was measured at the wall and the moment at which the velocity was measured at a distance of 10 mm from wall. The times appointed in velocity profiles measured by the laser-doppler method are those at the start of a scan. Due to the rapid change in the flow field of the boundary layer during the first

stage of heating a correction should be appropriated for this time delay. However, our observations were insufficient to achieve an accurate interpolation.

Hence the study done on velocity profiles and flow rates in the boundary layer must be considered to be qualitative, or at best semi-quantitative.

Appendix C

Container dimensions and some physical properties of test liquids

The experiments described in this thesis were performed with four containers of different size. The dimensions of these containers and the construction materials are presented in Table C.1. The experiments described, were performed with 8 different liquids. The most important physical properties of these liquids are presented in Table C.2.

Table C.1 Container dimensions and construction materials.

Container[1]	Diameter (m)	Height (m)	Wall thickness (mm)	Material
1	0.075	0.179	2	brass
2	0.178	0.277	2	copper
3	0.154	0.170	2	copper
4	0.236	0.273	2	brass

1. In the experiments described in Chapter 4 only container 2 was used. The experiments described in Chapter 5 were performed with containers 1 to 4.

Table C.2. Some physical properties of test liquids, at 30° C. Kinematic viscosity also at 100° C.

	ρ (kg/m³)	λ (W/m·K)	cp (J/kg·K)	β (K⁻¹)	$\nu_{30°C}$ (m²/s)	$\nu_{100°C}$ (m²/s)	Pr
Water	996	0.615	4180	5.6×10^{-4}	0.80×10^{-6}	0.30×10^{-6}	5
Sucrose solution 30 %	1123	0.514	3510	5.5×10^{-4}	2.12×10^{-6}	0.57×10^{-6}	16
Sucrose solution 40 %	1172	0.480	3275	5.3×10^{-4}	3.75×10^{-6}	0.79×10^{-6}	30
Sucrose solution 50 %	1225	0.447	3040	5.2×10^{-4}	8.31×10^{-6}	1.27×10^{-6}	69
Sucrose solution 60 %	1281	0.415	2800	5.0×10^{-4}	26.6×10^{-6}	2.43×10^{-6}	230
Glycerol solution 75 %	1189	—	—	—	17.8×10^{-6}	2.10×10^{-6}	110
Silicone fluid F111/100	964	0.159	1512	9.2×10^{-4}	80.6×10^{-6}	31.7×10^{-6}	700
Silicone fluid F111/10000	972	0.159	1512	9.2×10^{-4}	9270×10^{-6}	3310×10^{-6}	83000

Sources:

—P. Honig, 1953. Principles of Sugar Technology. Elsevier Publishing Company. Amsterdam/London/New York.

—National Research Council USA, 1926. International Critical Tables. McGraw Hill. New York/London.

—R. S. Norrish, 1967. Selected tables of physical properties of sugar solutions. Knapp, Drewett & Sons Ltd. Kingston upon Thames.

—Physical properties of glycerine and its solutions. Glycerine Producers Association. New York. No date.

—Technical documentation on silicone fluid. Imperial Chemical Industries. London. No date.

Appendix D

Numerical method for calculation of conduction heating in a cylindrical container

Transient conduction heating of a solid in a closed cylindrical container can be described by the following partial differential equation, assuming cylinder symmetry:

$$\frac{\partial T}{\partial t} = \alpha\left[\frac{\partial^2 T}{\partial x^2} + \frac{1}{r}\frac{\partial T}{\partial r} + \frac{\partial^2 T}{\partial r^2}\right] \tag{D.1}$$

For the coordinate system see Fig. 9. For this problem I assumed the following initial and boundary conditions:

at $t = 0$, $T = T_0$ for the whole container

at $t > 0$, $T = T_w$ at bottom and sidewall of the container

Further a head space is assumed to be present at the top of the container. The heat transfer through the head space can be characterized by a heat transfer coefficient $h_{\text{headspace}}$. By using a numerical method the heating can be simulated. Numerical solutions of similar heat conduction problems are, for example, extensively described by Jakob (1958).

If a grid size is chosen (i refers to r direction, j refers to x direction) Eqn (D.1) can be approximated by a finite difference equation (primes refer to the time level $t + \Delta t$):

a. At all nodal points except centre line and points adjacent to the head space

$$\frac{T'_{i,j} - T_{i,j}}{\Delta t} = \alpha\left[\frac{T_{i,j+1} - 2T_{i,j} + T_{i,j-1}}{(\Delta x)^2} + \frac{1}{r}\frac{T_{i+1,j} - T_{i-1,j}}{2(\Delta r)} + \frac{T_{i+1,j} - 2T_{i,j} + T_{i-1,j}}{(\Delta r)^2}\right] \tag{D.2}$$

b. At the centre line where both r and $\partial T/\partial r$ are zero $(1/r)(\partial T/\partial r)$ is replaced by $\partial^2 T/\partial r^2$ (see also Appendix A). Then:

$$\frac{T'_{i,j} - T_{i,j}}{\Delta t} = \alpha\left[\frac{T_{i,j+1} - 2T_{i,j} + T_{i,j-1}}{(\Delta x)^2} + 2\frac{T_{i+1,j} - 2T_{i,j} + T_{i-1,j}}{(\Delta r)^2}\right] \tag{D.3}$$

c. For points adjacent to the head space the method outlined by Jakob (1958), page 375, was used. It is assumed that $j = 1$ refers to points of the solid adjacent to the head space and $j = 0$ refers to the top cover with a temperature T_w. From an energy balance for a nodal point i, 1 it can be derived that

$$\frac{T'_{i,1} - T_{i,1}}{\Delta t} = \alpha \left[\frac{T_{i+1,1} - 2T_{i,1} + T_{i-1,1}}{(\Delta r)^2} + \frac{1}{r} \cdot \frac{T_{i+1,1} - T_{i-1,1}}{2(\Delta r)} + \right.$$
$$\left. + \frac{T_{i,2} - T_{i,1}}{(\Delta x)^2} + \frac{h_{head\,space} \cdot \Delta x}{\lambda} \cdot \frac{T_{i,0} - T_{i,1}}{(\Delta x)^2} \right] \quad (D.4)$$

From these equations the heating of the solid 'food' can be simulated, and temperature profiles at a certain time t can be calculated.

For the calculations referred to in Chapter 4 I used the following numerical values: $T_0 = 30°$ C, $T_w = 120°$ C (including top cover), $H = 200$ mm, $D = 180$ mm, $\Delta r = \Delta x = 10$ mm, $h_{head\,space} = 8$ W/m$^2 \cdot$ K (see Appendix E). For silicone fluid $\alpha = 0.116 \times 10^{-6}$ m^2/s, $\lambda = 0.16$ W/m $\cdot$ K.

Appendix E

Heat transfer through the head space of the container

Heat transport through the head space can be caused by radiation and by convection and conduction in the air layer. Since the metal lid will almost immediately assume the temperature of the heating medium and the liquid surface will have a lower temperature, effects of evaporation and condensation in the head space can be neglected. Another effect that has to be considered is heat conduction in the sidewall in the vertical direction, while the part of the sidewall joining the head space will have a higher temperature than the sidewall joining the liquid.

Radiation The lid and the sidewall joining the head space are considered as a hollow enclosure surrounding the liquid surface. Furthermore diffusive radiation is assumed. Problems of this kind were treated by Van der Held (1954) and Groeber et al. (1963). Heat transfer by radiation between surface of enclosure and liquid surface can be approximated by the formula of Christiansen:

$$q_{ls} = \{1/C_I + A_I/A_{II}(1/C_{II} - 1/C_s)\}^{-1}\{(T_I/100)^4 - (T_{II}/100)^4\} \qquad (E.1)$$

in which: q_{ls} = heat flux density to liquid surface (W/m²)

A_I = liquid surface (m²)

A_{II} = enclosure surface (m²)

C_s = emissivity of black body (W/m² · K⁴)

C_I = emissivity of liquid surface (W/m² · K⁴)

C_{II} = emissivity of surrounding surface (W/m² · K⁴)

T_I = temperature of liquid surface (K)

T_{II} = temperature of surrounding surface (K)

As emmisivity for a black body is assumed $C_s = 5.75$ W/m² · K⁴, for the liquid surface $C_I = 5.28$ W/m² · K⁴ and for the surrounding surface (cleaned copper or brass) $C_{II} = 1.15$ W/m² · K⁴, see McAdams (1954) and Handbook of Chemistry and Physics (1972). From Eqn (E.1) a heat transfer coefficient for radiation through the head space was calculated for different H/D ratios and different temperatures of the liquid surface (the wall temperature was assumed to be 121° C). This $h_{radiation}$ was related to the liquid surface area. The thus calculated $h_{radiation}$ varied from 4 to 6 W/m² · K.

122

Convection and conduction   During heating the temperature of top cover and sidewall will be higher than that of the liquid surface so that heat will be convected from the heated surfaces to the liquid surface. Heat transfer relations for horizontal enclosed plane gas layers heated from below are given by Groeber et al. (1963) and Jakob (1958). In the actual problem the top and sides of the horizontal gas layer are heated, which will cause a somewhat different convective flow. Because the side and the top are heated, a stable stratification in the head space arises. Certainly the convective heat transfer will be smaller than for a horizontal gas layer heated from below. Thus a correction for convective heat transfer in the head space will certainly not be underestimated by use of Jakob's (1958) approximation.

Jakob (1958), page 534, defined as a measure for the heat transport in a gas layer an equivalent thermal conductivity $\lambda_{convection}$, including the effect of conduction and convection. For $Gr > 4 \times 10^5$ the following correlation was found:

$$Nu = \frac{q_{ls}}{\Delta T} \cdot \frac{L_h}{\lambda} = \frac{\lambda_{convection}}{\lambda} = 0.068(Gr)^{\frac{1}{3}} \tag{E.2}$$

in which L_h is thickness gas layer and:

$$Gr = \frac{L_h^3 \cdot g \cdot \beta \cdot \Delta T}{\nu^2} \tag{E.3}$$

The heat conductivity, λ, of the vapour-air mixture in the head space was estimated at 0.03 W/m · K. Evaluation of Eqn (2) for this situation, ($Gr \simeq 5 \times 10^6$), results in $q_{ls}/\Delta T = h_{convection} = 2$ to 4 W/m^2 · K. This $h_{convection}$ is again applied to the liquid surface area.

Heat conduction in sidewall   The experiments were performed with partly filled containers. The wall of the container was heated with condensing steam, then h_{out} was high compared with h_{in}. The heat transfer between wall and the vapour-air mixture in the head space is negligible compared with the heat transfer between wall and liquid. Thus in the sidewall a temperature gradient arose, which caused a heat transport in the wall in vertical direction; so the sidewall acts like a fin. A numerical solution of this heat conduction problem showed that the contribution of this effect to the total heat flux can be neglected.

Conclusion   If the effects of radiation and convection and conduction are added an $h_{headspace} = 6 - 10$ W/m^2 · K is obtained. If this heat transfer coefficient for the head space is applied to the liquid surface area, the apparent heat transfer coefficient h' (Section 5.1, Eqn (36)) has to be corrected as follows:

$$\Phi_{total} = \Phi_{sidewall, bottom} + \Phi_{headspace} \tag{E.4}$$

or

$$h' \cdot \Delta T \cdot (\tfrac{1}{4}\pi D^2 + \pi DH) = h \cdot \Delta T \cdot (\tfrac{1}{4}\pi D^2 + \pi DH) + h_{headspace} \cdot \Delta T \cdot \tfrac{1}{4}\pi D^2 \tag{E.5}$$

This results in:

$$h = h' - h_{headspace} \cdot (1 + 4H/D)^{-1} \tag{E.6}$$

From Eqn (36) the apparent heat transfer coefficient h' is obtained, by applying Eqn (E.6) the true heat transfer coefficient for sidewall and bottom is obtained.

For water h' is about 1200 W/m² · K. If it is assumed that $h_{headspace} = 10$ W/m² · K and $H/D = \frac{1}{4}$, Eqn (E.6) leads to the following result:

$$h = 1200 - 5 = 1195 \text{ W/m}^2 \cdot \text{K}$$

Thus for water the effect of heat transfer through the head space is negligible.

For silicone fluid F111/10000 h' is about 30 W/m² · K. If assumed $h_{headspace} = 6$ W/m² · K and $H/D = \frac{1}{4}$, Eqn (E.6) in this case leads to:

$$h = 30 - 3 = 27 \text{ W/m}^2 \cdot \text{K}$$

Thus for the viscous silicone fluids and for small H/D ratios the heat transfer through the head space cannot be neglected.

Appendix F

Computational procedure for simplified simulation model

In the simulation model three liquid regions are distinguished: a boundary layer flow upwards at the wall, an upper stratified region in the core and a lower unstratified region in the core (see Fig. 45). For the simulation the core is discretized, the grid size corresponding to the size of a tank in the tanks-in-series model. Then each grid line corresponds with the centre of a tank. The computational procedure then is as follows:

1. A grid size Δx and a corresponding time step Δt are chosen.
2. The boundary layer flow rate, W, at the top of the unstratified region is calculated from Eqns (60–64). From Eqn (67) the temperature of the liquid leaving the boundary layer at the top is calculated. In Eqn (67) T_{in} is the liquid temperature of the unstratified region, while for the heat transfer coefficient, U, a value calculated from Eqn (41) is used.
3. The heat flux density from the bottom to the unstratified region is calculated from:

$$q_b = U(T_w - T_b) \tag{F.1}$$

The heating of the unstratified region in Δt is calculated from Eqn (49) which is approximated by:

$$T_{b,t+\Delta t} = T_{b,t} + \frac{q_b \Delta t}{X \rho c_p} \tag{F.2}$$

4. The downward velocity in the core, v_c, was calculated from Eqn (65).
5. The temperature rise in the stratified region is calculated for each grid line from Eqn (48), which is approximated by:

$$T_{i,t+\Delta t} = T_{i,t} + \frac{v_c \Delta t}{\Delta x} (T_{i,t} - T_{i-1,t}) \tag{F.3}$$

The subscript i refers to the ith grid line from above.
6. At the start of heating the thickness of the unstratified region is taken equal to the liquid height. Then at each time step a check is made whether the height of the unstratified region has to be changed by comparing the temperature at the base of the stratified region, T_c, with the temperature of the unstratified region, T_b. If $T_c > T_b$ the interface between stratified and unstratified region is shifted downwards by one grid size; if $T_c < T_b$ the boundary is shifted upward. If an adjustment of the height of the unstratified region takes place the temperature

125

rise of the unstratified region calculated from Eqn (F.2) is adjusted for the new height. If a linear change of the height is assumed with ΔX in Δt, a new temperature is calculated by using $X_{new} = X \pm \Delta X$. Thus in this simulation model the change of the height of the unstratified region proceeds with a step size ΔX.

7. The new value of the height of the unstratified region and the new temperature distribution in the liquid are then used for the next time-step. For the next time-step the procedure is started at point 2 again.

Appendix G

Effective heat diffusivity for a packed bed with stagnant fluid in pores

Heat transfer coefficient for conduction heating of a solid object

No exact mathematical representation is to be found in literature for transfer of heat by conduction in a porous medium that consists of spherical particles in a stagnant fluid. The numerous formulae suggested by various authors (see Krisher, 1956) are qualitative by nature and often based on drastically simplified models. We chose the approximation of Kunii & Smith (1960), who developed the following mathematical relation for the effective thermal conductivity:

$$\lambda_{\text{eff}}/\lambda_t = \varepsilon + \frac{\beta_0(1-\varepsilon)}{\Phi + \gamma(\lambda_t/\lambda_s)} \tag{G.1}$$

in which: β_0 = effective length between centre of two neighbouring solid particles divided by the particle diameter.

γ = effective length of a solid particle for heat transfer divided by the particle diameter

ε = porosity of packed bed

Φ = effective thickness of the fluid film adjacent to the surface of two solid particles divided by the particle diameter

λ_f = thermal conductivity of fluid

λ_s = thermal conductivity of solid phase.

In Eqn (G.1) Φ is defined as:

$$\Phi = \Phi_2 + (\Phi_1 + \Phi_2)\frac{\varepsilon - 0.260}{0.216} \quad \text{for} \quad 0.260 \leqslant \varepsilon \leqslant 0.476 \tag{G.2}$$

in which Φ_1 corresponds with the loosest packing and Φ_2 with the closest packing. Now Φ_1 and Φ_2 are functions of λ_s/λ_t and can be read from a figure given by Kunii & Smith (1960).

If we know the effective thermal conductivity, the effective thermal diffusivity can be calculated from:

$$\alpha_{\text{eff}} = \frac{\lambda_{\text{eff}}}{(\rho c_p)_{\text{bed}}} = \frac{\lambda_{\text{eff}}}{\varepsilon \rho_t c_{pt} + (1-\varepsilon)\rho_s c_{ps}} \tag{G.3}$$

If we consider pure conduction in an infinite homogenous, isotropic cylinder with $Bi = \infty$, the series solution of the averaged dimensionless temperature can be approximated for $\alpha_{\text{eff}}t/\frac{1}{4}D^2 > 0.20$ by:

127

$$\bar{\theta}(t) = u \exp\left[-\frac{v\alpha_{\text{eff}}t}{\frac{1}{4}D^2}\right] \tag{G.4}$$

For a flat plate of thickness H the analogous formula reads:

$$\bar{\theta}(t) = w \exp\left[-\frac{y\alpha_{\text{eff}}t}{\frac{1}{4}H^2}\right] \tag{G.5}$$

If the plate is heated at one surface only (the other surface being completely insulated) this formula becomes:

$$\bar{\theta}(t) = w \exp\left[-\frac{y\alpha_{\text{eff}}t}{H^2}\right] \tag{G.6}$$

In Eqns (G.4), (G.5) and (G.6) u, v, w and y are constants, see Carslaw & Jaeger (1965):

$$v = \beta_1 = 5.7831$$
$$y = \pi^2/4 = 2.4674 \tag{G.7}$$

in which β_1 is 1st root of $J_0(\beta) = 0$.

For the heating of a cylinder at sidewall and bottom, while the top is insulated, we have:

$$\bar{\theta}(t) = \frac{\bar{T} - T_w}{T_0 - T_w} = uw \exp\left[t\left(-\frac{v\alpha_{\text{eff}}}{\frac{1}{4}D^2} - \frac{y\alpha_{\text{eff}}}{H^2}\right)\right] \tag{G.8}$$

Further:

$$hA_c(T_w - \bar{T}) = V_c(\rho c_p)_{\text{eff}} \frac{\partial \bar{T}}{\partial t} \tag{G.9}$$

From Eqn (G.8) $\bar{T}$ and $\partial\bar{T}/\partial t$ can be calculated, which then results in:

$$h = \frac{\alpha_{\text{eff}} V_c(\rho c_p)_{\text{eff}}}{A_c}\left(\frac{5.7831}{\frac{1}{4}D^2} + \frac{2.4674}{H^2}\right) \tag{G.10}$$

128